ADDIS ABABA UNIVERSITY

SCHOOL OF GRADUATE STUDIES

ADDIS ABABA INSTITUTE OF TECHNOLOGY (AAiT)

CENTER FOR RENEWABLE ENERGY

Investigation of Exhaust Gases Driven Absorption Cooling System Case Study on Gambella, General Cargo Ship

A THESIS SUBMITTED TO THE SCHOOL OF GRADUATE STUDIES OF ADDIS ABABA UNIVERSITY IN PARTIAL FULFILLMENT OF THE DEGREE OF MASTER OF SCIENCE IN RENEWABLE ENERGY TECHNOLOGY

By: Beniam Getasetegn

Advisor: Dr. Solomon T/Mariam

July, 2025

Addis Ababa, Ethiopia

DECLARATION

I, Beniam Getasetegn, declare that this thesis is the result of my own work and that all source and material used for this thesis have been duly acknowledged. This thesis is submitted in partial fulfillment of the requirement for master's degree in renewable energy technology at Addis Ababa University and to be made available at the university's library under the role of the library. I confidently declare that this thesis has not been submitted to any institutions anywhere for the award of any academic degree, diploma, or certificate.

Name: Beniam Getasetegn

Signature: ----------

Date: 22/07/2025

ADDIS ABABA UNIVERSITY

ADDIS ABABA INSTITUTE OF TECHNOLOGY

SCHOOL OF MULTIDISCIPLINARY

CENTER OF RENEWABLE ENERGY

Exhaust Gases Driven Absorption Cooling System Case Study on Gambella, General Cargo Ship

By**:** Beniam Getasetegn

Approved by Board of Examiners:

Advisor	Signature	Date
Internal Examiner	Signature	Date
External Examiner	Signature	Date
Chairman	Signature	Date
School of Postgraduate Program	Signature	Date

ACKNOWLEDGMENT

First and above all I want to sincerely thank my God and his mother Saint Virgin Marry for being with me throughout my life and supporting me a lot in every walk of performing this thesis. I want to sincerely thank my advisor Dr. Solomon T/Mariam (Associate Professor) for his tireless help by showing me the key points on how the way to accomplish this work by guiding and directing me along the path. The advices and confidence that I received in my working time with him will serve me in every way of my career.

I also sincerely thank Ethiopian Shipping and Logistics Service Enterprise (ESLSE) crews specifically, Ch. Ing. Teshome, Technical Officer Bekri, Technical Officer Bekele Alemu and Technical Officer Dawit Ayele for helping and understanding me in getting an important data for this work.

At the end, I want to deeply thank my parent for their endless help during the worst time of my life that I gained to harden me by far and I dedicate this thesis work for them especially to my beloved mother Yeshi-embet Esubalew for her prayers, love and care that walked me for success.

ABSTRACT

In shipping transportation emission reduction has been a great concern for the last decades own to various reasons. Due to increment of oil prices, shipbuilders have been inspired to rise the vessel's overall fuel efficiency. Currently, these situations are initiated by emission controlled areas as well as taxation of CO_2. Recovering waste heat from low grade energy through vapor absorption refrigeration system is a promising way to improve engine efficiency and fuel consumption.

In this thesis, utilization of exhaust gas from marine engines as a heat input to vapor absorption system is examined using marine vessel Gambella as a case study ship. The absorption cycle uses $H_2O-LiBr$ solution as a circulating fluid. An exhaust gas analysis is computed based on six months of engine performance data and then thermodynamic analysis is computed and simulation analysis is performed using Excel for vapor absorption system.

This thesis focuses on performance enhancement of single effect vapor absorption system. By adding mixing chamber, flash gas removal and liquid suction heat exchanger into a single stage system, system performance is raised. Thermodynamic analysis is computed to compare the increment of performance on proposed cycle with ordinary and combined cycle. Simulation result shows that a proposed cycle COP is increased considerably by 38.23% and 3% relative to ordinary cycle and combined cycle respectively. Adding of vapor mixing chamber and flash gas removal accounts 35.23% increment on system performance and the remaining 3% is accounted by liquid suction heat exchanger. From the results the proposed cycle also considerably increased the cooling effect in an evaporator as well as an overall efficiency of marine diesel engine of the case study ship between 4 – 9%. Hence, introducing vapor mixing chamber and liquid suction heat exchanger to an ordinary cycle is a novel enhancement. Environmentally, utilizing the absorption system throughout sailing will diminish fuel utilization by 82.5 ton/year with fuel cost saving by 57,188.18 $/year and this results a payback period of 7 years for investment cost. This, in turn, decreasing emissions of NO_X, SO_X as well as CO_2 by cost effectiveness of 2.88 $/kg, 18.86 $/kg as well as 0.054 $/kg respectively and also reduces about 349.55 and 418.11 tons of CO_2e in 100years and 20 years using well to wake approach respectively.

Key words: Marine diesel engine, Exhaust gas, Absorption system, Cooling effect, COP

TABLE OF CONTENTS

DECLARATION i
ACKNOWLEDGMENT iii
ABSTRACT iv
NOMENCLATURE vii
LIST OF FIGURES ix
LIST OF TABLES xi
CHAPTER 1: INTRODUCTION 1
1.1. Background 1
1.2. Problem Statement 1
1.3. Objectives 2
1.3.1 General objective 2
1.3.2 Specific objectives 2
1.4. Significance and Scope of the Study 3
CHAPTER 2: LITERATURE REVIEW 4
2.1. Marine Engine Exhaust Gas Recovery Mechanisms 4
2.2. Absorption Refrigeration Machines 6
2.3. Working Fluid Pairs – Refrigerant-Absorbent and their Practical Problems 8
2.4. Heat Sources for Water-Lithium Bromide Absorption Cooling Systems 11
2.5. Environmental Impacts of Exhaust Gases and Refrigerants used on Board Vessels 11
2.5.1 Sulfur influence and dew point temperature of exhaust gas 12
2.6. Advancement of Absorption Mechanism and Arrangement 14
2.6.1 Working solution pairs 14
2.6.2 Integrated systems 14
2.7. Summary of Literature Review and Research Gap 17
2.7.1. Summary of literature review 17
2.7.2. Research Gap 18
CHAPTER 3: METHODOLOGY 19
3.1. Engine of Marine Vessel Gambella 19
3.2. Exhaust Gas Analysis 20
3.2.1 Energy potential of exhaust gas 23

3.3. Thermodynamic Analysis of a Proposed Vapor Absorption System 24
3.3.1 Operating principle 24
3.3.2 Design assumptions 25
3.3.3 Refrigeration capacity and performance 28
3.3.4 Mass and energy balance analysis 29
3.4. Environmental and Economic Analysis of Vapor Absorption Refrigeration System 33
CHAPTER 4: RESULT AND DISCUSSIONS 37
4.1. Exhaust Gas Analysis 37
4.2. VARS Analysis 38
4.3. Temperature Variation Effect on the Ordinary and Proposed cycle 40
4.3.1 Exhaust gas temperature variation effect 40
4.3.2 Effect of variation of generator temperature 43
4.3.3. Effect of condenser temperature variation 45
4.3.4. Effect of evaporator temperature variation 47
4.3.5. Effect of variation of absorber temperature 49
4.3.6 Effect of entrainment ratio variation and temperature of exhaust gas on a heat transfer rates 51
4.3.7. Heat exchanger effect 54
4.4. Environmental and Economic Results 55
CHAPTER 5: CONCLUSION AND RECOMMENDATIONS 61
5.1. Conclusion 61
5.2. Recommendations 62
REFERENCES 63
APPENDIX A 68
APPENDIX B 70
APPENDIX C 72
APPENDIX D 75

NOMENCLATURE

Abbreviations

ACE	Annual cost effectiveness
CC	Cooling capacity
COP	Coefficient of performance
ECA	Emission control areas
ER	Emission reduction
ESLSE	Ethiopian Shipping Lines and Logistics Service Enterprise
FT	Flash tank
HSFO	High sulfur fuel oils
IMO	International Maritime Organization
LSFO	Low sulfur fuel oils
LSHX	Liquid suction heat exchanger
MCR	Maximum continuous rating
ORC	Organic Rankine cycle
PM	Particulate matter
PPM	Parts per million
RC	Rankine cycle
RHX	Refrigerant heat exchanger
SHX	Solution heat exchanger
SMCR	Specific maximum continuous rating
UC	Unit cost
VARS	Vapor absorption refrigeration system

VARSU	Vapor absorption refrigeration system unit
VLSFO	Very low sulfur fuel oil
WC	Water column
WHRS	Waste heat recovery system

Symbols

χ	Concentration of LiBr (%)
$\dot{m}$	Mass flow rate (kg/s)
V	velocity (m/s)
h	Enthalpy (kJ/kg)
ε	Effectiveness (%)
n	Number of age
i	Interest rate (%)
C_p	Specific heat capacity (kJ/kg^{o}C)
T	Temperature (^{o}C)
ω	Entrainment ratio
λ	Circulation ratio
Q	Heat transfer rate (kW)

Subscript

a	Absorber
e	Evaporator
g	Generator
c	Condenser
exh	Exhaust gas

LIST OF FIGURES

Figure 2-1 Schematic of VARS (Samanta & Basu, 2016)..... 7
Figure 2-2 Commercialized single drum item, H_2O-LiBr system (Kumar, 2009). 10
Figure 2-3 Commercialized twin drum item, H_2O-LiBr system (Kumar, 2009)..... 10
Figure 2- 4 Refrigerant losses owing to AC from various kinds of vessel (IMO et al., 2014)..... 12
Figure 2- 5 Influence of sulphur amount in fuel on dew point temperature of exhaust gas 13
Figure 2- 6 Integrated FT-absorption-ejector VARS (Sirwan et al., 2013a). 16
Picture 3-1 Marine Engine system of Marine Vessel Gambella with engine type 6S40ME-B9-TII (Photo Captured by ESLSE Technical officer Bekele Alemu and reprinted with ESLSE permission)..... 19
Figure 3-1 Mass balance of the engine system……..23
Figure 3-2 A proposed single-stage H_2O-LiBr VARS. 24
Figure 3-3 Schematic and operation conditions of ordinary single-stage H_2O-LiBr VARS..... 26
Figure 3-4 P-T-X representation of single-stage H_2O-LiBr VARS..... 27
Figure 4-1 P−T−χ line diagram of the proposed system……39
Figure 4-2 Exhaust gas temperature effect on a heat transfer rate for each component of ordinary cycle. 40
Figure 4-3 Exhaust gas temperature effect on a heat transfer rate for each component of proposed cycle. 41
Figure 4-4 Effect of exhaust gas temperature on desorbed $\dot{m}r$, $\dot{m}ss$ and $\dot{m}ws$..... 41
Figure 4-5 Comparison of COP between a proposed, combined and an ordinary cycle. 42
Figure 4-6 (a) Effect of variation of generator temperature on heat transfer rate…….44
Figure 4-6 (b) Effect of variation of generator temperature on H_2O-LiBr concentration. 44
Figure 4-6 (c) Effect of variation of generator temperature on COP..... 45
Figure 4-7 (a)Effect of variation of condenser temperature on thermal load……46
Figure 4-7 (b) Effect of variation of condenser temperature on H_2O-LiBr concentration. 46
Figure 4-7 (c) Effect of variation of condenser temperature on COP..... 47
Figure 4-8 (a) Effect of evaporator temperature variation on a heat transfer rates. ……48
Figure 4-8 (b) Effect of evaporator temperature variation on H_2O-LiBr concentration..... 48
Figure 4-8 (c) Effect of evaporator temperature variation on COP. 49

Figure 4-9 (a) Effect of absorber temperature variation on heat transfer rates…….50

Figure 4-9 (b) Effect of absorber temperature variation on H_2O-LiBr concentration. 50

Figure 4-9 (c) Effect of absorber temperature variation on system COP. 51

Figure 4-10 (a) Entrainment ratio effect on condenser heat transfer rates with exhaust gas temperature……52

Figure 4-10 (b) Entrainment ratio effect on evaporator cooling load with exhaust gas temperature. 53

Figure 4-10 (c) Effect of entrainment ratio on system performance. 53

Figure 4-11 COP vs LSHX effectiveness…….54

Figure 4-12 Annual emission reduction after using VARSU……55

Figure 4-13 Exhaust gas based VARSU's overall lifecycle cost elements for 18 years of operation. ……...…….56

Figure 4-14 Yearly capital recovery cost of after implementing exhaust gas based VARSU……..57

Figure 4-15 Yearly cost of fuel saving after implementing exhaust gas based VARSU……..57

Figure 4-16 Yearly cost-effectiveness emission decrement for pollutants after implementing VARSU…….....58

Figure 4-17 Well-to-wake emissions of climate pollutants before applying VARSU……..59

Figure 4-18 Well-to-wake emissions of climate pollutants before applying VARSU……..60

LIST OF TABLES

Table 3-1 Engine rating at specific working conditions of T_{air} = 24ºC, T_{cw} = 18oC, p_{bar} = 1.015 bar, Δp_m = 300 mm WC(water column) 20
Table 3-2 Constants for Duhring enthalpy correlations of $H_2O-LiBr$ 28
Table 4-1 Results for different parameters of exhaust gas…….37
Table 4-2 Thermodynamic values for each stream lines of ordinary cycle. 38
Table 4-3 Thermodynamic values for each stream lines of auxiliary components of the proposed cycle. 38

CHAPTER 1: INTRODUCTION

1.1. Background

In the globe, 90% of all commercial freight is moved by ships, most of which run on fossil fuels. However, because of climate change and the growing cost of fuel, shipbuilders and owners are currently investigating more economical and environmentally beneficial ways (IMO, 2018).

It has been projected that the marine industry would continue to expand due to economic growth as well as population growth, particularly across Asia, Latin America, and Africa. To reach the 50% reduction in emissions target without adversely affecting the world economy and people's standard of living, larger ships with more advanced propulsion systems are preferable (Vahvanen, 2020).

The large vessels are ideal for long-haul transcontinental journeys between major hub ports (Sahriana et al., 2020). Ship designs that use air bubble lubrication or a hull shape can lower hydrodynamic drag force and thereby ship energy consumption. With MALS (Mitsubishi Air Lubrication System) installed for boats, Mitsubishi Heavy Industries has saved more than 5% on fuel. Studies show that reducing propulsion losses and power transmission can also be beneficial(Lee, 2014). Over the past ten years, there hasn't been much of an improvement in the thermodynamic efficiency of large ships using the diesel cycle (Manzela et al., 2010).

The study that will be covered in this master's thesis is centered on using ship engine waste heat to power absorption cooling systems. Because of this, it seeks to reduce the amount of energy needed to run the ship's cooling system, which will improve engine thermal performance and lessen greenhouse gas emissions.

1.2. Problem Statement

Nowadays, much emphasis is given to sustainability and energy efficiency. This has prompted researchers worldwide to take waste heat recovery from vehicle and marine engine gasses into consideration. Among the alternative technologies, the $H_2O-LiBr$ vapor absorption

refrigeration system has shown promise. It can be fueled by the exhaust gases from marine engines.

Despite the widespread adoption of heat recovery mechanisms, limited research has been dedicated to understanding how the properties of exhaust gases such as temperature and flow rate affect the efficiency of critical components (like the flash tank, liquid suction heat exchanger (LSHX), and mixing chamber). The resulting oversight limits the wider adoption of waste heat recovery technology in practical applications for cooling system.

Thus, the purpose of this MSc thesis is to examine how the performance of the auxiliary components in $H_2O-LiBr$ based vapor absorption refrigeration systems relates to the attributes of exhaust gases. By systematically analyzing these interactions, the study intends to contribute to the knowledge base surrounding low-grade waste heat utilization. Ultimately, enhancing system efficiency and expanding the applicability of waste heat recovery is the target of this research work. Hence, this research will address the current knowledge gaps and provide insights for future advancements in the design and integration of waste heat recovery systems.

1.3. Objectives

1.3.1 General objective

A general objective of this thesis work is investigating how an exhaust gases of marine engines of type "6S40ME-B9-TII" affect the performance of the auxiliary components of $H_2O-LiBr$ absorption refrigeration systems.

1.3.2 Specific objectives

- Analyze exhaust gas properties from the specified marine engines. This includes their changes while the ship is in operation.
- Compute thermodynamic analysis based on exhaust gas analysis for the $H_2O-LiBr$ vapor absorption refrigeration system (VARS).

- Examine how the properties of the exhaust gas affect the operation of key auxiliary parts of the refrigeration cycle (such the mixing chamber, LSHX, and flash tank), paying particular attention to temperature changes as well as heat transfer rate.
- Suggest modifications on the auxiliary components for better cooling capacity.
- Examine the environmental and economic benefits of the system.

1.4. Significance and Scope of the Study

Using dissipated heat from marine diesel engines of exhaust gases have great importance in keeping marine environment from pollution by reducing emissions and consumptions of fuel. This thesis will focus mainly on using the dissipated heat from marine diesel engine of exhaust gas for production of cooling effect.

The scope of this thesis work is to collect data from Ethiopian Shipping Lines and Logistics services about fuel consumption and operation condition of the selected vessel main engine system. Then determine available energy potential of exhaust gases and analyze the existing cooling potential and its performance. By using this waste energy, design a single effect VARS with performance enhancement devices to supplement the existing cooling system.

CHAPTER 2: LITERATURE REVIEW

2.1. Marine Engine Exhaust Gas Recovery Mechanisms

Cruise ships are among the most significant marine transportation modes in terms of air pollution due to their energy requirements for propulsion, electric generating, and air conditioning. Even with advancements in energy systems, such as the engines used, recovering exhaust gas energy through waste heat recovery systems (WHRS) remains a viable way to reduce the environmental impact of cruise ships. According to Shu et al., 2013, a review has been conducted about waste heat recovery aboard ships. This study demonstrated that the fundamental technologies of using of exhaust gas to recover heat by applying combined cycles, gas turbines, desalination, Rankine cycles (RC), and VARS for cooling production. The most useful of these are gas turbines, desalination plants, and Rankine cycles while absorption systems are not applicable in vessel. Zhu et al., 2020, who evaluated WHRS from marine engines, vouch for this outcome. Specifically, they mentioned that for engines with outputs more than 25 MW, RC in conjunction with power turbine works well. With the organic Rankine cycle (ORC) in place, tiny ships are advised to use it. Large ships are suited for CO_2 based power cycles.

Nonetheless, low thermal efficiency is a major problem with power application for dissipated heat. In their experimental investigation, Alshammari et al., 2018, measured the efficiency of an ORC in close proximity to 4.3% when it was attached to diesel engine running at steady state. Regardless of some articles discussing it, the published work analysis reveals that, as of now, dissipated heat cannot be used on board ships for cooling purposes. Absorption systems are the most widely applicable system used to produce cooling. Chaboki et al., 2021, propose a $H_2O-LiBr$ absorption system through energy, exergy, and surrounding analysis, they show that the recommended system can diminish total irreversibility by 31% and save USD 45,078 in annual punishment costs related to CO_2 emissions. Salmi et al., 2017, who analyzed absorption chillers using $H_2O-LiBr$ and NH_3-H_2O as the operating fluid, also found identical results. Cao et al., 2015, simulated an increase in electric COP from 3.6 for conventional chiller to 9.4 for VARS.

In order to bring down fuel consumption without affecting the vessel's energy outputs, Bo et al., 2021, executed a thermodynamic examinations of a tri-generation system that combines humidification desalination unit, booster ejector cooling cycle, and Kalina cycle for generating fresh water, refrigeration, and energy. Another study reported by Zhang et al., 2021, made simulation prototype for unique coupled system aboard a cruise ship that utilizes dissipated heat to power an ejector cooling system and transcritical CO_2 ORC. They claimed that as compared to the usual system, this system exhibited considerable thermodynamic improvements.

A heat-operated ejector cooling system powered by dissipated energy from a minor marine engine with nominal power output of 100 − 250 kW was experimentally investigated by Butrymowicz et al., 2021. The tested device consumes 75 kW of recovered heat from gasses to generate 30 kW of cooling. Furthermore, hot water can be provided and the thermal load can be attained by using energy from cooling of water jacket, which essentially meets thermal energy requirement for the whole mid-sized ship's. Identical research team suggested doing a tested investigation on cooling system with ejector for AC run by dissipated heat and utilizing R1234ze, an eco-friendly refrigerant. By applying a broad range of temperatures to the available source, they illustrated the viability of employing piston engine dissipated heat to run a system and attained a greatest COP of 0.33.

Manzela et al., 2010, made a tested analysis for VARS utilizing exhaust gas as heat source. According to their task, they assigned a tested research on exhaust gases heat accessibility and VARS result on engine performance, exhaust discharges, and vehicle energy savings. To do this, they tested at a successful car engine in VARS that was coupled to an exhaust pipe-mounted bench test dynamometer. They examined the engine at 25%, 50%, and 75% by varying throttle valve opening. According to the results, the inclusion of VARS reduced carbon monoxide emissions while enhancing hydrocarbon discharges.

Ouadha & El-Gotni, 2013, performed research on marine diesel engine by applying NH_3−H_2O based VARS. According to their work, the engine consumes about 48% of the given power and the remaining release to the surrounding. They combine the engine with VARS to apply this

dissipated heat lessen the coolant load. Simulation findings reported that system COP fluctuates between 0.6057 and 0.6937 due to varying of SHX capacity between 70 and 100 respectively. According to the results system performance is enhanced by rising desorber and chiller temperature or diminishing absorber and condenser temperatures.

Fernández-Seara et al., 1998, performed WHRS in a trawler chiller ship to run NH_3−H_2O based VARS by utilizing engine exhaust for cooling purpose onboard. The fishing ship has 4−stroke diesel engine with power varying between 700 − 1200 kW hence at high as well as uniform load of an engine, heat is recovered from the exhaust at the time of fishing. Simulation findings revealed that this kind of WHRS is viable for chiller trawler vessels.

2.2. Absorption Refrigeration Machines

Ferdinand Carré created VARS for the first time in 1823, and it was initially applied in the late 1700s. In contrast to the compression system, an absorption system unit uses waste energy from a source rather than electricity. In VARS, there is two working fluids (absorbent and refrigerant), which are isolated and combined at distinct phases of a refrigeration system. H_2O−LiBr and NH_3−H_2O are most widely applicable fluid pairs of solutions. Stability, a high enthalpy of vaporization, affordability, accessibility, non-corrosiveness, and environmental friendliness are desirable characteristics for fluid pairs in VARS (Manzela et al., 2010).

AC and cooling systems can be driven by VARS, which uses heat energy instead of electricity. Large trawling fishing vessels require a continuous refrigeration chain for proper refrigeration. VARS has been used to produce ice and cooling. However, dissipated heat is now widely used to power VARS in cruise vessel HVAC systems, food items cooling cycles as well as cargo hold refrigerating in cooled cargo vessels (Manzela et al., 2010).

The useable heat sources for operating VARS in the study on geothermal waste heat reported by Keçeciler et al., 2000, have a temperature ranges from 50 − 200°C. This indicates exhaust gases, scavenge air cooler as well as jacket water are crucial energy sources to run VARS.

Heat is emitted when refrigerant vapor goes to condenser. After passing through the expansion valve, liquid refrigerant goes to evaporator and heat is introduced. Next, a vapor refrigerant moves to absorber, where a weak absorbent solution absorbs it. Heat is also rejected into the surroundings during the absorption cycle and a weak solution is further pressurized into desorber where dissipated energy is utilized. This energy vaporizes refrigerant and a fresh cycle is initiated and the absorber receives strong solution back. To maximize the cycle performance overall, heat is transmitted into the solution via SHX and going toward the desorber (Samanta & Basu, 2016). Figure 2-1 below shows VARS with solution and refrigerant heat exchanger.

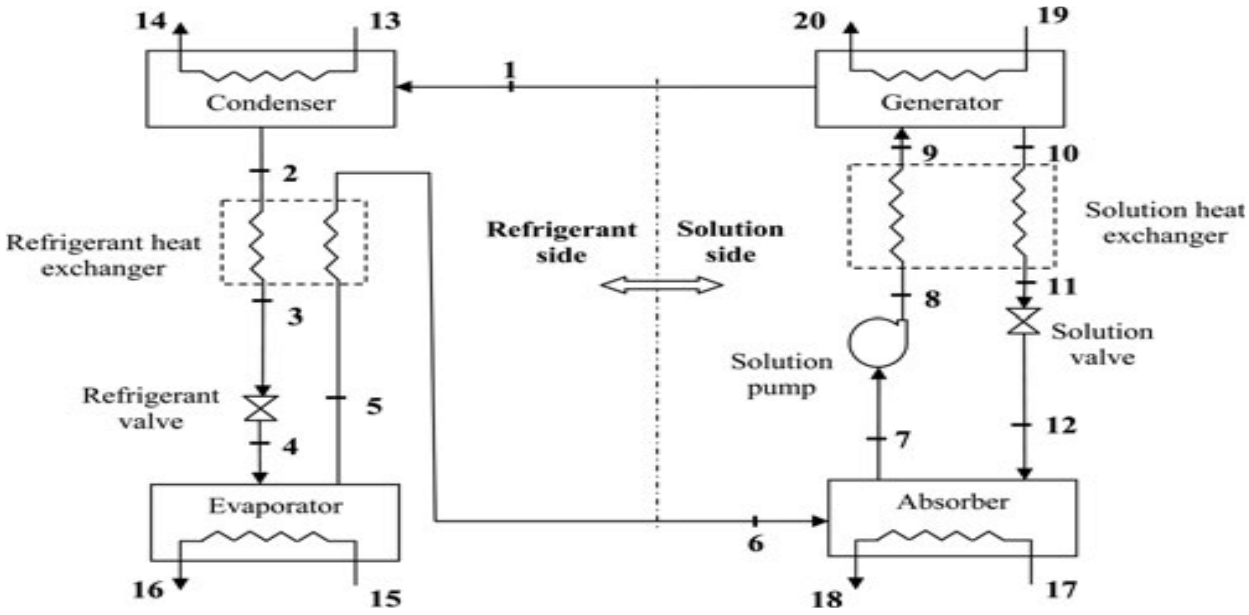

Figure 2-1 Schematic of VARS (Samanta & Basu, 2016).

The benefit of VARS is that it can use many dissipated heat sources, which allows for the customization of a system to best suit the requirements of each vessel. Chiller temperature, heat source temperature and working solution determine performance. NH_3−H_2O systems typically have a COP between 0.5 and 0.6 while H_2O−LiBr system have COP between 0.8 − 0.9. Towards H_2O−LiBr solution, chiller temperatures have to be above 0^oC while in NH_3−H_2O systems chiller temperatures must be suitable for freezing (Guangrong, 2017; Ouadha & El-Gotni, 2013).

Mathapati et al., 2014, performed research on VARS using NH_3−H_2O pair for AC of a car utilizing dissipated heat of same car that was before rejecting into waste in the surrounding. For exhaust gas application, mathematical prototype is created by them. The vehicle's cooling effect is taken into account, and a workable analysis is carried out to compute how much energy is contained in the car's exhaust gas.

2.3. Working Fluid Pairs – Refrigerant-Absorbent and their Practical Problems

The fluid pairings that are cycling in VARS are NH_3−H_2O and H_2O−LiBr. For a variety of reasons, H_2O−LiBr is among the most significant solutions. Not only is water non-explosive, cheap, non-toxic, and has also a good vaporization of latent heat. The application temperatures applied in VARS, where the pressure ranges are sub-atmospheric, are a shortcoming of employing water as a refrigerant. When LiBr is associates with H_2O, a considerable internal temperature gap between heat sources and sinks is controlled, that results to a significant temperature rise. Owing to H_2O in H_2O−LiBr solution is non-volatile and does not react with LiBr. Hence, the pure water vapor exits the generator and the system does not require rectifier or analyzer. However, NH_3−H_2O has a number of substantial advantages over H_2O−LiBr pair. The vapor of ammonia has a strong affinity for water as an absorbent. Aside from the large latent heat quantity of ammonia refrigerant, both elements are also strongly soluble with various working circumstances, and these mixtures are highly fixed as well as fitted with almost all materials (Kurem & Horuz, 2001).

However, both types of pairs have drawbacks. Since, lithium bromide is salt which may get solidified if the solution reaches its precipitation region, carry has to be taken in determining temperature, pressure and concentration. This crystallization leads to seal an operating chamber. This implies that a cooling system that uses LiBr requires amendment regularly during which the cycle must be stopped, which reduces system performance and raises operating expenses. By using greater temperatures and double or triple VARS, the chance of crystallization can be reduced (Salehi et al., 2019). Alongside to the crystallization issue, other shortcomings include extreme viscosity, corrosion, and restricted solubility (Kurem & Horuz, 2001). Salehi et al., 2019 applied H_2O−LiBr to analyze crystallization issue in various kinds of VARS. They discovered that at maximum temperature of absorber, there was a dramatic drop in solution pressure of when exiting

expansion valves, which caused some of the solution to evaporate and enhanced the concentration of the solution. This indicates that crystallization at the entrance of desorber's, close to expansion valve, becomes dangerous. They also demonstrated how crystallization occurs at temperatures higher in the absorber and lower in the condenser. To handle crystallization, ternary fluids have to be applied to enhance solubility or introduce inhibitors (Kamali et al., 2018)

Three common practical challenges in H_2O−LiBr systems are pressure drop, air leakage and crystallization. Relative to cooling water temperature, pressure of condenser must be existed at a specific point to avoid crystallization. This is performed by controlling cold water flow to a condenser (Kumar, 2009).

External air discharges into a system since it works as a vacuum throughout. Thus, an air purifying system is applied practically. Friction should reduce pressure drop owing to extreme specific volume of vapor and moderate working pressures. There are two kinds of commercialized H_2O−LiBr systems: single-stage (effect) as well as multi-stage(effect) systems (Kumar, 2009), Figure 2-2 and Figure 2-3. In commercial systems, twin and single drum combinations are also applied for better performance.

Two working pressures are crucial in single effect systems: condenser−desorber pressure and chiller−absorber pressure. This system can be grouped into twin drum and single drum item. Since chiller and absorber work at similar pressure and could be enclosed in one vessel, like that desorber and condenser could be housed on the other and these two items perform with a unit pressure. Hence, a twin drum contains of two housings working with high and low part of pressures.

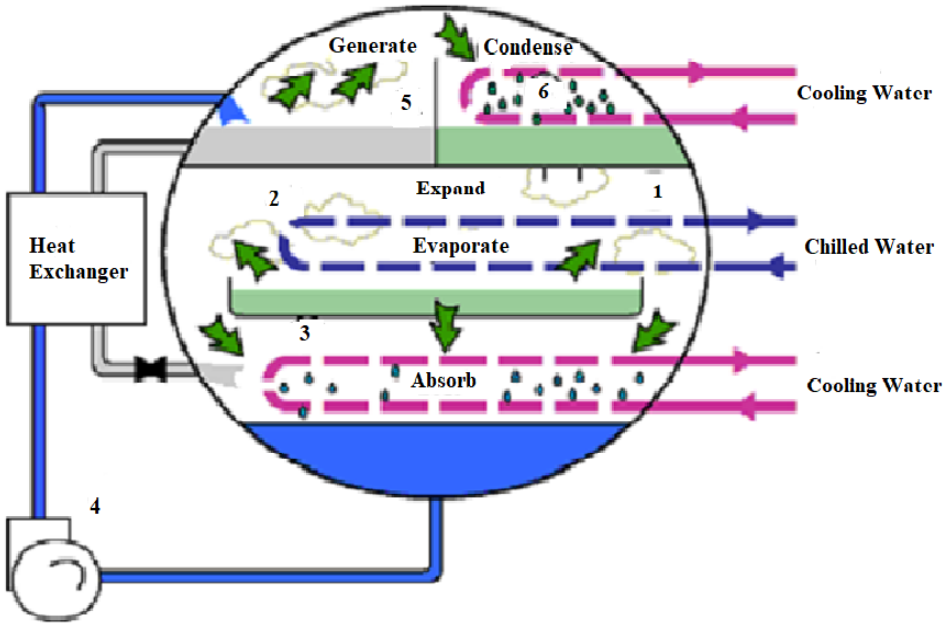

Figure 2-2 Commercialized single drum item, H_2O-LiBr system (Kumar, 2009).

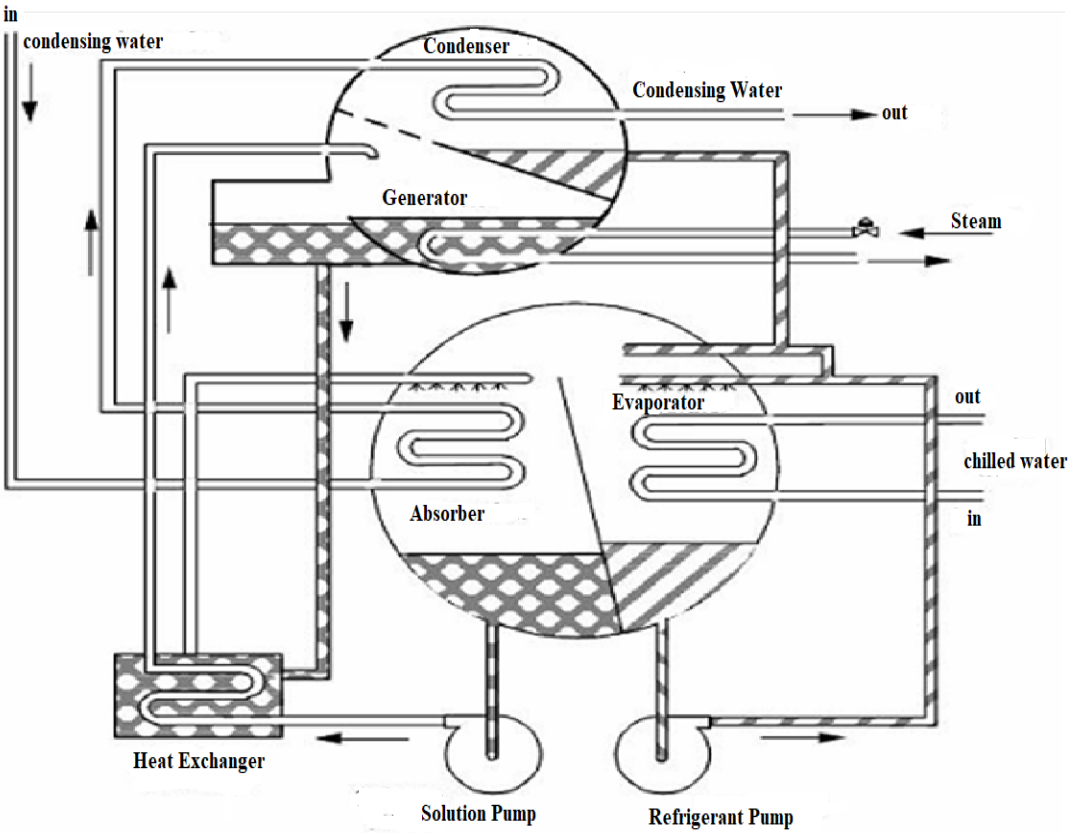

Figure 2-3 Commercialized twin drum item, H_2O-LiBr system (Kumar, 2009).

2.4. Heat Sources for Water-Lithium Bromide Absorption Cooling Systems

When it proceeds to applications of dissipated heat and renewable energy, VARS is crucial. This dissipated heat may exhaust from the engine or industry. Numerous heat sources can be applied to run $H_2O-LiBr$ systems. Systems that have huge potential are mostly run by hot water, steam, or waste exhaust gas. Gas and oil are directly applied to run small-scale potential systems (Kumar, 2009).

In single−effect VARS, an absorber working under 40^oC and a condenser working with 46^oC, therefore a heat source that have 120^oC is needed to give cooled water at 7^oC. In this system, COPs gained fall between 0.6 − 0.8, while for multi−effect VARS, it is between 1.2 − 1.4 (Kumar, 2009).

2.5. Environmental Impacts of Exhaust Gases and Refrigerants used on Board Vessels

In 2012, emissions of international shipping are assumed to be 796 million tonnes CO_2 as well as 816 million tonnes CO_{2e} for Greenhouse gases (GHG) blending CO_2, CH_4 and N_2O. International shipping reports for approximately 2.2% and 2.1% of global CO_2 and GHG emissions on a CO_2 equivalent (CO_{2e}) basis, respectively (IMO et al., 2014). Furthermore, recent researches of vessel emissions reveal that a shipping-associated particulate matter (PM) discharges are responsible for around 60,000 of cardiopulmonary as well as lung cancer deaths/year across the coasts (Convention et al., n.d.).

Besides to these emissions, a refrigerants utilized onboard vessels for AC (air conditioning) as well as cargo cooling duties are additional source of vessel emission. These refrigerants are either ozone−depleting substances, like chlorofluorocarbons (CFCs), or their substituents, like hydro fluorocarbons (HFCs), tetrafluoroethane (R134a), as well as solution of pentafluoroethane, trifluoroethane and tetrafluoroethane (R404a) have considerable global warming potential (EU, 2024). According to recent studies, an average yearly phase-out's of refrigerants from a world fleet makes an AC devices accountable for approximately 69.8% of an overall loss of refrigerants. From this about 30.2% loss is associated with a cooling device. Figure 2-4 indicates AC refrigerant losses contributed by each kind of vessel. From the figure a highest accounts of a refrigerant losses are from general cargo as well as cruise ships (IMO et al., 2014).

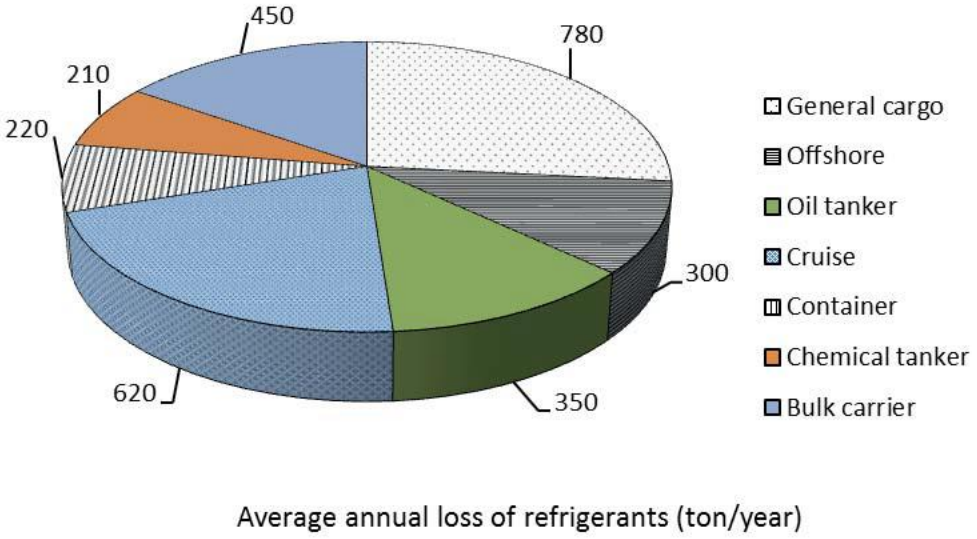

Figure 2-4 Refrigerant losses owing to AC from various kinds of vessel (IMO et al., 2014)

Owing to a continuous rise of discharge from vessels, IMO published a set of regulations concerning this issue in the form of the "International *Convention* for the Prevention of Pollution from Ships (MARPOL)", Annex VI. Regulation 14 restricts SO_X and PM discharges, while Regulation 13 and a design indexes for energy efficiency restrict NO_X and CO_2 discharges, respectively (Seddiek, 2015).

Onboard, ships cooling system commonly uses vapor compression refrigeration systems. These systems are driven by electrical energy and have high COP as well as low purchase price. However, the systems have contribution to greenhouse gas and ozone layer depletion when the system refrigerant is phased out (Riffat & Qiu, 2004). Regulation 12 of the MARPOL convention, Annex VI, issued by IMO, states that: new installations containing ozone-depleting substances are prohibited on all ships from January 2020 (IMO, 2009).

2.5.1 Sulfur influence and dew point temperature of exhaust gas

Petroleum contains broadly of hydrocarbons as well as different values of mixtures of nitrogen, oxygen as well as sulfur. In crude oil, sulfur is a principal excess element next to carbon and hydrogen. Sulfur in petroleum is caustic to materials and have negative effect for catalyst efficiencies. The usual bunker fuels are kindly huge residual ratio of petroleum purifying. Their burning provides substantial rejections of CO, SO_X, NO_X as well as particulate matter (PM). For

restricting rejection of risky pollutants of air, sulfur have to be lessen in the fuels to a very low level. The International Maritime Organization (IMO) has executed a strict rule on sulfur content for marine fuel oils. From January 1, 2020 ahead, sulfur amount in fuels utilized on vessels working outside particular emission control areas (ECA) is not greater than 0.5% (5,000 ppm S). Based on IMO-2020, fuels own a sulfur amount between 1−3.5% is called high sulfur fuel oils (HSFO) while sulfur amount smaller than 1% is low sulfur fuel oils (LSFO). VLSFO means fuel < 0.5% S (Yang et al., 2023).

A substantial factor restricting the utilization of dissipated heat found in exhaust gas is low-temperature corrosion. It is the outcome of the occurrence of SO_X as oxidation results of sulphur presented in the fuel. Sulphur is oxidized to SO_2 and, if there is catalyst, to SO_3. SO_3 consecutively join with water to get sulphuric acid (H_2SO_4). H_2SO_4 is in a gaseous condition at a high temperature, have not any possibility to corrode components that have direct contact. Its condensation takes places when the temperature in the area occupied with exhaust gas drops under the dew point. Subsequently, the acid condensates and directly combines with metal components (Behrendt, 2019). Figure 2-5 illustrates how the sulphur amount in fuel influences exhaust gas dew point.

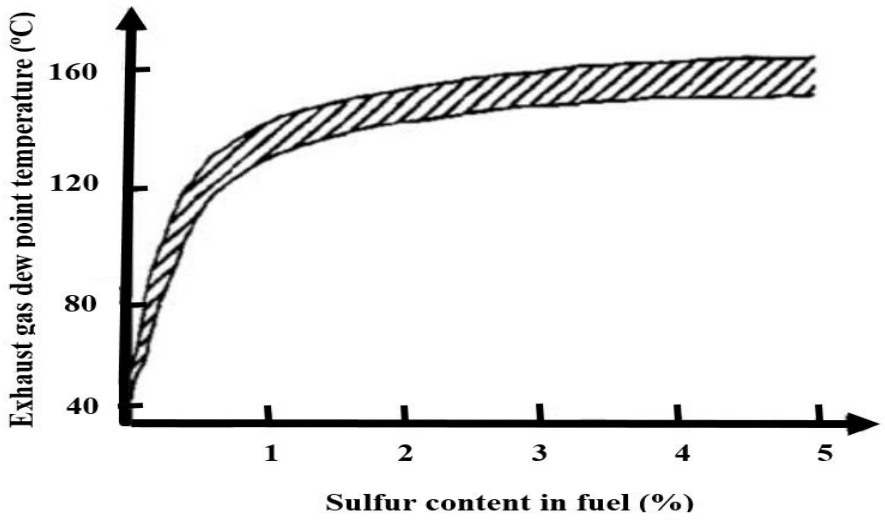

Figure 2-5 Influence of sulphur amount in fuel on dew point temperature of exhaust gas

(Behrendt, 2019).

Dew point is noticed in a shaded space in Figure 2-5 owing to a variable mixtures of SO_X, that is reliant on situations in exhaust gas pipe as well as roles of catalysts. For avoiding this circumstances takes place at the time of burning of fuel carrying above 1% of sulphur, exhaust gas temperature towards the WHRS have not to be under 160°C (Behrendt, 2019).

The working demands for the safe keeping of environment state that the SO_X rejection should be restricted as well as minimized. In confined areas, like Baltic Sea, it is needed to combust fuels with < 0.1% sulphur amounts, optional fuels, like LNG, or it has to be assemble an equipment in exhaust gas pipes that diminishes SO_X in the exhaust gas (Behrendt, 2019).

Taking into account the quantity of heat recovered from exhaust gas, a principal effective solution is utilizing fuels that have low sulphur content or elective fuel owing to the chance to cool exhaust gas to small temperatures between 110−120°C (Behrendt, 2019).

2.6. Advancement of Absorption Mechanism and Arrangement

2.6.1 Working solution pairs

Selecting proper pair of working fluid is a key issue in absorption cycle since COP is greatly affected by fluid thermodynamic characteristics. When taking proper fluid pair to apply in VARS, the following factors must be taken into account (Holmberg & Berntsson, 1990):

- High latent heat of vaporization as well as concentration working fluid in absorbent;
- Thermodynamically good characteristics like viscosity, and thermal conductivity;
- Cost effectiveness, chemical stability, and surrounding-friendliness.

2.6.2 Integrated systems

Different evaluations of VARS have proved that fundamental elements influencing system efficiency are auxiliary components, material qualities, and design of systems. To achieve good performance, auxiliary components as well as supported elements have efficiently affected ordinary single-stage VARS. The following explains how auxiliary components, like distillation columns, flash tanks, ejectors, as well as HX, influence VARS performance.

Heat exchangers for solutions and refrigerants

Solution heat exchanger (SHX), found between absorber and desorber, is a basic subcomponent of an absorption cycle which is applied to efficiently recover of thermal energy of concentrated fluid return back from desorber to absorber. The diluted fluid which leaves absorber is heated by recovered heat before going to generator. Therefore, heat demands in desorber becomes diminished and enhance system COP.

Aphornratana, 1995, performed an tested task and shows that by applying SHX and system COP enhanced considerably by 60%. Sözen, 2001, analyzed an examination about effect of HXs' on the performance of $H_2O{-}NH_3$ VARS. According to his result system efficiency has being significantly affected by applying a SHX. However, utilizing RHX as well as SHX had no considerable influence on COP. In a different paper, Koehler et al., 1988, demonstrate that RHX has a minimum role in an $H_2O{-}$LiBr system while SHX is crucial to optimizing COP.

Karamangil et al., 2010, carried out a task for evaluating the effect of both HXs on the system COP. He observed that SHX had extreme significant influence on COP and increased by 66%. But, there have being a small rise on COP by applying both HXs.

Flash tank

Most multi-pressure systems are attached to the flash tank (FT) in order to enhance its cooling capacity (CC) as well as COP. Sirwan et al., 2013, suggested a novel design on single-stage VARS and in his design a flash tank have being placed between chiller and condenser for rising CC in a chiller, be seen in Figure 2-5. According to the reported results the introduced system which involve FT and ejector, revealed maximum COP but minimum efficiency has been attained by ordinary VARS. In recent years, Abed et al., 2015, investigated ejector-flash tank combination for $NH_3{-}H_2O$ VARS for giving better system's efficiency.

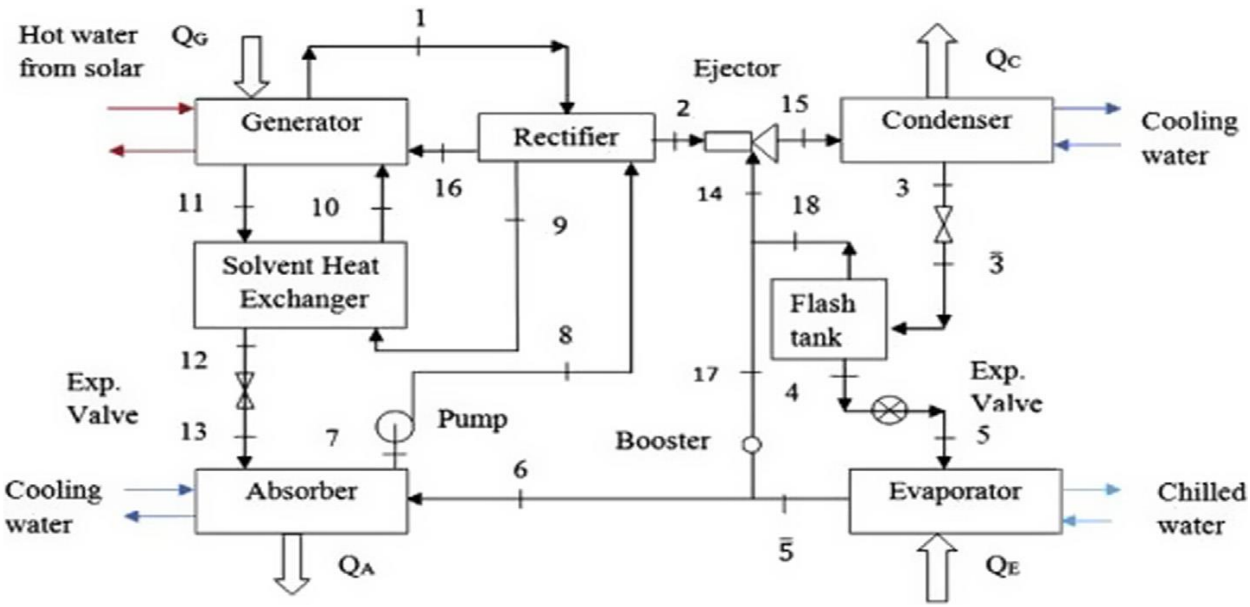

Figure 2- 6 Integrated FT-absorption-ejector VARS (Sirwan et al., 2013a).

Ejector

Ejector is one of the auxiliary components combined into VARS to enhance energy efficiency. By arranging ejector in single-stage VARS, 2−pressure configuration has been changed to a triple-pressure. This leads to diminish desorber temperature and circulation ratio and then system's work at better condenser and absorber temperatures. An ejector-VARS implies a multiple−effect VARS yet with few elements. Due to ordering of ejector in VARS, two groups of triple-pressure combination system are there: (1) ejector placed at an absorber inlet to recover pressure from an absorber as well as enhancing a reaction between fluids found in an absorber. (2) ejector found between desorber and condenser (Aphornratana & Eames, 1998; Farshi et al., 2013; D.-W. Sun et al., 1996).This kind of ejector position is run by the vapor of high-pressure side refrigerant extracting from desorber directing to rise refrigerant vaporization and then resulting better CC of a system.

Sun et al., 1996, revealed a joined H_2O−LiBr ejector VARS. In this arrangement ejector have being found in the middle of condenser and desorber. This cycle has been a proper design for applying dissipated heat. In contrast to the usual single-stage system, a capability of modern joined system has been boosted by 50%.

Bellos & Tzivanidis, 2018, performed evaluation on enhancing of a LiBr−H_2O ejector VARS run using parabolic trough kind of solar collectors. According to their report the joined cycle efficiency has been improved by 60.9% in contrast to ordinary VARS through identical working situations.

2.7. Summary of Literature Review and Research Gap

2.7.1. Summary of literature review

Nowadays, high depletion of fossil fuel reserves has lead different researchers across the globe to give focus and study further on the VARS' performance enhancement. Rankine cycle in power plants, vapour compression system for refrigeration, IC engines of cars utilizes high quality of thermal energy and because of irreversibility created in a cycle, huge quantity of energy is emitted to a surrounding as low quality of energy.

According to the manuscript review, it has been noticed that lot of thermodynamic studies have been performed on different VARS configurations with conventional and alternate working solutions. Thermodynamic analysis is usually carried out from two aspects either by using first law analysis or second law analysis. As far as VARS is concerned, energy analysis mainly deals with evaluation of COP and heat loads in the VARS elements. Often parametric calculation is done to evaluate the impact of components' temperatures as well as other working variables on VARS performance with a help of energy analysis.

Further, the circulating fluid employed in the system has a direct impact on a VARS's efficiency. Specifically, when it considering VARS that utilizes salt mixture, crystallization is a key issue which needs anticipated concentration. Besides, the crystallization behaviors of different salt mixtures are several and consequently, one system that is necessary for a distinct range of circulating situations cannot be important for other working circumstance of temperatures. Extreme concentration of salt in the mixture is crucial for this circumstance.

H_2O−LiBr is a potential working fluid pair that may utilized in VARS for cooling or AC task. In contrast to NH_3−H_2O through similar running situations, several studies shown that H_2O−LiBr based VARS has superior system efficiency based on energy analysis.

System performance improvements can be done by different mechanisms. The first one is by selecting the proper working fluid pair by considering suitable thermodynamic characteristics. Introducing system components and subcomponents such as SHX and RHX for efficient thermal energy recovery, ejector for successful energy utilization, and flash tank for enhancing system performance.

2.7.2. Research Gap

As can be seen, there aren't many research discussing how to improve VARS performance and cooling capability by utilizing mixing chamber, flash tank and LSHX. While some authors simply employ FT, others make use of the ejector and FT. The study conducted by Abed et al., 2015, is the one that demonstrates how applying these three subcomponents can be coupled to improve performance. In fact, even in cases where the engine's waste heat is insufficient, these subcomponents are critical to enhancing system performance particularly in port stay of a vessel if properly utilized.

LSHX is applied to get adequate amount of subcooling and superheating by exchanging heat with a warm circulating fluid from a flash tank with the cool working fluid from a chiller. This helps to enhance cooling capacity (CC) and COP. Flash gas removal also applied to remove flash gas or water vapor at an intermediate pressure before going to evaporator. This flash gas formed during the throttling process and by temperature lift and have to recompress to the condenser unless it increases the pressure drop to the evaporator. This further increases both COP and CC and helps for safe operation of the evaporator. Finally, introduce ejector in the middle of generator and condenser for mixing vapors which comes from FT and generator and also to provide energy effectiveness. However, when the pressure of condenser increases beyond the limit, the mixing situation interferes and the vapor which comes from the flash tank return back to the evaporator and the ejector completely losses its operation (Chunnanond & Aphornratana, 2004). Hence, to overcome this kind of condition the ejector is substituted by vapor mixing chamber in this thesis. Therefore, this modification is a good remedy to fill the research gap. In this thesis heat recovery is made using exhaust gases from marine diesel engine to meet the current request of AC and refrigeration. This can be achieved by modified the ordinary single stage vapour absorption device by adding subcomponent such as FT, LSHX and vapor mixing chamber.

CHAPTER 3: METHODOLOGY

3.1. Engine of Marine Vessel Gambella

The ship is general cargo ship having 166 m long, 27 m width, and has a carrying capacity of 28119 dead weight. The engine type is 6S40ME−B9−TII beside conventional MAN Diesel turbocharger kind TCA as well as fastened pitch propeller. Its data are available from MAN Diesel and Turbo series product manual and ESLSE (ESLSE, 2022).

6S40ME−B9−TII engine type is electronically managed a 2−stroke engines with camshaft for handling exhaust valves. This engine is constructed with 6 cylinders, 40 cm of cylinder bore diameter, 177 cm stroke as well as nominal power yield of 6810 kW at 146 rpm. VLSFO as well as diesel oil are fuel alternatives of an engine (Man, 2018). The quantitative values of engine system performance are listed in Appendix A.

Picture 3-1 Marine Engine system of Marine Vessel Gambella with engine type 6S40ME-B9-TII (Photo Captured by ESLSE Technical officer Bekele Alemu and reprinted with ESLSE permission)

When the engine is on, exhaust gas primarily flows through turbo charger to improve engine efficiency then goes into oil fired boiler to deliver heat for the generation of hot water for various purposes on board and finally leaves the system.

3.2. Exhaust Gas Analysis

The mass of exhaust gas as well as temperature along the service rating are determined by considering the six months' data of the engine rating and exhaust gases properties that are annexed in Appendix A, these data are reported for specific working conditions, Table 3-1. (Man, 2018).

Table 3-1 Engine rating at specific working conditions of T_{air} = 24°C, T_{cw} = 18°C, p_{bar} = 1.015 bar, Δp_m = 300 mm WC(water column)

Engine Rating	Power P, kW	Speed n, rpm
Nominal MCR ($P_{L1,}$ n_{L1})	6810	146
Specified MCR ($P_{M,}$ n_M)	5789	131.4
Matching Point ($P_{O,}$ n_O)	5789	131.4
Service Rating ($P_{S,}$ n_S)	4631	122

Numerical analysis is performed for service rating being 80% of specified MCR (maximum continuous rating) power of an engine. Equations from (3.1) to (3.11) are equations used to determine a correction factor for selection of specified MCR, ambient conditions and engine load.

A) Selected designated MCR point M as well as matching point:

$$P_M = \frac{P_M}{P_{L1}} \times 100\% = 85\% \quad (3.1)$$

$$n_M = \frac{n_M}{n_{L1}} \times 100\% = 90\% \quad (3.2)$$

Change of determined amount of exhaust gas $\Delta m_M\%$ in % amount of L_1 as well as free of P_O

$$\Delta m_M\% = 14\ln\frac{P_M}{P_{L1}} - 24\ln\frac{n_M}{n_{L1}} = 0.25 \quad (3.3)$$

Temperature variation of exhaust gas ΔT_M at point M, given in °C after turbocharger in relation to L_1 as well as acceptable for $P_O = P_M$.

$$\Delta T_M = 15\ln\frac{P_M}{P_{L1}} + 45\ln\frac{n_M}{n_{L1}} = 7.2 \quad (3.4)$$

Additional temperature variation of exhaust gas when matching point O smaller than 100% of M:

$$P_O = 100\%\left(\frac{P_O}{P_M}\right) = 1 \quad (3.5)$$

$$\Delta T_O = -0.3(100 - P_O\%) = 0 \quad (3.6)$$

B) Ambient conditions as well as back-pressure:

$$\Delta M_{amb}\% = 0.03(P_{bar} - 1000) - 0.41(T_{air} - 25) + 0.19(T_{CW} - 25) - 0.011(\Delta P_M - 300) = -0.47\% \quad (3.7)$$

$$\Delta T_{amb} = -0.01(P_{bar} - 1000) + 1.6(T_{air} - 25) + 0.1(T_{CW} - 25) + 0.05(\Delta P_M - 300) = -1.75^oC \quad (3.8)$$

C) Engine load:

Service rating = 80% (MCR power) (3.9)

Variation of mass of exhaust gas, at part load:

$$\Delta m_S\% = 37\left(\frac{P_S}{P_M}\right)^3 - 87\left(\frac{P_S}{P_M}\right)^2 + 31\left(\frac{P_S}{P_M}\right) + 19 = 7.1\% \quad (3.10)$$

Exhaust gas variation of temperature, at part load:

$$\Delta T_S = 280\left(\frac{P_S}{P_M}\right)^2 - 410\left(\frac{P_S}{P_M}\right) + 130 = -18.8^oC \quad (3.11)$$

By using ‘‘List of Capacities’’ from engine design data which is annexed in appendix B and the above computed values of correction factor, mass as well as temperature of exhaust gas is computed as:

M_{L1} = 56400kg/hr

T_{L1} = 265^{o}C

$$M_{exh} = M_{L1} \times \frac{P_M}{P_{L1}} \left\{1 + \frac{\Delta m_{M\%}}{100}\right\} \times \left\{1 + \frac{\Delta M_{amb\%}}{100}\right\} \times \left\{1 + \frac{\Delta m_{S\%}}{100}\right\} \times \frac{P_{S\%}}{100} \quad (3.12)$$

$$T_{exh} = T_{L1} + \Delta T_M + \Delta T_O + \Delta T_{amb} + \Delta T_S \quad (3.13)$$

In equations (3.13), owing to the operation conditions of an engine, the temperature of exhaust gas fluctuates with ±15^{o}C respectively (Man, 2018).

Amount of air utilized for combustion is estimated as 98.2% of computed amount of exhaust gas:

$$M_{air} = 0.982 M_{exh} \quad (3.14)$$

Marine engine system mass balance is needed to analyze the amount of exhaust gas. Therefore, in order to do that use the following assumptions.

a) System is open and steady.

b) T_{∞} = 297K

c) V_{air} < 3m/s

d) Take gases as ideal gas.

e) Consider a ship at 100% load of SMCR.

Mass is conserved in rate form, that is:

$$\sum \dot{m}_{in} = \sum \dot{m}_{out} \quad (3.15)$$

Figure 3-1 shows mass balance in a marine diesel engine.

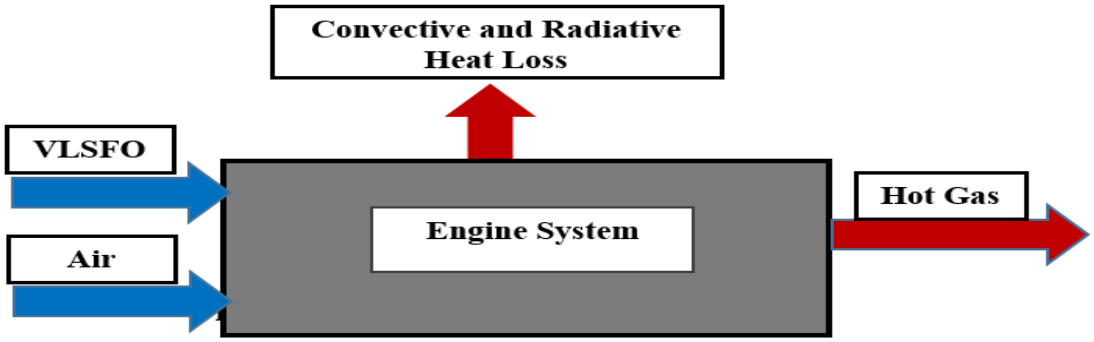

Figure 3-1 Mass balance of the engine system.

3.2.1 Energy potential of exhaust gas

As discussed in section 2.5 in the literature review by taking into account the quantity of heat utilized from exhaust gas, a particular solution is applying fuels that have low sulphur content to cool exhaust gas to small temperatures between 110 − 120°C (Behrendt, 2019). Therefore, in this research, 120^{o}C is taken as the final temperature of an exhaust gas in the analysis based on fuel type (VLSFO) fed to an engine.

Nevertheless, an exhaust gas temperature which is computed in equation (3.13) is already utilized by oil fired boiler to produce hot water for different purposes on board. After production of hot water, exhaust gas temperature is 170 $\pm$ 15^{o}C which is a final temperature released to a surrounding (see Appendix A). This temperature has a good energy potential to generate cooling effect applying single stage VARS until it reaches dew point temperature (110 −120^{o}C).

The exhaust gas boiler thermal power output at full engine load is given by computing exhaust gas temperature level, mass flow and heat capacity. By applying Silva and Costa correlations, an exhaust gas heat capacity is computed as (Arun Bangotra, 2017):

$$C_{P,exh} = (962.097 + 0.1509T_{exh})J/kgK \quad (3.16)$$

The oil fired boiler efficiency is estimated between 0.85 – 0.95. According to Johnson et al., 2015, a boiler efficiency η_B = 0.9 is taken. The generated thermal power by the exhaust gas boiler can be determined as (Behrendt, 2019):

$$Q_B = \eta_B \dot{m}_{exh} C_{P,exh} (T_{B,in} - T_{B,out}) \quad (3.17)$$

Energy potential of an exhaust gas goes to a surrounding is calculated as:

$$Q_g = \dot{m}_{exh} C_{P,exh} (T_{g,in} - T_{g,out}) \quad (3.18)$$

3.3. Thermodynamic Analysis of a Proposed Vapor Absorption System

3.3.1 Operating principle

The key elements of the proposed VARS are an ejector, expansion valves, a desorber, a condenser, a chiller, and an absorber. Additional auxiliary parts consist of the LSHX, SHX, and flash tank. H_2O-LiBr solution serves as the cycle's working fluid.

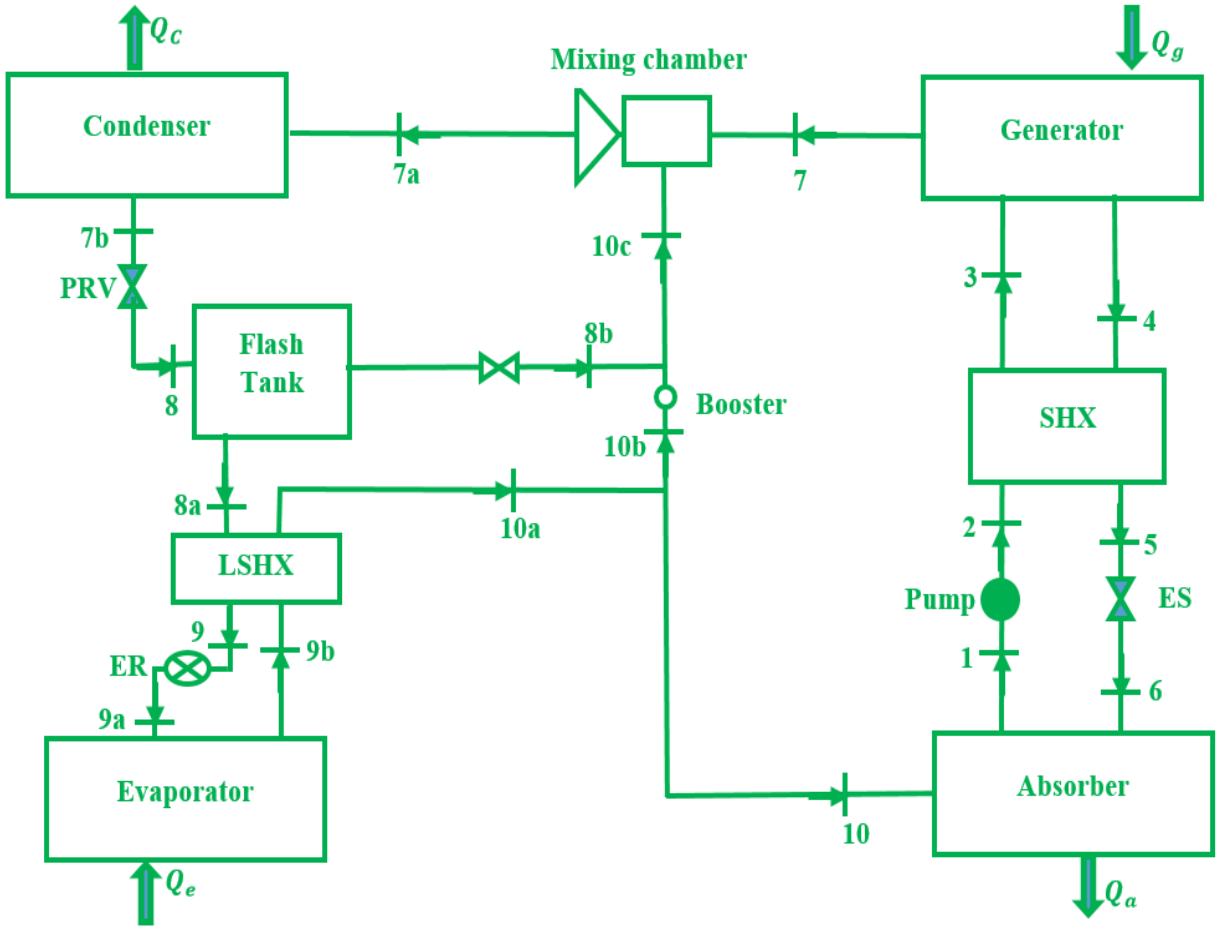

Figure 3-2 A proposed single-stage H_2O-LiBr VARS.

As indicated in Figure 3-2 a weak solution is pressurized by solution pump from absorber (low pressure) to the generator via a SHX. Inside a generator, mixtures of H_2O and LiBr is separated by a high-pressure operating situation. Following its vaporization, the water vapor travels to the mixing chamber (primary pass) combines with water vapor (secondary pass) from (10C) it is a blend of (8b) from a FT and (10b) from a booster. A refrigerant is pressurized isentropically by a booster. In the condenser, the mixture of water vapor condenses. Through a pressure-reducer valve (7b) the pressure of condenser reduces to flash tank pressure and the condensate liquid water is sent to the flash tank, where part of water vapor separated from the liquid. A vaporized water is extracted from a mixing line (10c) by the mixing chamber (secondary pass), while a remaining liquid part flows to LSHX and it becomes subcooled by exchanging heat from vapor which comes from the evaporator at low temperature. The subcooled liquid which comes from LSHX goes to an evaporator via expansion valve where the flash tank pressure reduces to an evaporator pressure and then low−pressure liquid water at an evaporator is prepared to initiate cooling effect. In a cooling cycle, liquid water vaporizes and then a vapor is extracted by a strong solution and creates a weak solution in absorber. Eventually, a SHX allow a high temperature strong mixture to exchange heat with low temperature weak solution and reduces its temperature and goes to solution expansion valve and reduces the generator pressure to an absorber pressure and then strong mixture goes to an absorber, for restarting an absorption process.

3.3.2 Design assumptions

According to an energy potential of exhaust gas to produce refrigeration effect, single stage VARS with adding some subcomponent is designed in this work. The capacity of the exhaust gases has the potential to address the required cooling load of the cabins in the selected vessel safely. To perform system analysis, the following assumptions are used (Palacios-Bereche et al., 2012):

- System elements are in steady situations.
- Pressure drops in system elements are neglected.
- Refrigerant exiting the generator is saturated vapor.
- SHX and LSHX efficiency: $\varepsilon = 0.7$.
- The mixing performance of the mixing chamber; $\omega = 0.6$
- Pump: isentropic.

- Valves operated adiabatically and influence of kinetic energy is ignored.

Operating conditions and system's size for each element are computed depends on the demand of cooling load of the cabins. According to the data collected from the ESLSE that are annexed in appendix C, the total cooling load of a selected ship is 380kW. The following are the selected design parameters for this system (Khalil, 2024):

- Refrigerant temperature and pressure in evaporator: $T_e = 5^oC$, $p_e = 0.872kPa$
- Generator temperature: $T_g = 85^oC$
- Condenser temperature and pressure: $T_c = 40^oC$, $p_c = 7.38kPa$
- Absorber temperature: $T_a = 35^oC$.
- The p−T−χ chart is generated at room temperature (p = 101.325kPa) by considering installing VARSU in the engine room.

Figure 3-3 indicates a p−T−χ system schematic of single effect vapor absorption system and Figure 3-4 indicates a p−T−χ line diagram of a system on Duhring enthalpy chart which indicates the path of H_2O-LiBr with their operating conditions based on the above assumptions.

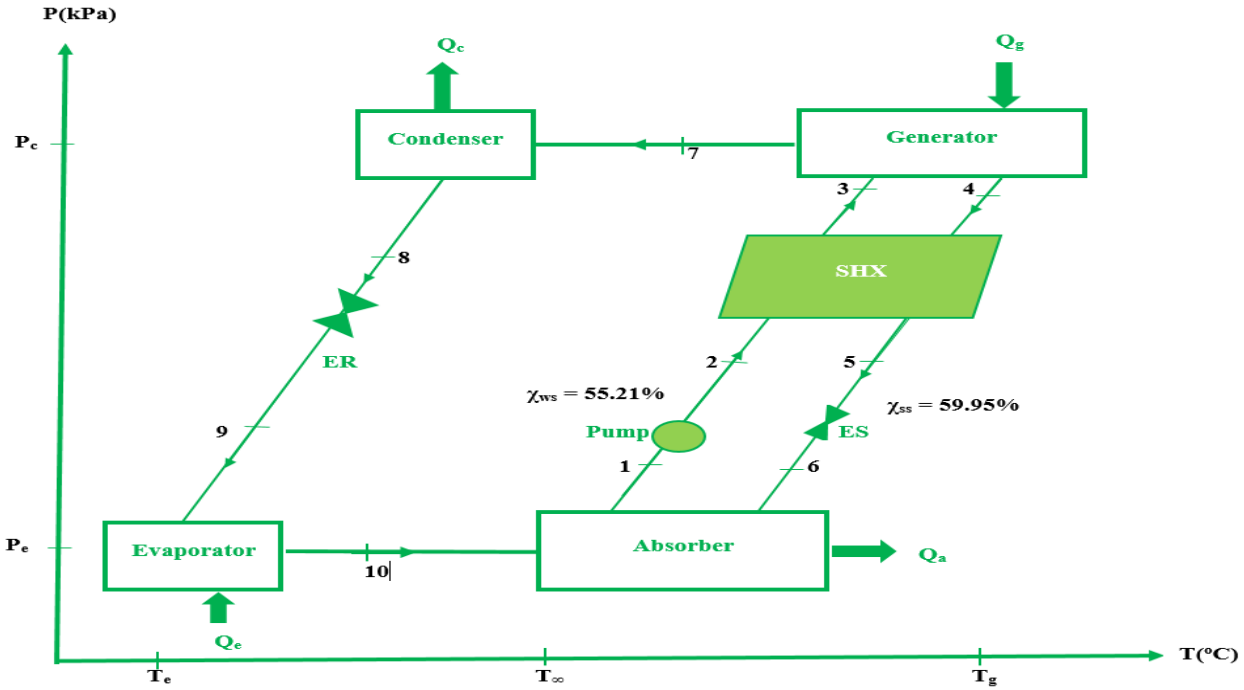

Figure 3-3 Schematic and operation conditions of ordinary single-stage H_2O-LiBr VARS.

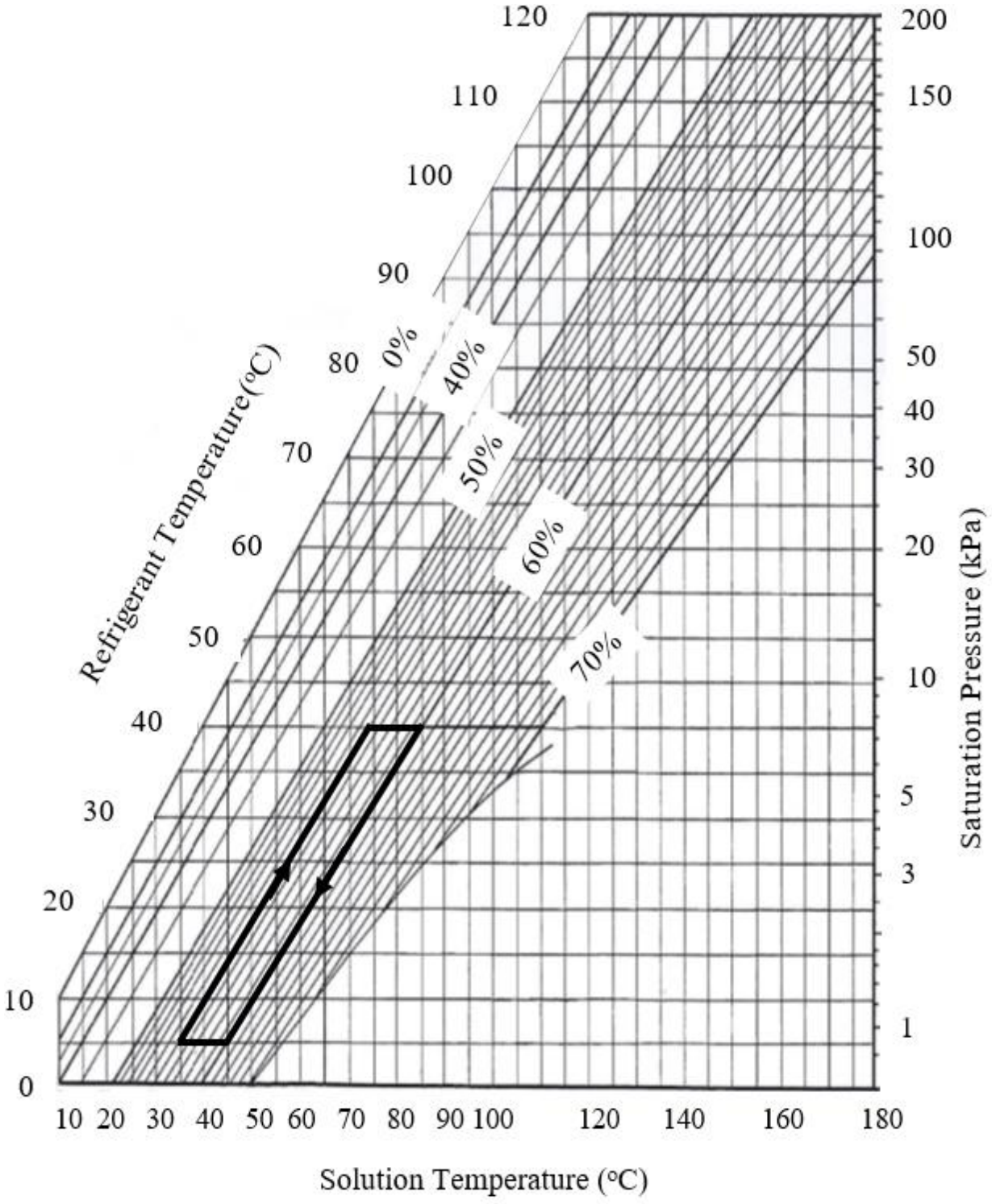

Figure 3-4 P-T-χ representation of single-stage H_2O-LiBr VARS.

In this thesis, the H_2O-LiBr single-stage and the proposed VARS computed by applying first law of thermodynamics and also the system enthalpy at each stream line computed using Excel by applying Duhring enthalpy correlation (equation 3.19).

$$h = \sum_0^4 A_n \chi^n + t \sum_0^4 B_n \chi^n + t^2 \sum_o^4 C_n \chi^n \quad (3.19)$$

Where

h is enthalpy in kJ/kg

t is temperature in ^oC and its range is $15 < t < 165^oC$.

χ is concentration in % LiBr and its range is $40 < \chi < 70\%$ LiBr.

Table 3-2 Constants for Duhring enthalpy correlations of $H_2O-LiBr$

A_n	B_n	C_n
$A_0 = -2024.33$	$B_0 = 18.289$	$C_1 = -3.70088214E2$
$A_1 = 163.309$	$B_1 = -1.1691757$	$C_2 = 2.8877666E-3$
$A_2 = -4.88161$	$B_2 = 3.248041E-2$	$C_3 = -8.1313015E-5$
$A_3 = 6.302948E-2$	$B_3 = -4.034184E-4$	$C_4 = 9.9116628E-7$
$A_4 = -2.913705E-4$	$B_4 = 1.8520569E-6$	$C_5 = -4.4441207E-9$

3.3.3 Refrigeration capacity and performance

Equations (3.19) and (3.20) are applied to compute weak and strong solution concentration (Khalil, 2024).

$$\chi_{ws} = \frac{49.04 + 1.125T_a - T_e}{134.65 + 0.47T_a} \quad (3.20)$$

$$\chi_{ss} = \frac{49.04 + 1.125T_g - T_c}{134.65 + 0.47T_g} \quad (3.21)$$

Then the circulation ratio (λ) and mass of weak solution is then given by:

$$\lambda = \frac{\dot{m}_{ss}}{\dot{m}_r} = \frac{\chi_{ws}}{\chi_{ss} - \chi_{ws}} \quad (3.22)$$

$$\dot{m}_{ws} = \dot{m}_{ss} + \dot{m}_{r} \quad (3.23)$$

Where;

$\dot{m}_{ws}$ = mass of weak solution;

$\dot{m}_{ss}$ = mass of strong solution;

$\dot{m}_{r}$ = mass of refrigerant vapor;

χ_{ws} = concentration of weak solution and

χ_{ss} = concentration of strong solution.

The refrigeration capacity of the designed single-stage VARS is calculated as;

$$Q_e = \dot{m}_r(h_4 - h_3) \quad (3.24)$$

COP of VARS is determined as:

$$COP = \frac{Q_e}{Q_g + W_P} \quad (3.25)$$

3.3.4 Mass and energy balance analysis

This analysis is used to determine a heat transfer rate (Q) for each system element and the overall system performance (COP). Each element has been taken as a control volume with entrance as well as exit streams. Mass and energy equations in each elements of a system are given and a cycle can be evaluated as follows:

Absorber

$$\dot{m}_1 = \dot{m}_6 + \dot{m}_{10} \quad (3.26)$$

$$\dot{m}_1 h_1 = \dot{m}_6 h_6 + \dot{m}_{10} h_{10} - Q_a \quad (3.27)$$

Where

$\dot{m}_1 = \dot{m}_{ws}$; $\dot{m}_6 = \dot{m}_{ss}$ and $\dot{m}_{10} = \dot{m}_r$

h_1 = h at T_a and χ_{ws}; $h_6 = h_5$; h_{10} = h at T_{10a} and $p_1 = p_6 = p_a = p_e = p_{sat}$ at T_e

Pump

$$p_1 = p_e \text{ and } p_2 = p_c \quad (3.28)$$

$$\dot{m}_1 = \dot{m}_2 \quad (3.29)$$

$$h_1 = h_2 \quad (3.30)$$

Where

$p_c = p_{sat}$ at T_c

Solution heat exchanger

$$\dot{m}_2 h_2 + \dot{m}_4 h_4 = \dot{m}_3 h_3 + \dot{m}_5 h_5 \quad (3.31)$$

Where

$\dot{m}_2 = \dot{m}_3 = \dot{m}_{ws}$;

$\dot{m}_4 = \dot{m}_5 = \dot{m}_{ss}$;

$h_4 = h$ at T_g and χ_{ss}; $p_2 = p_4 = p_3 = p_5 = p_c$ and

h_5 is computed from the above equation (3.31) and h_3 is determined from the equation (3.32) below;

$$\varepsilon_{SHX} = \frac{h_3 - h_2}{h_4 - h_2} \quad (3.32)$$

Generator

$$\dot{m}_3 = \dot{m}_4 + \dot{m}_7 \quad (3.33)$$

$$\dot{m}_3 h_3 = \dot{m}_4 h_4 + \dot{m}_7 h_7 + Q_g \quad (3.34)$$

Where

$\dot{m}_7 = \dot{m}_{ws}$; $\dot{m}_4 = \dot{m}_{ss}$ and $\dot{m}_7 = \dot{m}_r$

$h_7 = h_v$ at T_g and $p_3 = p_4 = p_5 = p_g = p_c$

Solution expansion valve

$$\dot{m}_5 = \dot{m}_6 \quad (3.35)$$

$$h_5 = h_6 \quad (3.36)$$

Where

$\dot{m}_5 = \dot{m}_6 = \dot{m}_{ss}$

Mixing Chamber

$$\dot{m}_{7a} = \dot{m}_{10c} + \dot{m}_7 \quad (3.37)$$

$$\dot{m}_{7a}h_{7a} = \dot{m}_{10c}h_{10c} + \dot{m}_7h_7 \quad (3.38)$$

Entrainment ratio (ω):is the performance of the mixing chamber and is computed as (Abed et al., 2015):

$$\omega = \frac{\dot{m}_{10c}}{\dot{m}_7} \quad (3.39)$$

$$\dot{m}_{7a} = (1 + \omega)\dot{m}_7 \quad (3.40)$$

$$h_{7a} = \frac{h_7 + \omega(h_{10c})}{1+\omega} \quad (3.41)$$

$$\dot{m}_{10c}h_{10c} = \dot{m}_{8b}h_{8b} = \dot{m}_{10b}h_{10b} \quad (3.42)$$

$$\dot{m}_{10c} = \dot{m}_{8b} + \dot{m}_{10b} \quad (3.43)$$

$$\dot{m}_{10b} = \dot{m}_{10a} - \dot{m}_{10} \quad (3.44)$$

Where

$\dot{m}_7 = \dot{m}_{10} = \dot{m}_r$

$\dot{m}_{10a} = \dot{m}_{8a}$; $p_7 = p_{7a} = p_{10c} = p_c$

From steam table: $h_7 = h_v$ at T_7, $T_7 = T_g$; $h_{8b} = h_v$ at T_{ft}; $h_{10b} = h_{10a} = h_{10}$; h_{10c} is determined above from equation (3.42).

Condenser

$$\dot{m}_{7a} = \dot{m}_{7b} \quad (3.45)$$

$$\dot{m}_{7a}h_{7a} = \dot{m}_{7b}h_{7b} + Q_C \quad (3.46)$$

Where

From steam table: $h_{7b} = h_f$ at T_{7b}; $T_{7b} = T_c$; $p_{7a} = p_{7b} = p_8 = p_c$

Pressure-reducer valve

$$\dot{m}_8 = \dot{m}_{7b} \quad (3.47)$$

$$h_8 = h_{7b} \quad (3.48)$$

Where

From steam table: $T_8 = T_{ft}$ and $p_8 = p_{ft}$ which is determined below from equation (3.51)

Flash tank

$$\dot{m}_8 = \dot{m}_{8a} + \dot{m}_{8b} \quad (3.49)$$

$$\dot{m}_8 h_8 = \dot{m}_{8a} h_{8a} + \dot{m}_{8b} h_{8b} \quad (3.50)$$

An intermediate pressure for flash tank is determined as (Abed et al., 2015):

$$P_{ft} = \sqrt{P_e P_c} \quad (3.51)$$

Where

$\dot{m}_8 = \dot{m}_{7b} = \dot{m}_{7a}$

$T_8 = T_{8a} = T_{8b} = T_{ft}$; $T_{ft} = T_{sat}$ at P_{ft}

From steam table: $h_8 = h_f$ at T_c; $h_{8a} = h_f$ at T_8; $h_{8b} = h_v$ at T_8

Hence, the unknown parameter $\dot{m}_{8b}$ is determined from equation (3.52) and is given as:

$$\dot{m}_{8b} = \frac{\dot{m}_{8a}(h_8 - h_{8a})}{h_{8b} - h_{8a}} \quad (3.52)$$

Liquid suction heat exchanger

$$\dot{m}_{8a} = \dot{m}_9 = \dot{m}_{9b} = \dot{m}_{10a} \quad (3.53)$$

$$\dot{m}_{8a} h_{8a} + \dot{m}_{9b} h_{9b} = \dot{m}_9 h_9 + \dot{m}_{10a} h_{10a} \quad (3.54)$$

The effectiveness of LSHX is given as:

$$\varepsilon_{LSHX} = \frac{T_9 - T_{8a}}{T_{9b} - T_{8a}} \quad (3.55)$$

Where

From steam table: $h_9 = h_f$ at T_9; $h_{8a} = h_f$ at T_8; $h_{9b} = h_v$ at T_{9b}; $p_{8a} = p_9 = p_{ft}$

and h_{10a} is determined from the above equation (3.54)

Refrigerant expansion valve

$$\dot{m}_9 = \dot{m}_{9a} \quad (3.56)$$

$$h_9 = h_{9a} \quad (3.57)$$

Where

$\dot{m}_9 = \dot{m}_{8a}$

$p_9 = p_{ft}$ and $p_{9a} = p_e$

Evaporator

$$\dot{m}_{9a} = \dot{m}_{9b} \quad (3.58)$$

$$\dot{m}_{9b}h_{9b} = \dot{m}_{9a}h_{9a} + Q_e \quad (3.59)$$

Where

$\dot{m}_{9a} = \dot{m}_{8a}$

From steam table: $h_{9a} = h_f$ at T_9; $h_{9b} = h_v$ at $T_{9a} = T_{9b}$ and $p_{9a} = p_{9b} = p_e$

3.4. Environmental and Economic Analysis of Vapor Absorption Refrigeration System

The emissions from auxiliary engine is determined as (Browning et al., 2009):

$$E = P \times LF \times A \times EF \quad (3.60)$$

Where

E is emissions in grams

P is MCR power in kW

LF is load factor (0.17)

A is activity in hrs

EF is emission factor for different pollutants in g/kWh

Annual emission reduction (ER_{VARSU}) at the time of sailing after applying VARS unit (VARSU) can be computed as:

$$ER_{VARSU} = P_E T_s F_e \quad (3.61)$$

Where

P_E is an electric power saved in kW at sailing,

T_s is annual sailing hours per year, and

F_e is an engine emission factor in g/kWh.

Annual cost-effectiveness is a cost which is to payed for IMO as a penalty due to the emission of different pollutants from the vessels. VARSU is a measure of emission decrement. Annual cost-

effectiveness for emission after using VARSU on a vessel (ACE_{VARSU}) relative to the decrement of each kind of pollutant emissions can be computed as: (Epa et al., 2016)

$$ACE_{VARSU} = \frac{C_{ti}}{ER_{VARSU}} \quad (3.62)$$

Where, C_{ti} is overall yearly cost of VARSU which involves capital, maintenance as well as operating costs in ($/year) and is determined as:

$$C_{ti} = AMR + C_{ins} + C_{m\&o} + C_{HE} \quad (3.63)$$

Where

AMR is yearly initial money recovery

C_{ins} is installation cost

$C_{m\&o}$ is yearly maintenance and operating cost

C_{HE} is heat exchanger cost

When applying VARSU, AMR is defined as in terms of unit cost (UC), an anticipated life time of a vessel after implementing VARSU (n), as well as the rate of interest (i) and is given by:

$$AMR = UC \times \frac{i(1+i)^n}{(1+i)^n - 1} \quad (3.64)$$

Fuel saving (m_{fs}) after VARSU at the time of cruising depends on generator specific fuel utilization (b_{eg}) in g/kWh, the saved electrical energy during sailing (P_E) in kW, and the number of cruising hours per year (T_s) and hence, m_{fs} is given by:

$$m_{fs} = b_{eg} P_e T_s \quad (3.60)$$

A fuel saving cost (C_{fs}) is determined in terms of the mass of fuel saved, fuel prices (C_f in $/ton), and fuel price change per year(PI) and is computed as:

$$C_{fs} = m_{fs} C_f (1 \pm PI)^n \quad (3.61)$$

The payback period is the time throughout that a project will pay to the financier the capital funded in the project by that financier and is computed as (Oyelakun et al., 2025):

$$\text{Payback Period} = \frac{\text{Initial investment}}{\text{Annual net cash flow}} \tag{3.62}$$

Climate metrics such as Global Warming Potential (GWP) and Carbon dioxide equivalent (CO_2e) applied for contrasting emissions of pollutants owing to their effect on the global climate. CO_2e is the value of CO_2 that have similar climate effect over a specified time horizon. The time horizon decides GWP values since it is a measure of waiting time of a gas in the atmosphere. There are 2 time horizons 20 and 100 years' time horizon (Report & Horizon, 2021).

To determine CO_2e of emission of pollutants from ship, in this research well to walk approach (WTW) is applied since this approach considers the overall processes from the supply chain of fuel pathways to all GHG intensity of the final fuel utilized on board a ship. This approach mostly analyzed pollutants that have well known GWP such as CO_2, CH_4, N_2O and BC (black carbon) (Comer & Osipova, 2021).

A ship's CO_2e_{WTW} (in g CO_2e) is computed in terms of the mass of fuel the ship consumed (FC in g) as well as a well-to-wake carbon dioxide equivalent factor (CEF_{WTW} in g CO_2e/g fuel) for that fuel (Comer & Osipova, 2021).

$$CO_2e_{WTW} = FC(CEF_{WTW}) \tag{3.63}$$

CEF_{WTW} is computed based on well to tank (WTT) emissions related with extracting, processing as well as transporting a fuel as well as tank to well (TTW) emissions related with utilizing fuel on board the ship (Comer & Osipova, 2021).

$$CEF_{WTW} = CEF_{WTT} + CEF_{TTW} \tag{3.64}$$

Where:

CEF_{WTT} = well-to-tank CO_2e factor, in gCO_2e/g fuel

CEF_{TTW} = tank-to-wake CO_2e factor, in gCO_2e/g fuel

CEF_{WTT} is computed by considering each climate pollutant emission factors (EF_{WTTp}) as well as related 100-year or 20-year GWP for each pollutant (GWP_p). The CEF_{TTW} is computed in a similar way:

$$CEF_{WTT} = \sum(EF_{WTTP} \times GWP_P) \quad (3.65)$$

$$CEF_{TTW} = \sum(EF_{TTWP} \times GWP_P) \quad (3.66)$$

Where:

CEF_{WTT} = well-to-tank CO_2e factor, in gCO_2e/g fuel

CEF_{TTW} = tank-to-well CO_2e factor, in gCO_2e/g fuel

EF_{WTTp} = well-to-tank pollutant emission factor p, in g/g fuel

EF_{TTWp} = tank-to-well pollutant emission factor p, in g/g fuel

GWPp = 100-year or 20-year GWP of pollutant p,

The fluids used for cooling systems are gases with GWP that can be 2,000 - 15,000 times greater than CO_2. By considering GHG with their addition, yearly GHG emissions attributable for the utilization of cooling system equipment can be computed as (Environnement et al., 2025):

$$E_{GHG,cooling} = \frac{[(Q_n \times k)+(C \times X \times A)+(Q_n \times Y \times (1-Z))]}{100} \times GWP_i \times 0.001 \quad (3.67)$$

Where:

$E_{GHG,cooling}$ = emissions of GHG attributable for cooling equipment, in tons of CO_2e/year

Q_n = refrigerant amount introduced to new device, in kg

GWP_i = GWP of refrigerant i

0.001 = conversion factor from kg to tons

k = initial emissions (%)

C = overall potential of equipment, in kW

X = yearly operating emissions (%)

A = operating years

Y = remaining initial load (%)

Z = efficiency of recovery (%)

CHAPTER 4: RESULT AND DISCUSSIONS

4.1. Exhaust Gas Analysis

Based on the analysis of exhaust gas which is stated in section 3.2, the computed results are shown in Table 4-1 for equations (3.12) – (3.18).

Table 4-1 Results for different parameters of exhaust gas

Parameters	Results	References
M_{exh} (kg/s)	13.29	(Man, 2018)
T_{exh} (^oC)	258 ± 15	(Man, 2018)
M_{air} (kg/s)	13.05	(Man, 2018)
VLSFO (kg/s)	0.24	(Man, 2018)
$C_{p,exh@T=120^oC}$ (kJ/kgK)	1.021	(Arun Bangotra, 2017)
$T_{B,in}$ (^oC)	258 ± 15	(see Appendix A)
$T_{B,out}$ (^oC)	170 ± 15	(see Appendix A)
$T_{g,in}$ (^oC)	170 ± 15	(see Appendix A)
$T_{g,out}$ (^oC)	120	(Behrendt, 2019)
Q_B (kW)	1096.78 ± 130.41	(Behrendt, 2019)
Q_g (kW)	725.63 ± 217.16	(Behrendt, 2019)

An exhaust gas mass flow rate and temperature leaving a marine engine is $\dot{m}_{ex,gas}$ = 13.29 kg/s and $T_{ex,gas}$ = 258 ± 15^{o}C respectively. This huge amount of energy has been utilized to produce hot water for cooking and for other accommodation purpose on board. Based on Behrendt, 2019, energy potential analysis, the boiler recovered about 1MW of energy from exhaust gas and then the exhaust gas leaving the boiler with 170 ± 15^{o}C to the atmosphere. Hence, in this thesis by considering the sulfur content and dew point temperature, this huge amount of energy potential can be recovered again for cooling production using VARS until it reaches dew point. Based on the analysis, the exhaust gas supplied appreciable amount of energy (725.63 ± 217.16kW) to the generator for producing enough amount of cooling effect in VARS.

4.2. VARS Analysis

In this section the values of different thermodynamic parameters which is equated in equations from (3.19) − (3.59) to find the performance in both proposed and ordinary cycles that are stated in section 3.3 are tabulated in table 4-2 and 4-3. Sample calculations can be shown in Appendix D. As explained in section 4.1, the values of exhaust gas temperature are fluctuated between 170 ± 15^{o}C. Therefore, the values which is tabulated under table 4-2 and 4-3 is by considering $\dot{m}_{ex}$ = 13.29 kg/s, T_{exh} = 155^{o}C, T_c = 40^{o}C, T_e = 5^{o}C, T_a = 35^{o}C and T_g = 85^{o}C and Figure 4-1 shows the path of refrigerant and H_2O−LiBr mixture with their operating conditions and system component on P−T−χ line diagram for the proposed system.

Table 4-2 Thermodynamic values for each stream lines of ordinary cycle.

Stream	p(kPa)	T(^{o}C)	$\dot{m}_r$ (kg/s)	χ(%)	Quality	h(kJ/kg)
1	0.872	35	2.150	55.21	−	84.06
2	7.38	35	2.150	55.21	−	84.06
3	7.38	75.11	2.150	55.21	−	166.85
4	7.38	85	1.980	59.95	−	202.33
5	7.38	44.32	1.980	59.95	−	112.43
6	0.872	44.32	2.150	59.95	−	112.43
7	7.38	85	0.170	−	1	2651.9
8	7.38	40	0.170	−	0	167.57
9	0.872	5	0.170	−	0.059	167.57
10	0.872	5	0.170	−	1	2510.6

Table 4-3 Thermodynamic values for each stream lines of auxiliary components of the proposed cycle.

Stream	p(kPa)	T(^{o}C)	$\dot{m}_r$(kg/s)	χ(%)	Quality	h(kj/kg)
7	7.384	85	0.170	−	1	2651.9
7a	7.384	63.79	0.272	−	1	2616.30
7b	7.384	40	0.272	−	0	167.57
8	2.538	40	0.272	−	0	167.57
8a	2.538	21.32	0.264	−	−	89.33

8b	2.538	21.32	0.008	−	1	2540.47
9	2.538	9.89	0.264	−	0	41.55
9a	0.872	5	0.264	−	−	41.55
9b	0.872	5	0.264	−	1	2510.60
10	0.872	31.16	0.170	−	1	2558.38
10a	0.872	31.16	0.264	−	1	2558.38
10b	0.872	31.16	0.094	−	1	2558.38
10c	2.538	30.21	0.102	−	1	2557.00

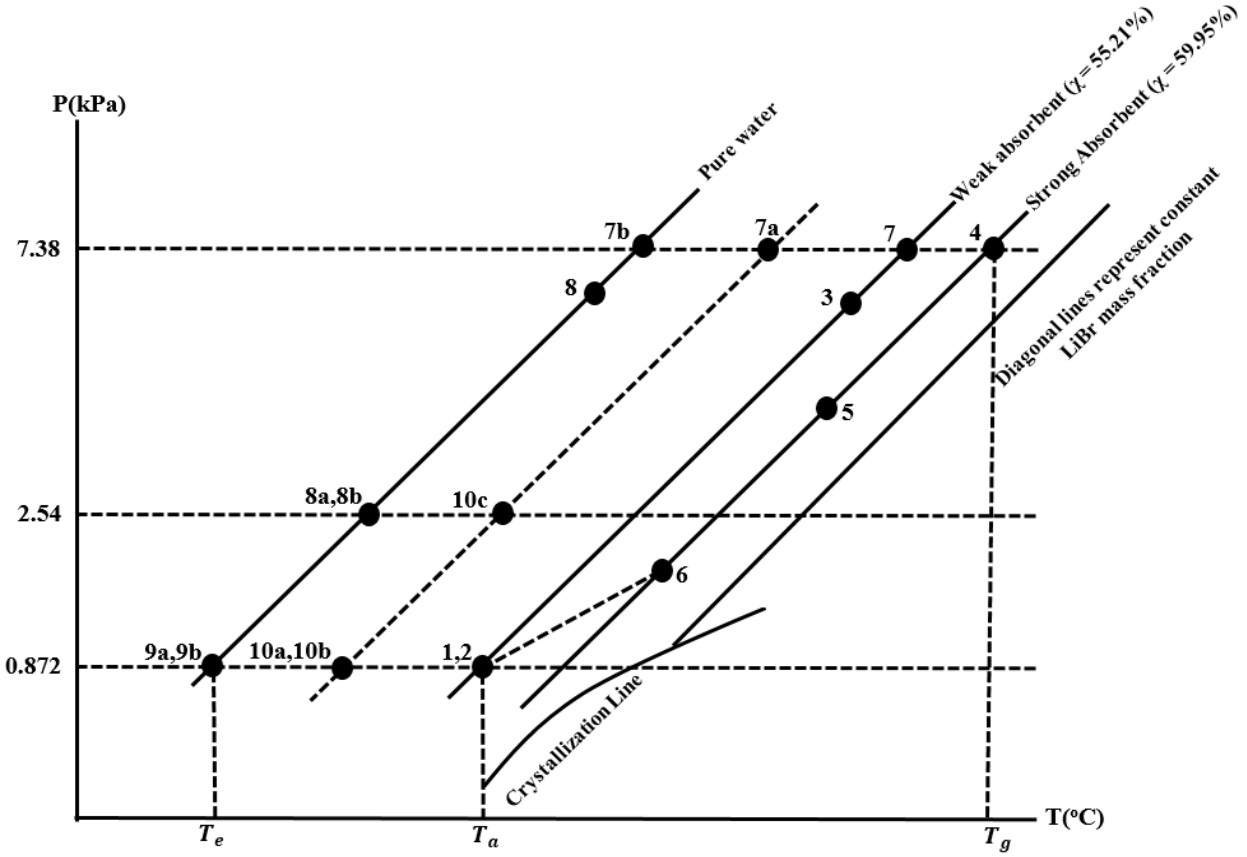

Figure 4-1 P−T−χ line diagram of the proposed system.

Owing to hot exhaust gas variation which is supplied to the generator, the heat transfer rate (Q) for each system component and system performance also varied in proposed and ordinary cycle. The cooling effect (Q_e) and system performance varies between 398.32 kW – 726.34 kW and 0.782 – 0.770 respectively in the ordinary system, 625.07 − 1149.54 and 1.228 – 1.219 in the combined system suggested by (Sirwan et al., 2013) while in the proposed system varies between 644.41kW – 1185.13 kW and 1.266 – 1.257 respectively within variation of heat source supply temperature of 170 ± 15°C. These amount of cooling effect production addresses the required amount of cooling

effect in the case study ship of marine vessel Gambella on all of the above stated cycles, since the cooling demand on board is 380 kW. Therefore, the remaining cooling effect can be utilized for preserving foods (like, milk products) at 5^{o}C in the catering compartment. In this case, applying VARS in these three systems increases a marine diesel engine overall efficiency of a case study ship by 2.9 – 5.3% for ordinary system, 4.6 – 8.4% for combined system and 4.7 – 8.7% for proposed system.

Simulation results are shown in this chapter in section 4.3 for the performance of the marine engine exhaust gas driven VARS using Excel. The influence of temperature variation of inlet exhaust gas which is supplied to generator for heating water lithium bromide solution is shown in Figure 4-2.

4.3. Temperature Variation Effect on the Ordinary and Proposed cycle

4.3.1 Exhaust gas temperature variation effect

Exhaust gas temperature variation effect on a heat transfer rate for each system component and system COP for both ordinary and proposed cycle is shown in Figure 4-2, 4-3 and 4-4.

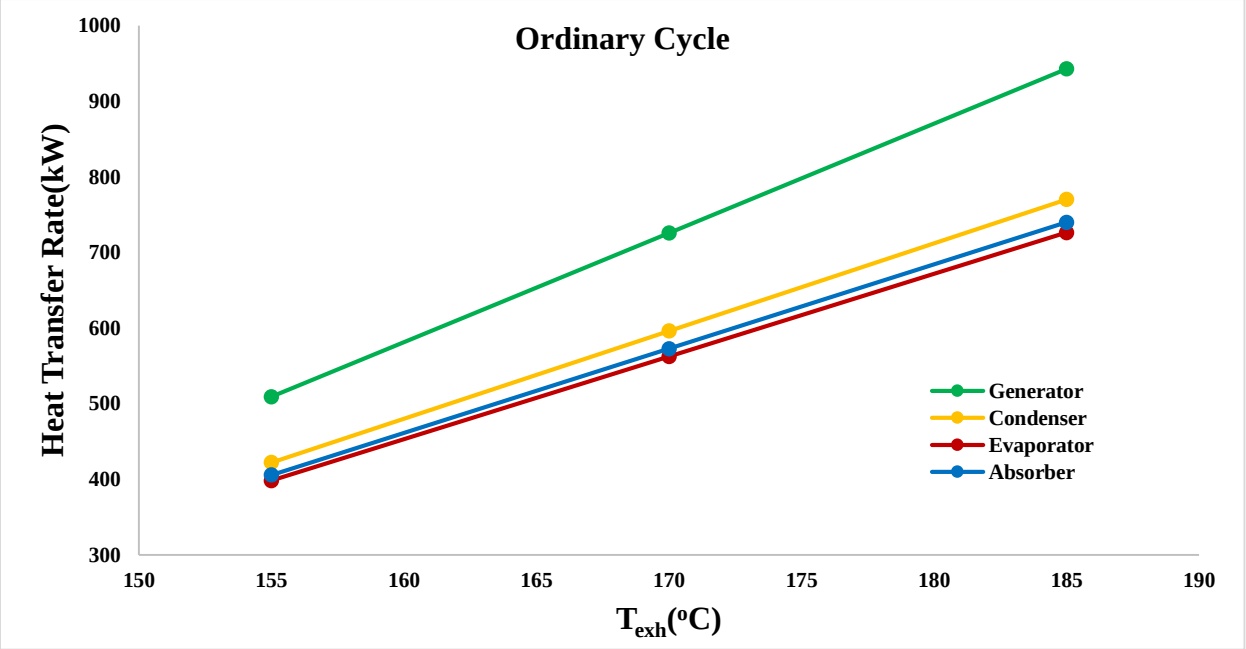

Figure 4-2 Exhaust gas temperature effect on a heat transfer rate for each component of ordinary cycle.

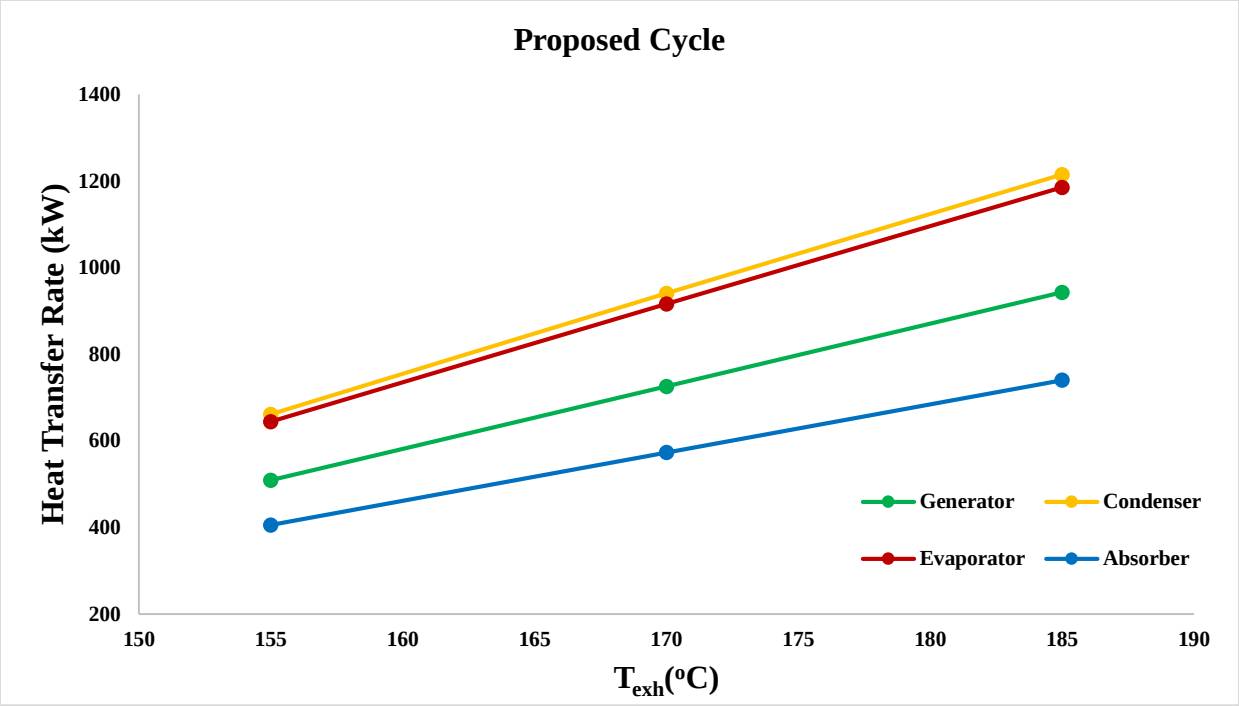

Figure 4-3 Exhaust gas temperature effect on a heat transfer rate for each component of proposed cycle.

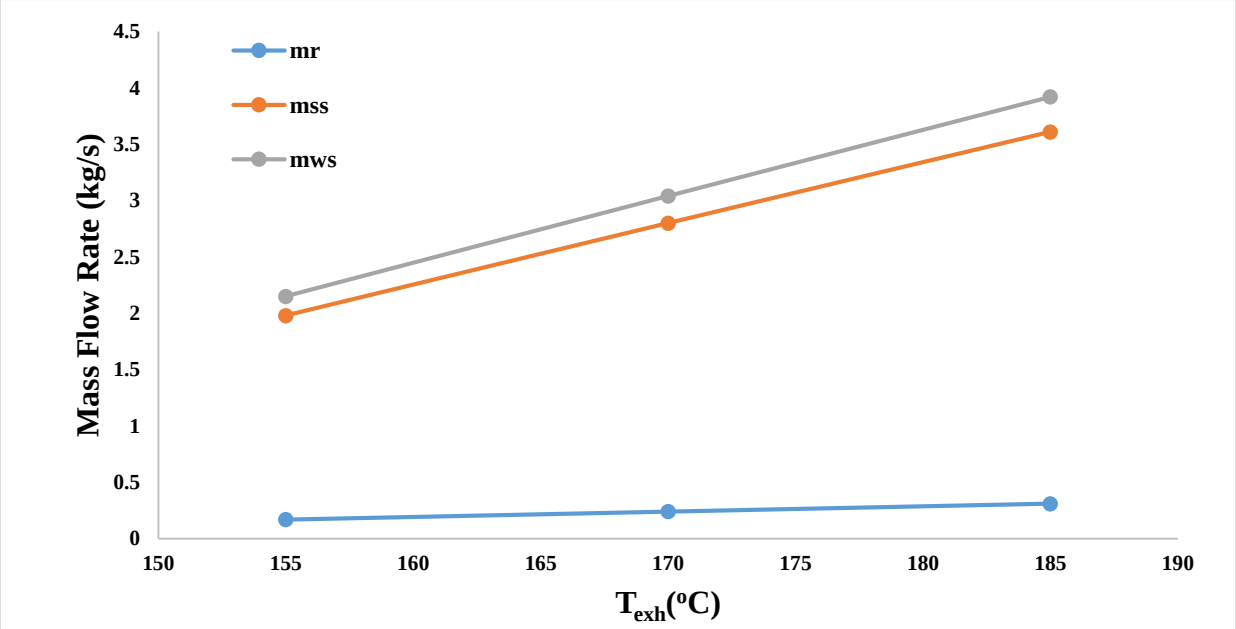

Figure 4-4 Effect of exhaust gas temperature on desorbed ṁr, ṁss and ṁws.

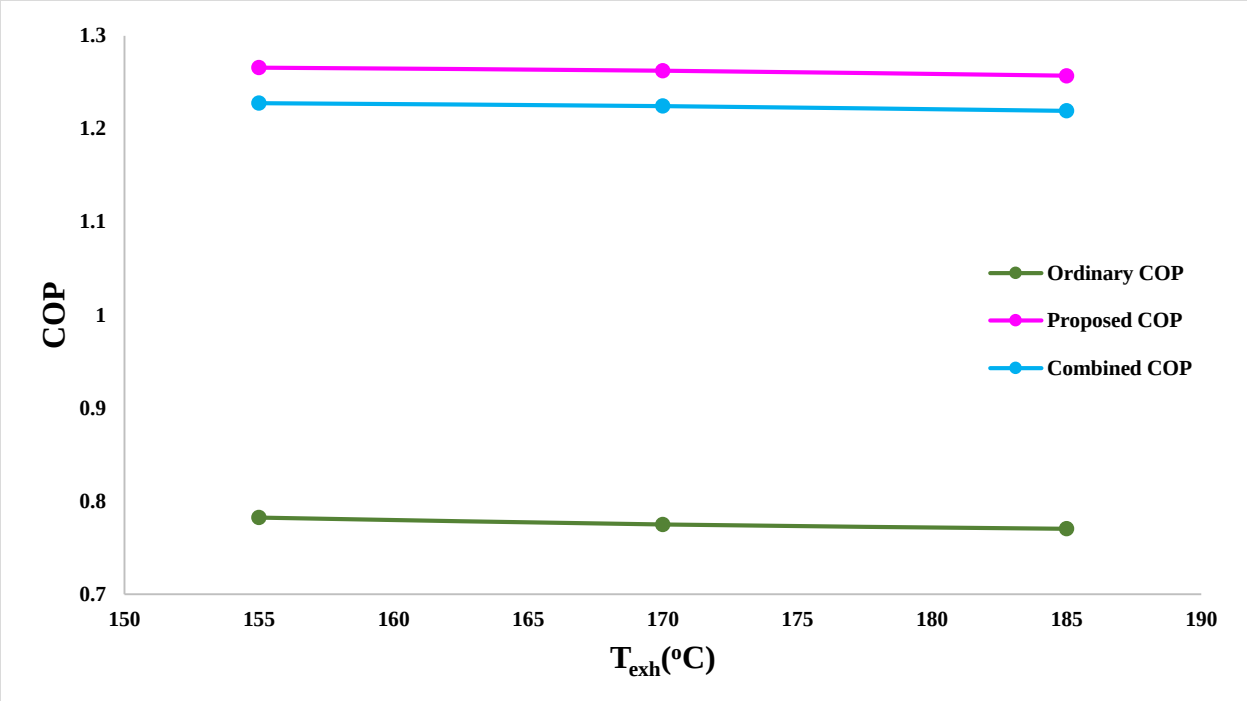

Figure 4-5 Comparison of COP between a proposed, combined and an ordinary cycle.

As indicated in the above Figure 4-2 and 4-3, a heat transfer rate of an ordinary and a proposed cycle starts increasing considerably until the exhaust gas temperature reaches 185^{o}C. The figure shows linear increment in a heat transfer rate in all system components when varying the inlet exhaust gas temperature.

In this design the heat input source for generator(Q_g) and an absorber heat transfer rate (Q_a) is the same in all the above stated cycle. When an exhaust gas temperature rises linearly, a desorbed mass flow of refrigerant rises slightly. However, a weak as well as strong solution of water lithium bromide leaving the desorber increases linearly as shown in Figure 4-4. This has a direct considerable effect on the evaporator cooling load (Q_e) and condenser heat transfer rate (Q_c) but there is no significant effect on system COP.

The COP would be expected to rise considerably with increment of exhaust gas temperature, however as exhaust gas temperature rises, a heat transfer rate for the other system components also rises with respect to change of temperature of exhaust gas as shown in Figure 4-2 and 4-3. As shown in Figure 4-5, due to a combined effect of the auxiliary components introduced to the

ordinary cycle, a COP of a proposed cycle is maximum, and its way is identical to a combined and an ordinary cycle.

4.3.2 Effect of variation of generator temperature

As indicated in Figure 4-6 (a), temperature of generator (T_g) was varied from 76 to 95℃. As T_g increases, concentration of strong solution and system performance increases in ordinary, combined and the proposed cycle. However, the increase in system COP is not appreciable after 85^{o}C, it is almost the same as shown in Figure 4-6 (c). In these cycles, when T_g increases, a generator and an absorber heat transfer rate starts to decrease highly until it reaches 85^{o}C. After 85^{o}C, it decreases slightly that is why system COP increases gradually. A condenser heat transfer rate (Q_c) is increased with increment of T_g as indicated in Figure 4-6 (a). If T_g rises, a $H_2O-LiBr$ concentration coming from a generator as well as temperature of weak solution increases as shown in Figure 4-6 (b). Thus, the enthalpy (h_3) is raised by interchanging heat with a strong solution in a SHX. As T_g rises, strong solution enthalpy is increased and this leads to reduce the circulation ratio. Weak solution concentration, evaporator heat transfer rate (Q_e) and entrainment ratio of a mixing chamber is not affected by T_g increment. T_g should not be greater than 95℃ to prevent crystallization of LiBr, because a strong solution concentration should not be exceeded 65%. Therefore, the proposed cycle evidently has a higher COP in contrast to a combined as well as an ordinary cycle. Thus, a selected value of 85^{o}C for generator temperature is adequate.

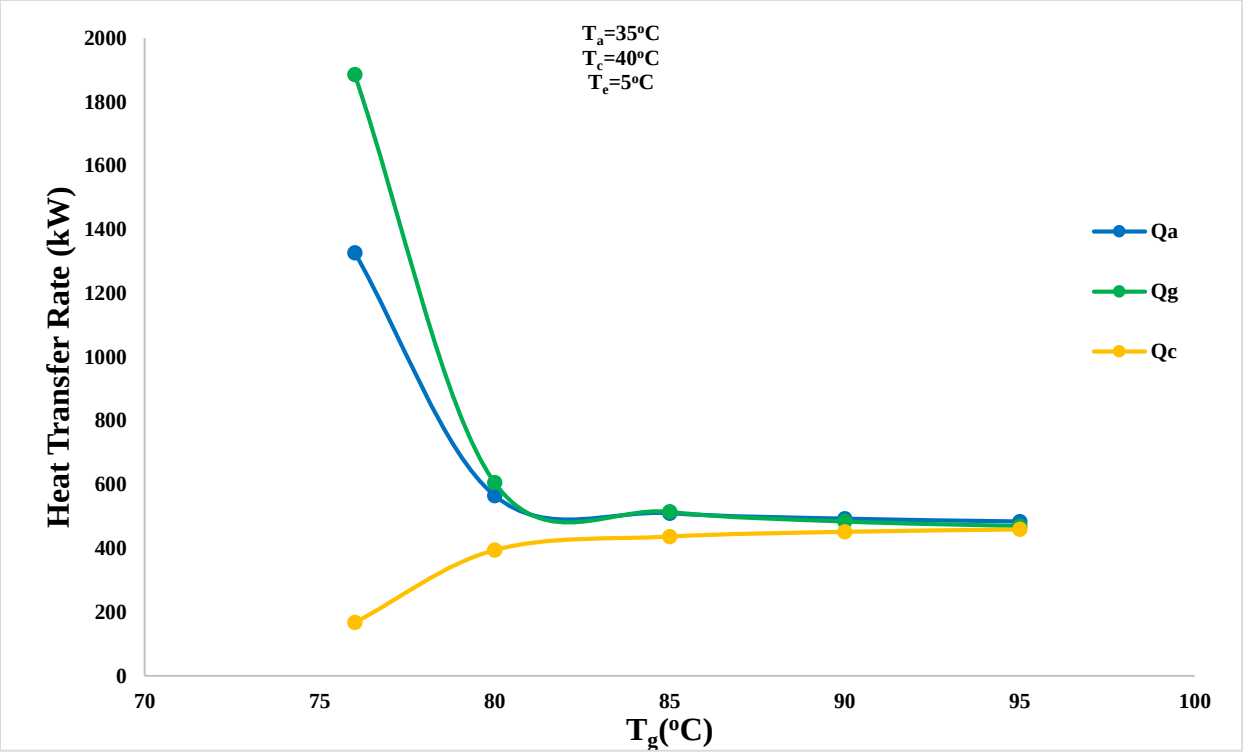

Figure 4-6 (a) Effect of variation of generator temperature on heat transfer rate.

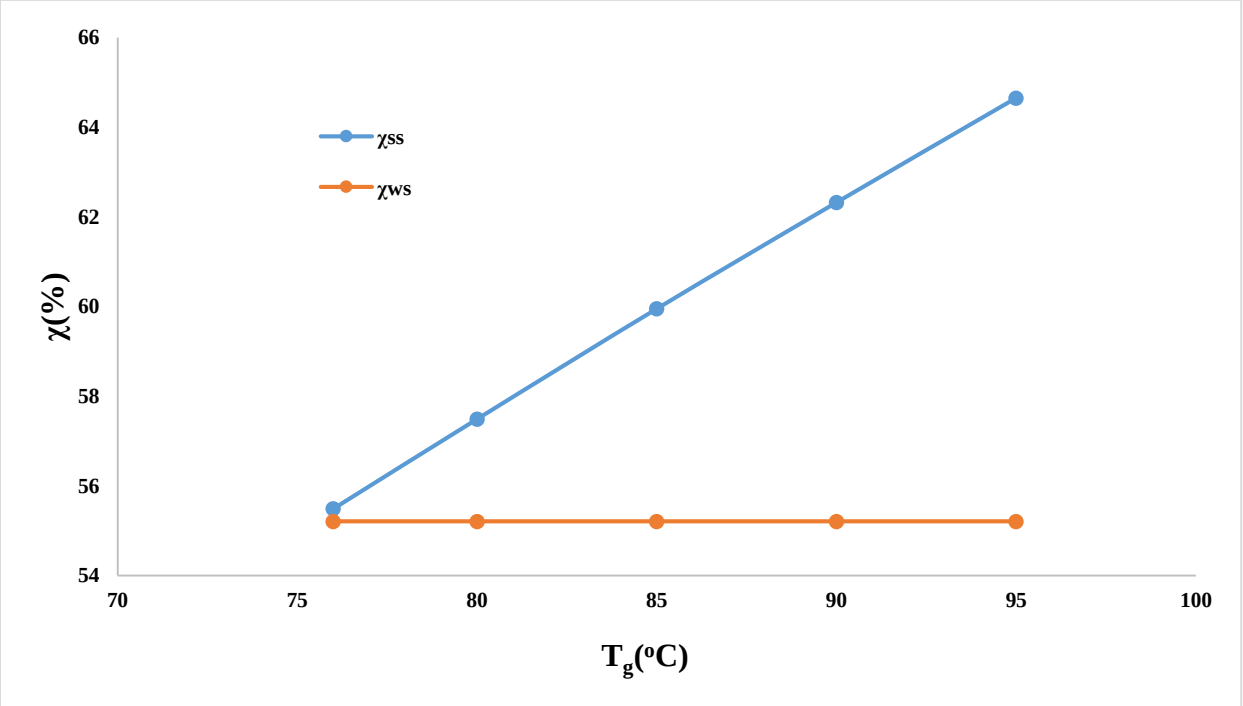

Figure 4-6 (b) Effect of variation of generator temperature on H_2O-LiBr concentration.

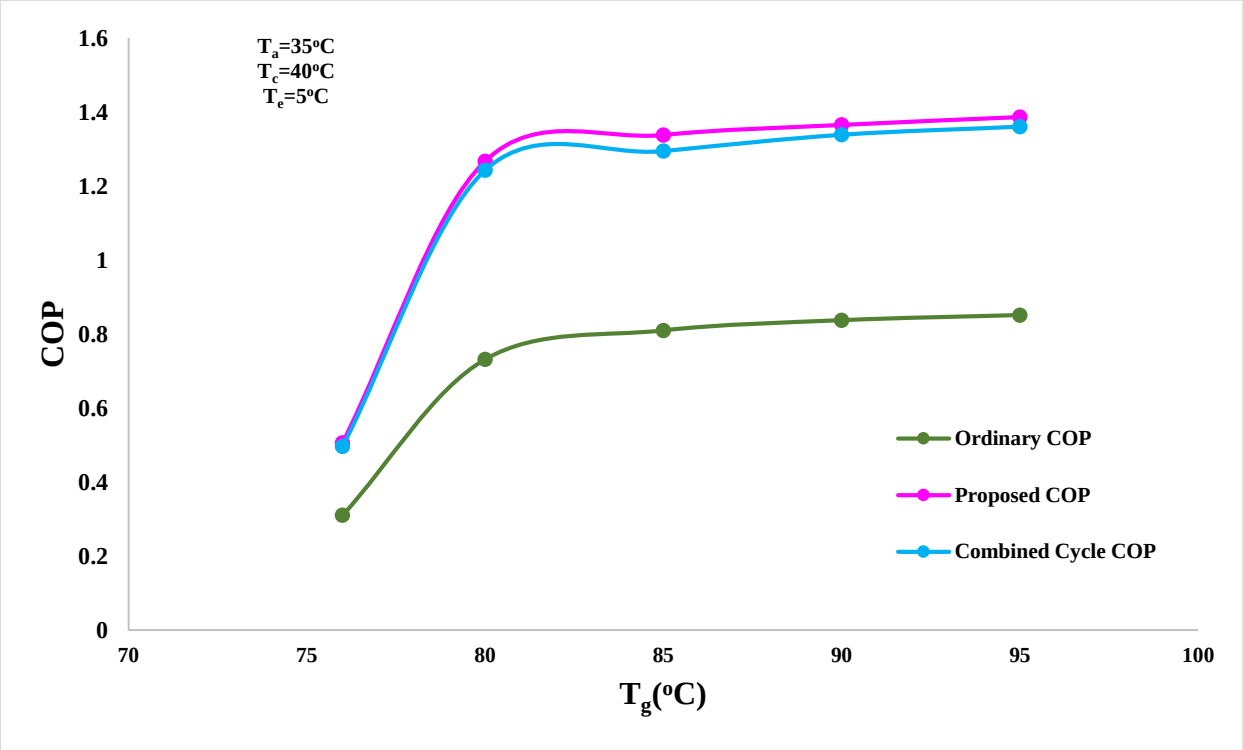

Figure 4-6 (c) Effect of variation of generator temperature on COP.

4.3.3. Effect of condenser temperature variation

As indicated in Figure 4-7 (a), heat transfer rates of different components are changed as condenser temperature (T_c) is changed. When T_c rises, a condenser pressure (p_c) rises and a concentration of strong solution (χ_{ss}) reduces. Owing to increment of p_c, a quantity of saturated liquid enthalpies coming from a condenser also rises and this leads to a decrement of a heat transfer rates of condenser. By minimizing χ_{ss}, a circulation ratio rises and a generator and an absorber heat transfer rates rises very slightly till the temperature reaches 40°C then they increased in a considerable manner. However, increment of condenser temperature does not affect weak solution concentration. Increment of condenser temperature leads to increase the generator and condenser pressure, and a decrease in χ_{ss} in a generator as shown in Figure 4-7 (b). This causes an increment of the circulation ratio and a decrement on a mass flow of refrigerant that is desorbed from a generator and this leads to reduce system performance as shown in Figure 4-7 (c). In this case also, the proposed cycle has a highest COP in contrast to a combined as well as an ordinary cycle. Thus, the selected condenser temperature (40°C) is good selection.

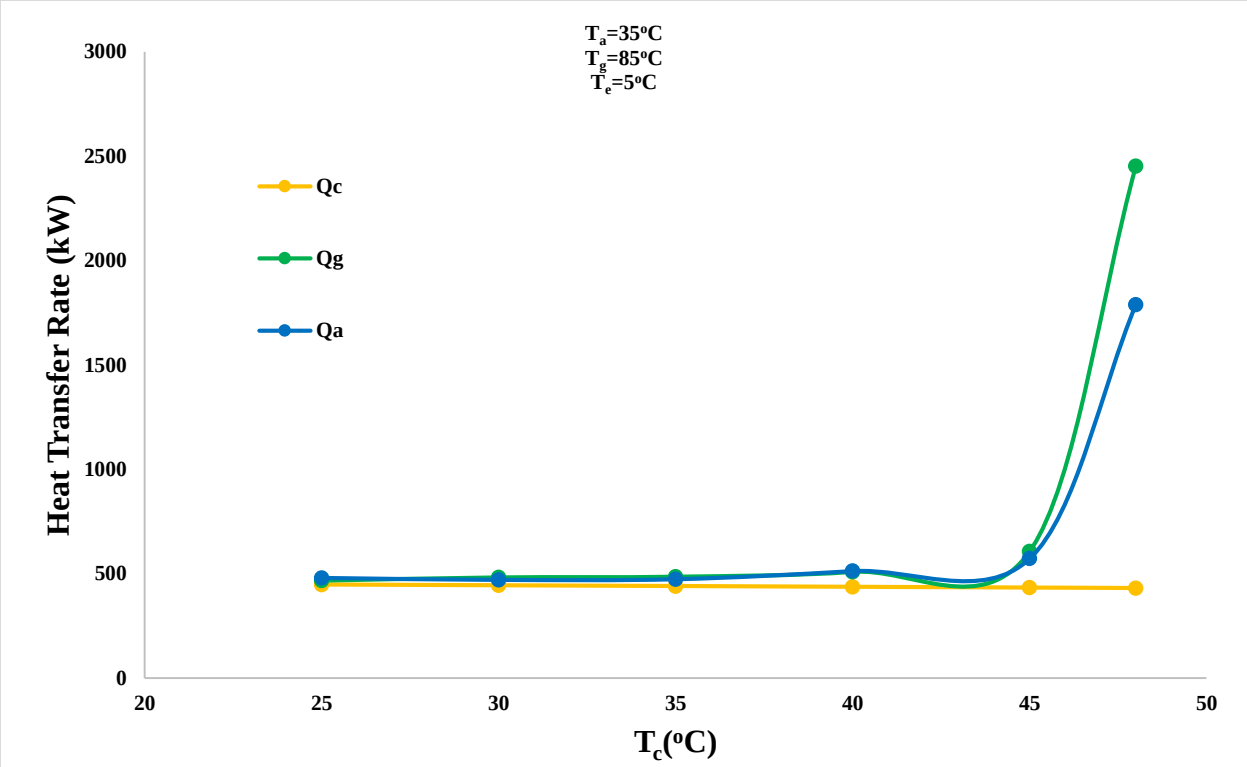

Figure 4-7 (a) Effect of variation of condenser temperature on thermal load.

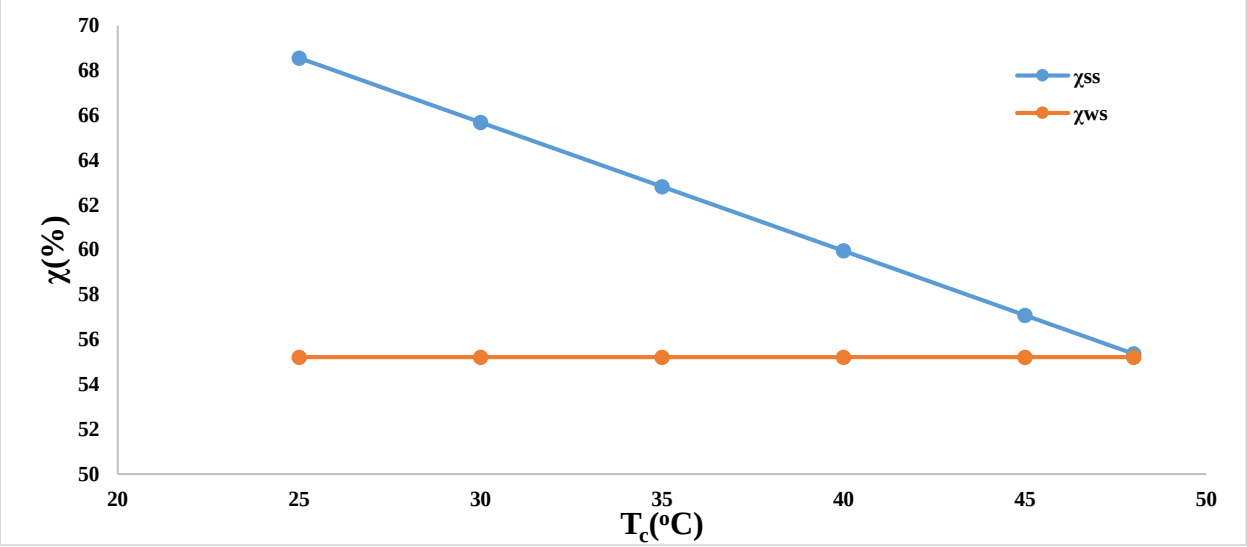

Figure 4-7 (b) Effect of variation of condenser temperature on H_2O-LiBr concentration.

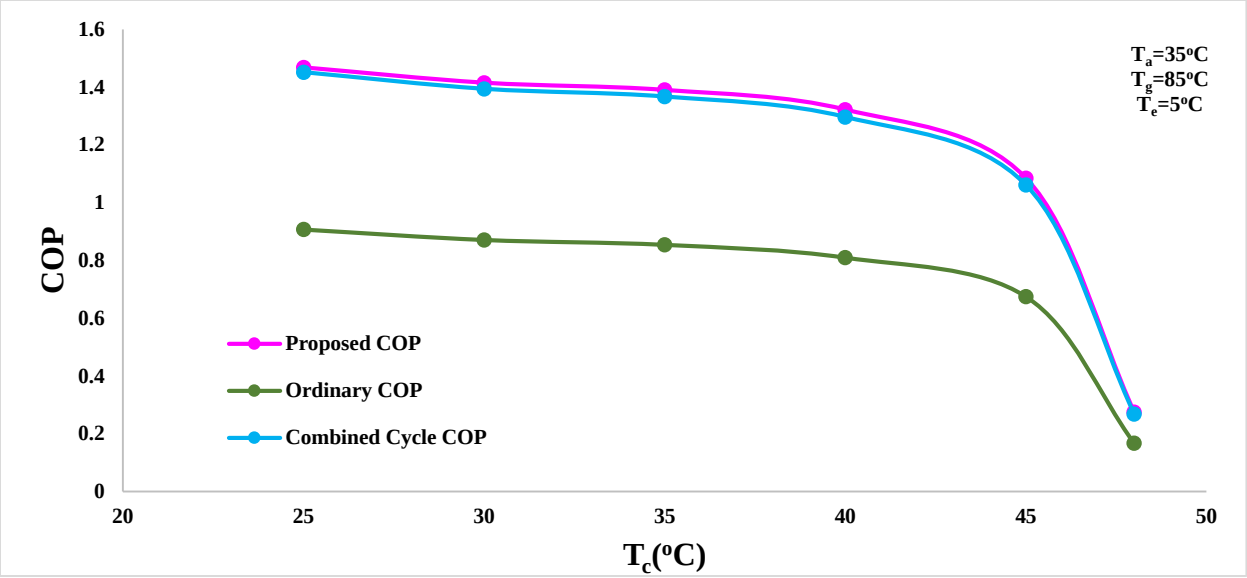

Figure 4-7 (c) Effect of variation of condenser temperature on COP.

4.3.4. Effect of evaporator temperature variation

Evaporator temperature variations with the heat transfer rates are observed in Figure 4-8 (a). The generator and an absorber heat transfer rates reduces as the evaporator temperature rises, while the evaporator heat transfer rates rises very slightly when the evaporator temperature rises. However, cooling cycles working under high evaporator temperatures is meaningless in refrigeration or air-conditioning (D. Sun, 1997). As evaporator temperature (T_e) rises, a weak solution concentration (χ_{ws}) also reduces. This leads to decreases the circulation ratio of the solution that is extracted from the absorber to produce an adequate amount of refrigerant vapor as shown in Figure 4-8 (b). This result reduces the strong solution flow rate which is extracting from a generator and goes to an absorber, and hence a heat exchanged amount in a generator reduces. In addition, a low flow rate of the strong solution reduces its potential to absorb vapor refrigerant in an absorber. Hence, as a result a reduction in a heat transfer rates to a generator because of an increment of evaporator temperature, system performance increases as shown in Figure 4-8 (c). In a proposed and combined cycle, when T_e rises, evaporator and flash tank pressure rises and this leads to rise a vapor flow rate goes to a mixing chamber. By using LSHX in the proposed system, evaporator heat transfer rates (Q_e) is increased. Thus, a results indicate that a proposed cycle has a highest COP than a combined as well as an ordinary cycle. Thus a considered evaporator temperature (5°C) is the best selection.

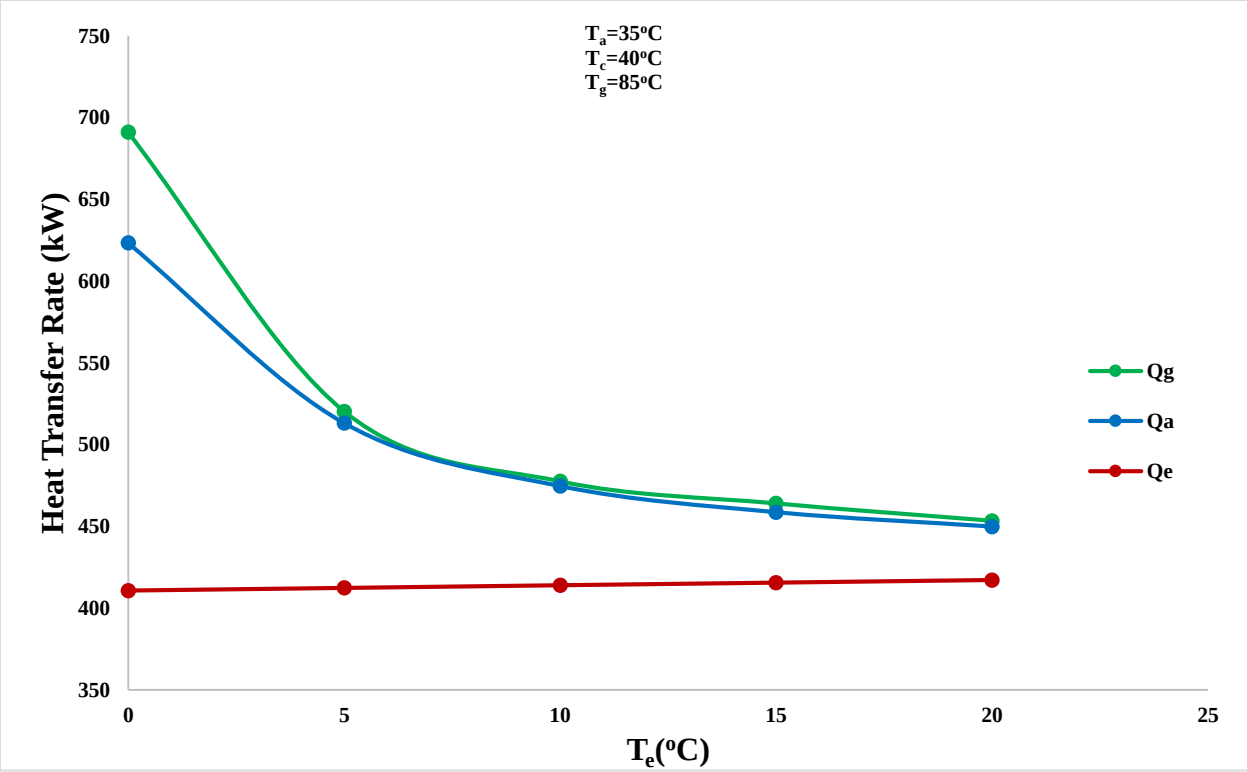

Figure 4-8 (a) Effect of evaporator temperature variation on a heat transfer rates.

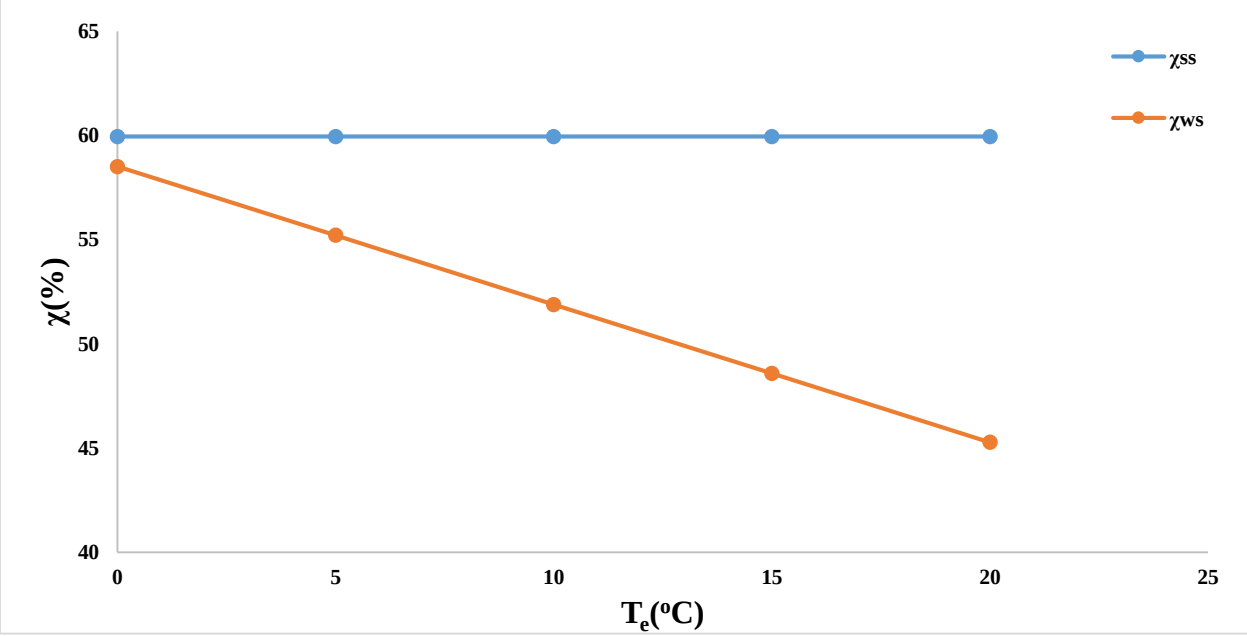

Figure 4-8 (b) Effect of evaporator temperature variation on H_2O-LiBr concentration.

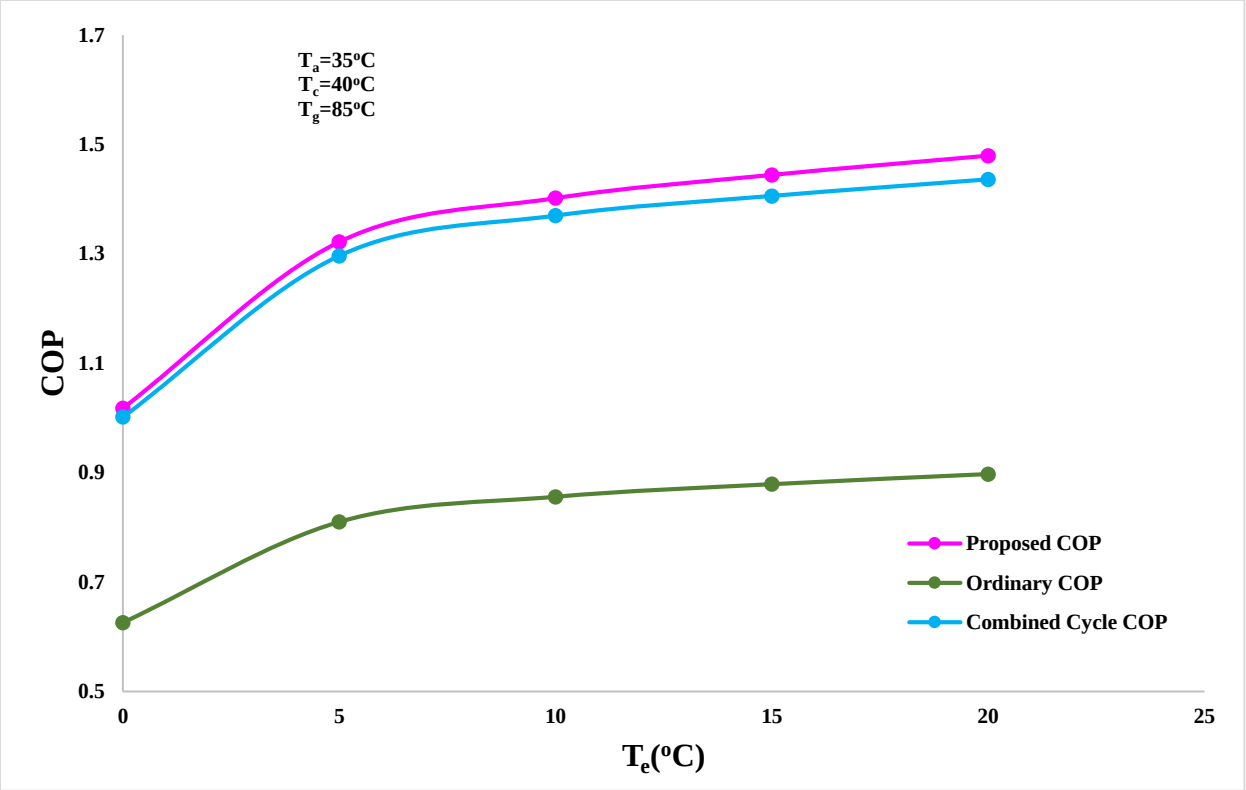

Figure 4-8 (c) Effect of evaporator temperature variation on COP.

4.3.5. Effect of variation of absorber temperature

As indicated in Figure 4-9 (a), a generator and an absorber heat transfer rates rises when absorber temperature (T_a) rises. Hence, system COP is reduced with increment of T_a as shown in Figure 4-9 (c). When T_a rises, a weak solution concentration come close to a strong solution concentration and this leads to rise circulation ratio as indicated in Figure 4-9 (b). But, the concentration of strong solution and a heat transfer rates in evaporator and condenser is not influenced by T_a variation and remains the same in ordinary, combined and proposed cycles. In this case to prevent crystallization, it is essential to reduce a heat transfer rate of the absorber and its temperature. In the analysis, increment of absorber temperature after 43°C is going to crystallization. Thus, the selected value of absorber temperature (35°C) is the proper selection. Based on Figure 4-9 (c), the proposed cycle generally shows higher system performance in the proposed system relative to combined and ordinary cycle.

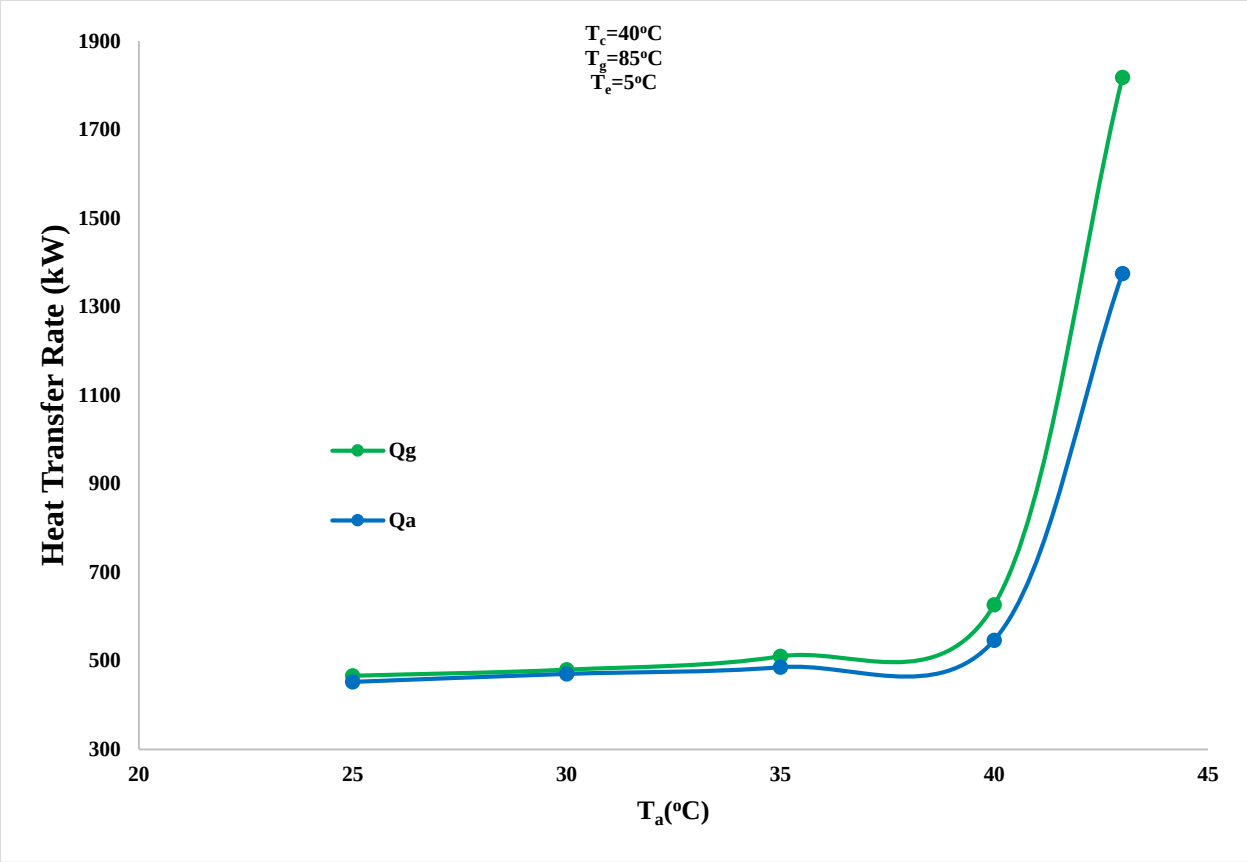

Figure 4-9 (a) Effect of absorber temperature variation on heat transfer rates.

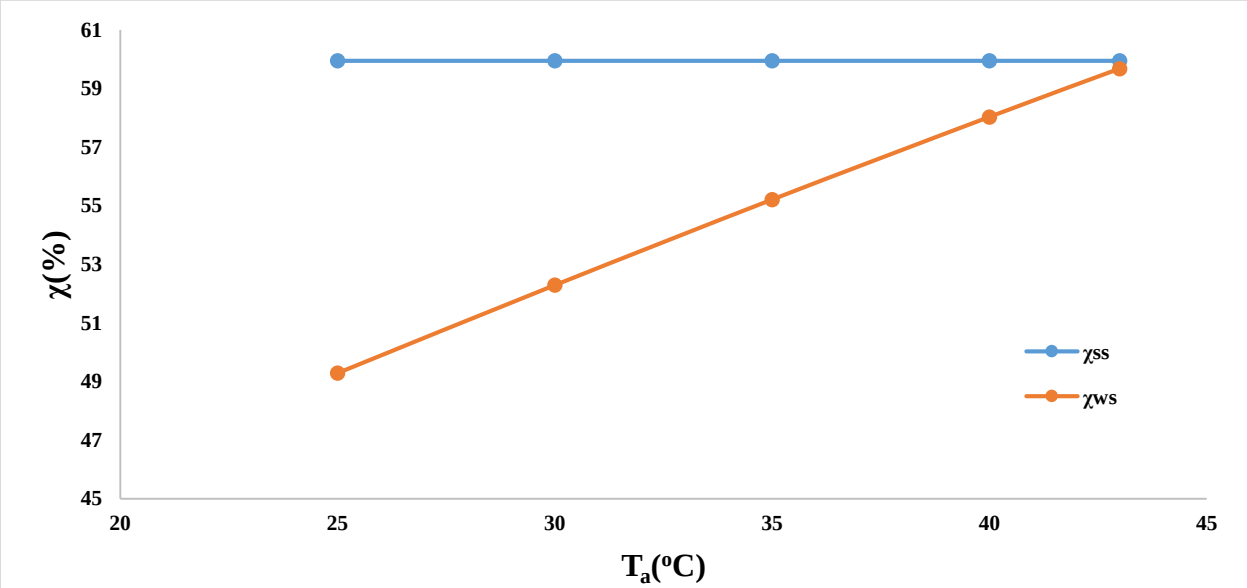

Figure 4-9 (b) Effect of absorber temperature variation on H_2O-LiBr concentration.

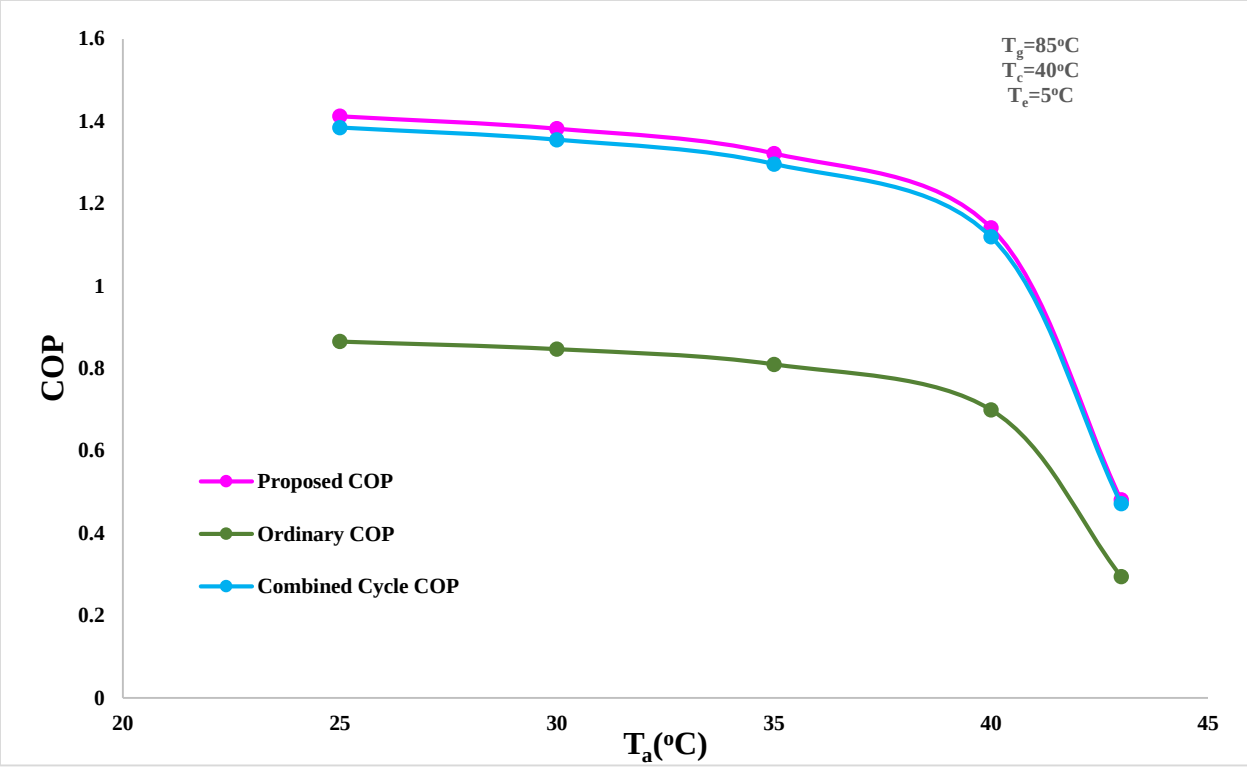

Figure 4-9 (c) Effect of absorber temperature variation on system COP.

4.3.6 Effect of entrainment ratio variation and temperature of exhaust gas on a heat transfer rates

In the proposed and combined system, temperature of exhaust gas (T_{exh}) has a linear effect on a mixing chamber on both primary and secondary flow. If T_{exh} rises, a flash gas which is removed in a flash tank is raised significantly by 25% in both the proposed and combined system. This rises the mass of saturated vapor in a secondary flow which get in a mixing chamber and this leads to increase a heat transfer rates on a condenser and evaporator. Since, a mass of desorbed refrigerant increases with rising of exhaust gas temperature in generator and this linearly affect the entrainment ratio as indicated in Figure 4-10 (a) and (b). If an entrainment ratio (ω) rises, the efficiency of a mixing chamber also rises and this leads to decrease the inlet temperature of condenser by 2.7°C within 0.1 increment of entrainment ratio. It is anticipated to reduce a heat transfer of condenser, but it increases linearly by 6.5% relative to constant T_{exh}. This is due to an increment of saturated vapor which is coming from flash gas removal and generator. The entrainment ratio increment also increased the cooling effect of the evaporator by 6.3% and this

results improving system COP by 30% relative to ordinary cycle and this percentage increment is reduced by 14.3% when the entrainment ratio is increased by 0.1 as shown in Figure 4-10 (c). However, a mass flow of refrigerant which passes to an absorber remains constant. Due to this reason, a heat transfer rate on the generator is similar to the ordinary cycle like absorber and this results increasing performance significantly. Hence, the proposed design can increase values to a system with variation of T_{exh} as compared to an ordinary cycle.

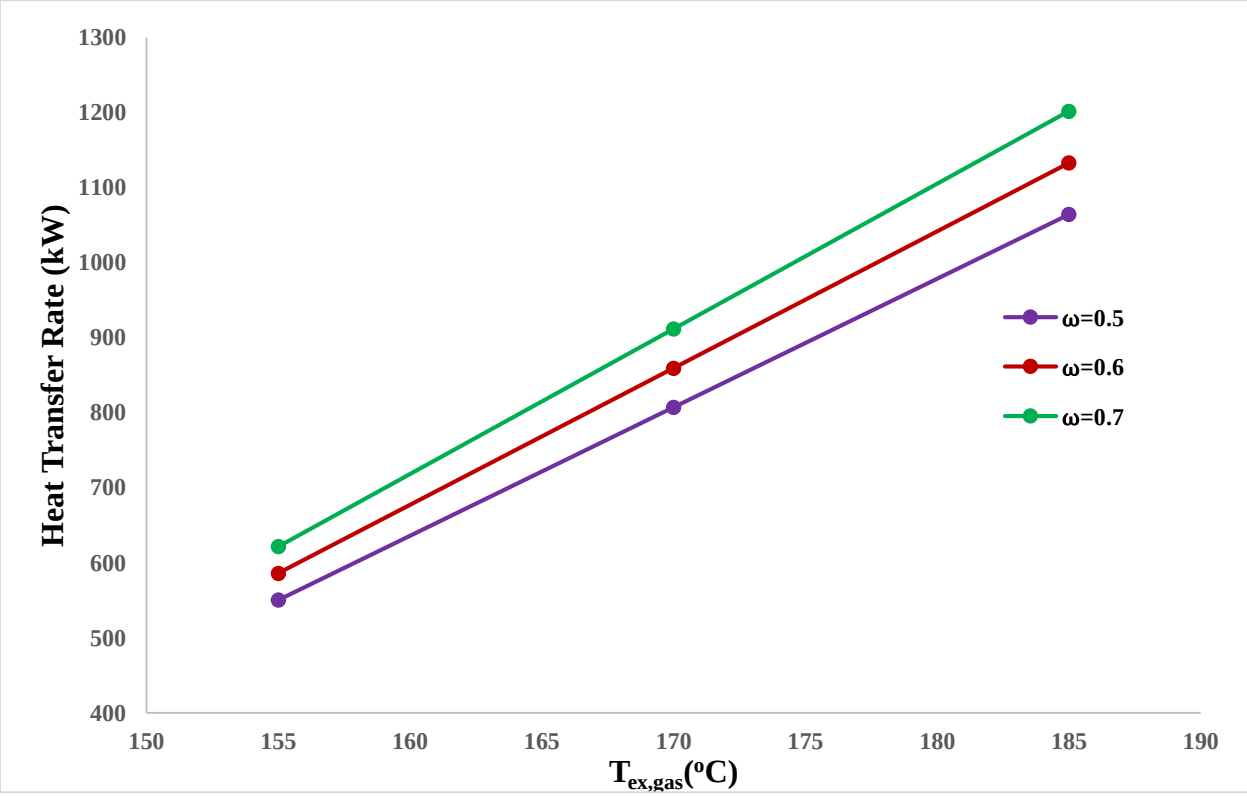

Figure 4-10 (a) Entrainment ratio effect on condenser heat transfer rates with exhaust gas temperature.

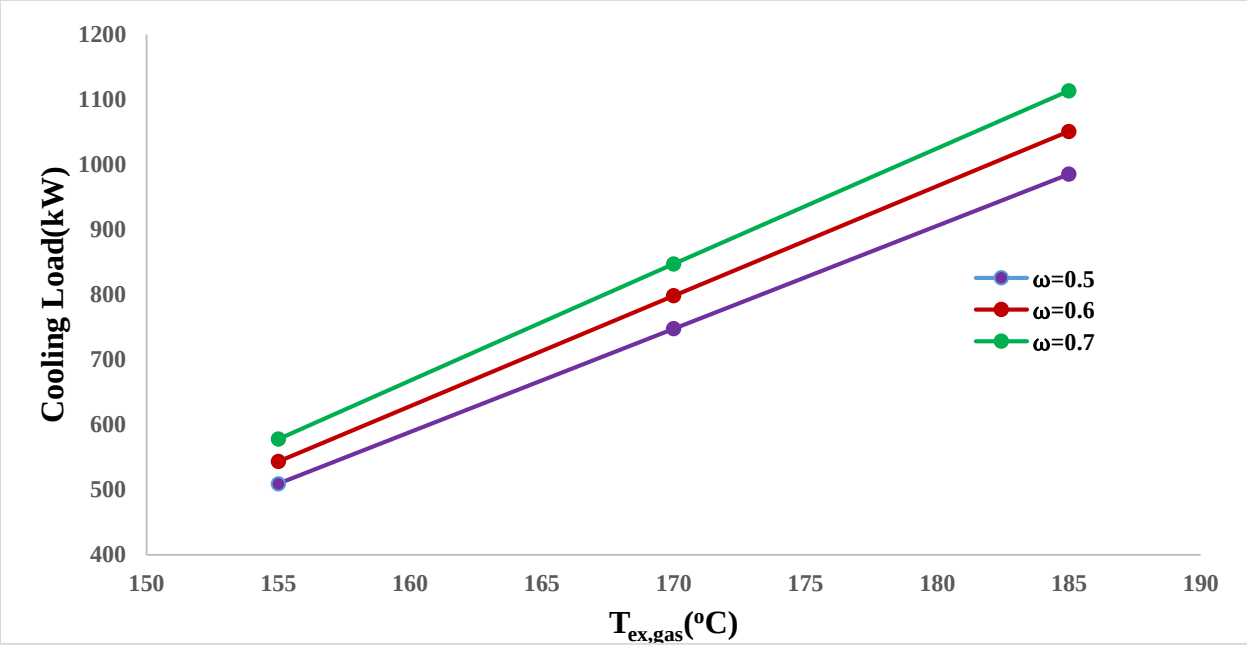

Figure 4-10 (b) Entrainment ratio effect on evaporator cooling load with exhaust gas temperature.

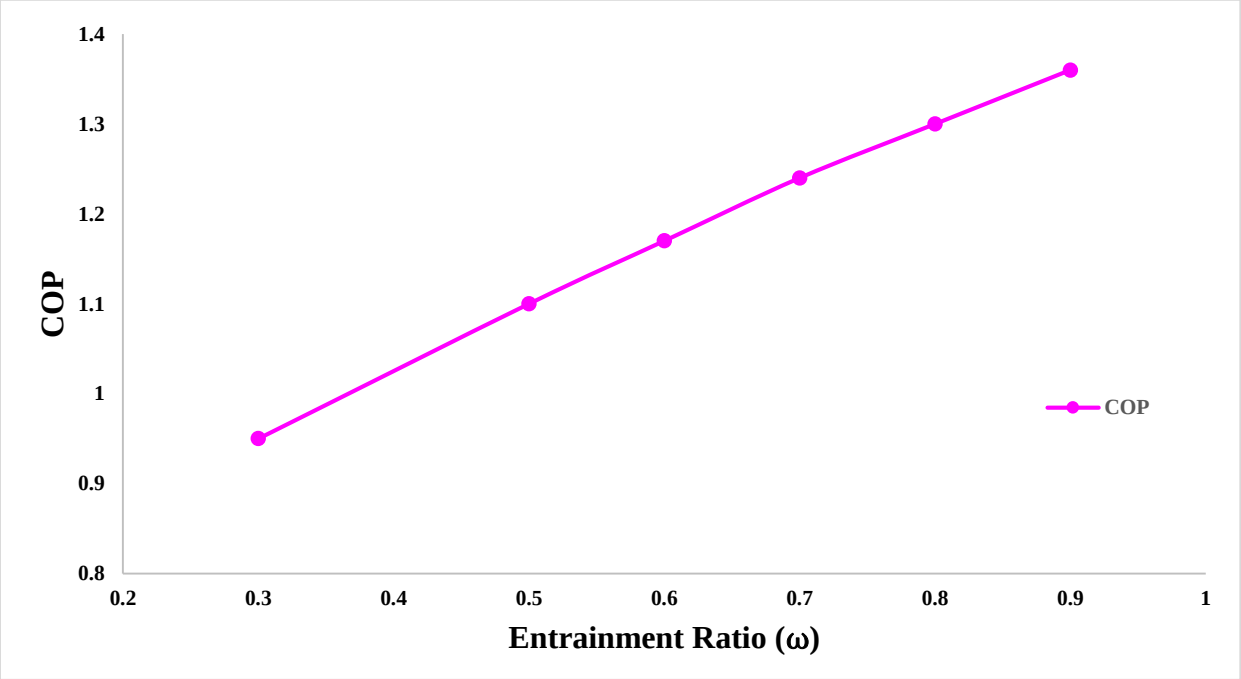

Figure 4-10 (c) Effect of entrainment ratio on system performance.

4.3.7. Heat exchanger effect

In the proposed design, the booster is installed between LSHX and flash tank vapor streamline to pressurize a vapor to a mixing chamber. By installing LSHX, a refrigerant goes to evaporator is subcooled since a refrigerant goes to evaporator approximately has low enthalpy, while the heat of a saturated vapor extracted from evaporator and pass into an absorber and mixing chamber is raised. Consequently, a heat transfer rates of these elements rise slightly.

When LSHX effectiveness rises, a refrigerant is more subcooled. Hence, a cooling capacity rises considerably as well as linearly since a liquid refrigerant passing a throttling valve with low temperature eliminates its heat to a refrigerant vapor exiting from evaporator.

In this thesis, the LSHX effectiveness is 70%. Figure 4-11 indicates system COP versus LSHX effectiveness at different points. The COP of the system increased slightly by 3% within 20% variation of effectiveness.

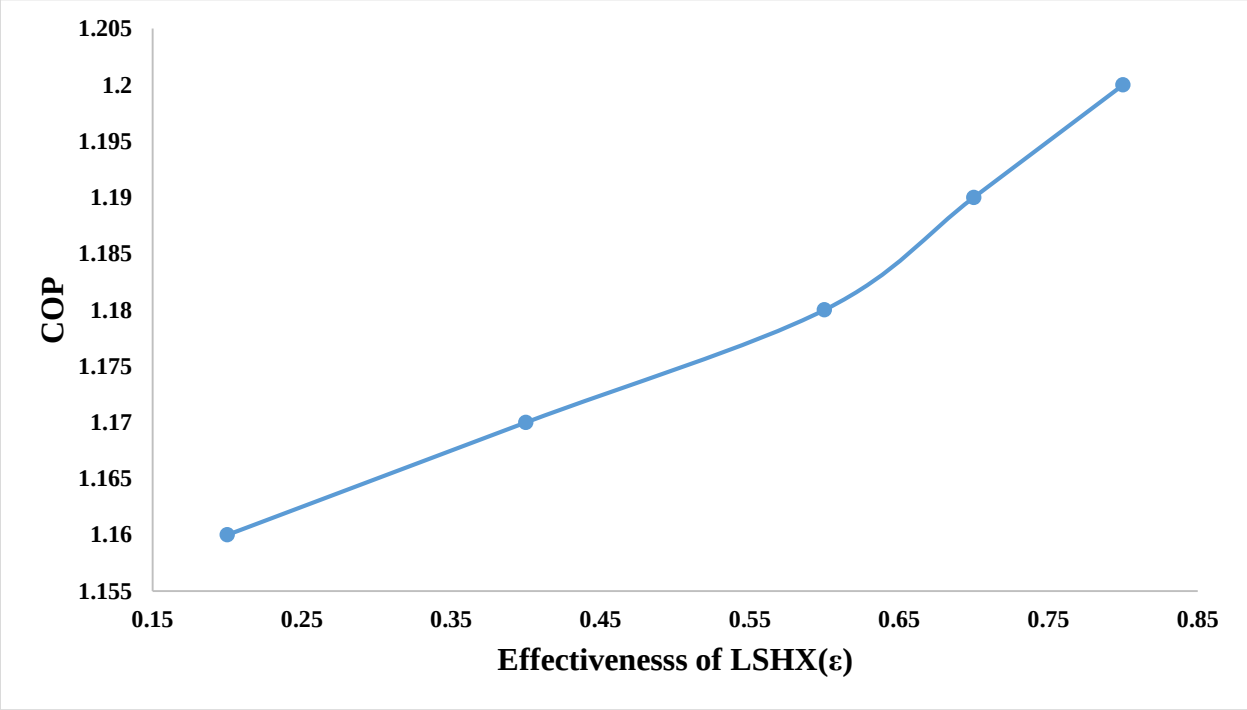

Figure 4-11 COP vs LSHX effectiveness.

4.4. Environmental and Economic Results

Basically, applying VARSU will results to save an auxiliary engines power requirement as well as reduction in emission and fuel consumption. In this case study investigations, results are indicated that about 82.5 ton/year fuel is saved with current price of fuel 673 $/ton by applying using VARSU. The emission factors (in g/kWh) for marine gas oil (MGO) which is fueled for moderate speed diesel engines with 0.5% sulfur, are 13.90, 0.32, 0.40, 1.10, 2.12 and 690.71 for NO_X, PM, HC, CO, SO_X, and CO_2 emissions respectively, during sailing (Browning et al., 2009). As shown in Figure 4-12 environmental advantages is observed when contrasting a yearly emission decrement in ton/year after implementing VARSU. Annual emissions (in ton /year) of auxiliary engines are 33.94, 0.78, 0.98, 2.69, 5.18 and 1686.66 for NO_X, PM, HC, CO, SO_X and CO_2 respectively. When the ship is in cruise mode, applying VARSU will down these emissions to 14.45, 0.33, 0.42, 1.14, 2.20 and 717.86 ton/year respectively by considering about 128.5 kw electrical energy consumption for AC, the auxiliary engine MCR power 1776 kW and the annual sailing hours of a case study vessel 8088 hr (see Appendix C).

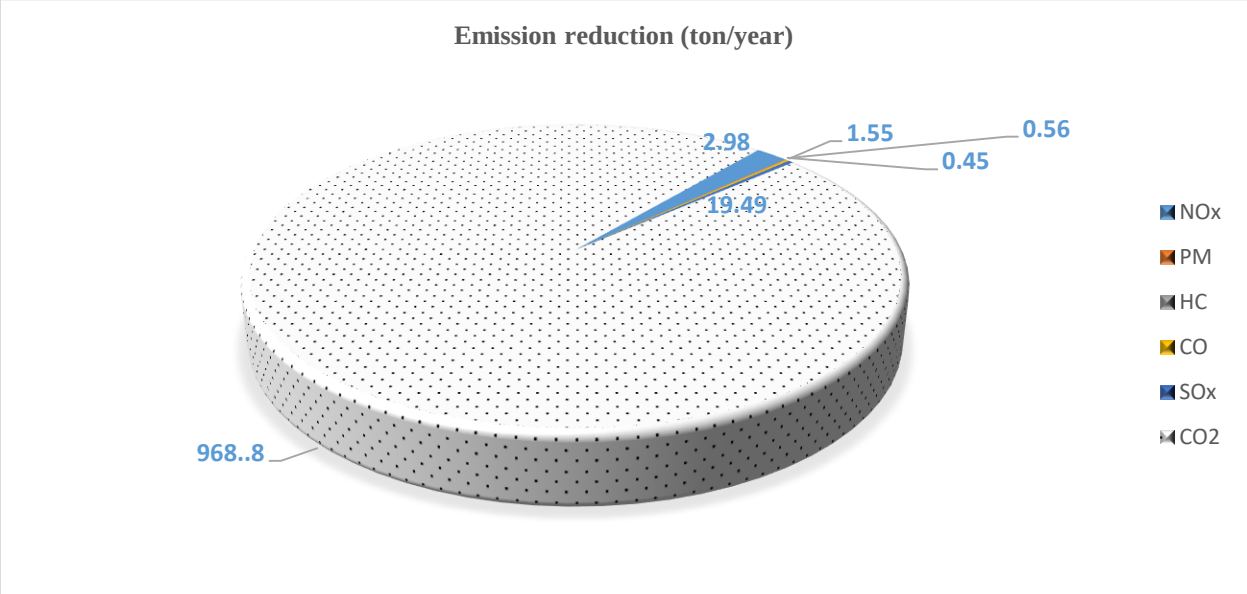

Figure 4-12 Annual emission reduction after using VARSU.

Economically, VARSU application is decided from a yearly installation costs as well as its time of recovery. The VARSU capital cost is ranges between 500 $/kW − 700 $/kW and an installation cost accounting 12% of capital cost. A yearly maintenance as well as operating costs are 0.008

$/kWh and 8 $/kW respectively. For a proposed VARSU application with considering some added components, the capital as well as installation costs are $224,104.2 with annual fuel saving of 57,188.18 $/year. The initial cost of HX is $10,572 which is 5.7% of exhaust gas based VARSU capital cost (Ammar, 2018). A VARSU's total lifecycle cost (LCC) depends on the vessels life time as well as a remaining operating years after the installation. Figure 4-13 indicates the exhaust gas based VARSU's LCC over 18 years of operation with considering 30 years of the average life time of vessel (Mikelis, 2008). The exhaust gas based VARSU's capital cost is $200,868 representing 48.68% of LCC. The operating and maintenance costs are $54,720 and $109,440, representing 13.24% and 26.48% of LCC. Hence, computing the overall LCC will leads to decision about installation of VARSU. Energy decrement and maintenance costs is the key points for decision.

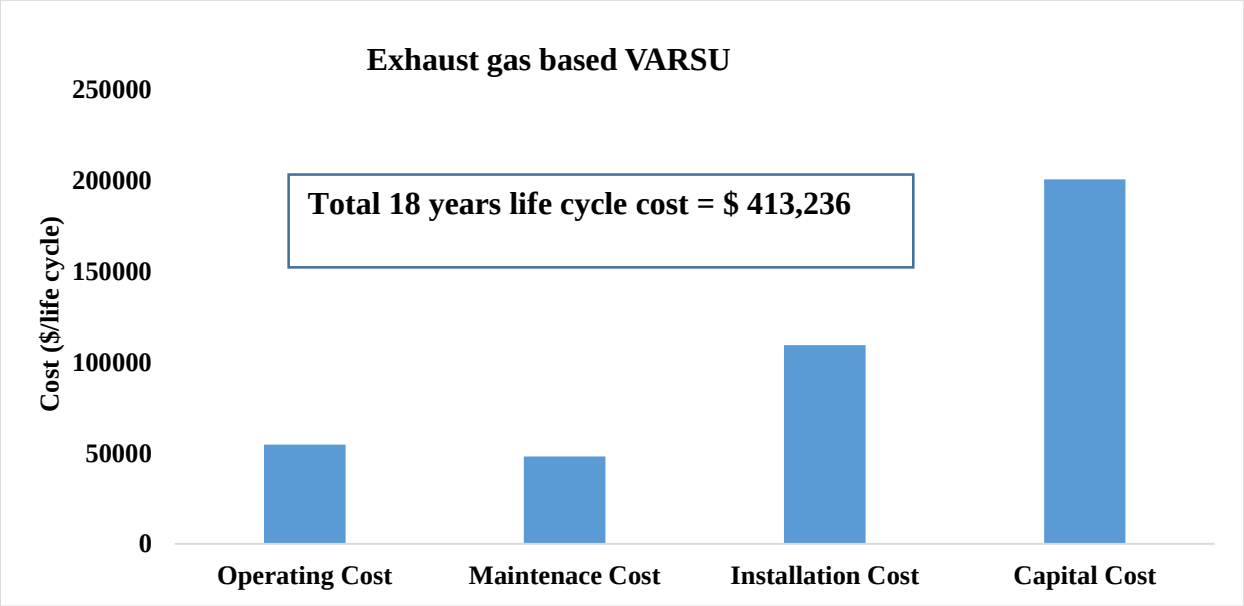

Figure 4-13 Exhaust gas based VARSU's overall lifecycle cost elements for 18 years of operation.

Moreover, the time required for money recovery should be taken into account for the economic decision when applying VARSU. Figure 4-14 and 4-15 indicates the yearly initial recovery cost and fuel saving cost with payback periods for exhaust gas based VARSU. In this case study, the yearly capital money recovery cost is 57188.18 $/year for exhaust gas based VARSU with i = 10% (Ammar, 2018). The payback time intervals should be in contrast with the applicable economic

life of a vessel. Thus, the payback period becomes 7 years and then the yearly fuel saving cost at 18th years is about $94,523.34 with 3% increment of fuel price.

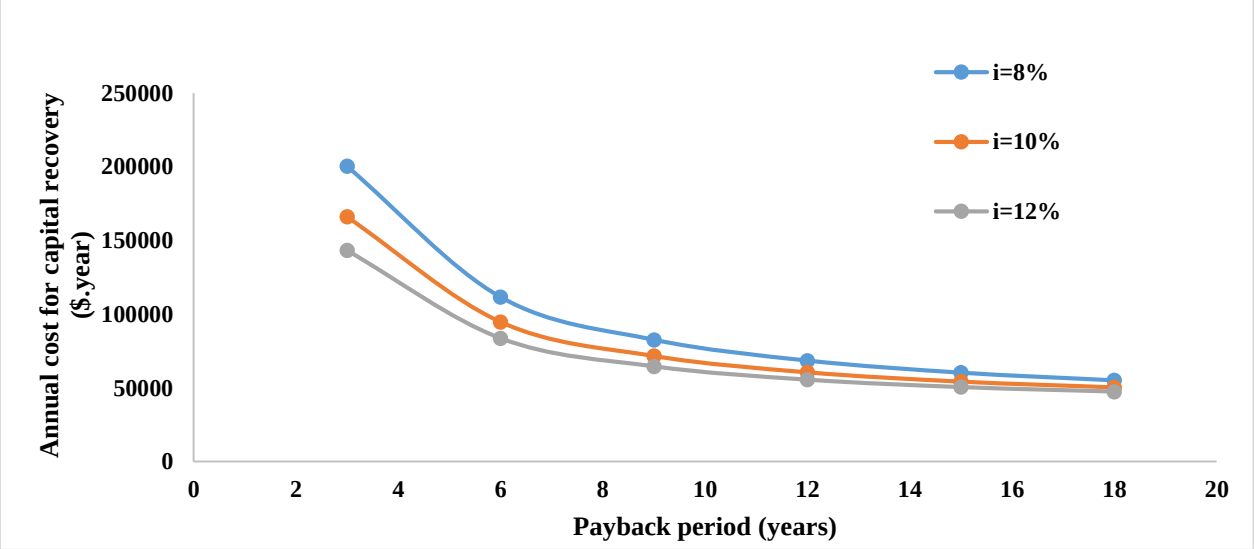

Figure 4-14 Yearly capital recovery cost of after implementing exhaust gas based VARSU.

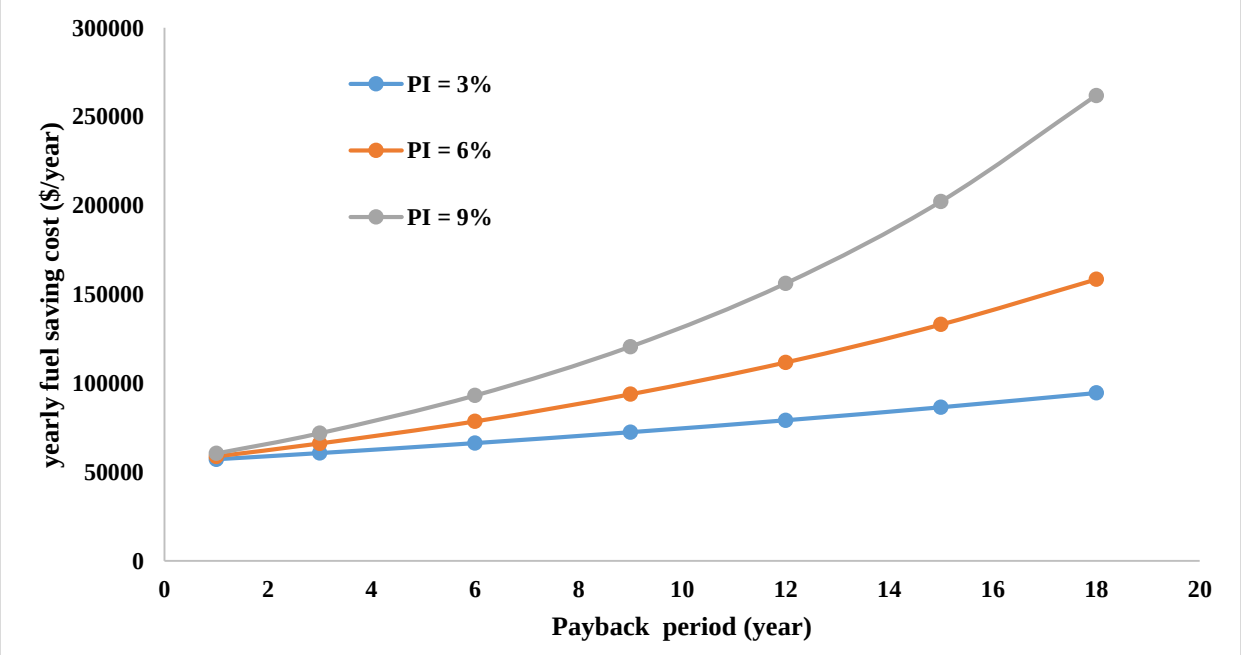

Figure 4-15 Yearly cost of fuel saving after implementing exhaust gas based VARSU.

Another eco−environmental advantage of applying VARSU for the main engine is decrement of cost effectiveness due to emission reduction of each pollutant. Figure 4-16 shows the computed

emission cost-effectiveness decrement for pollutants. A lesser yearly emission cost effectiveness, a greater economic advantage due to decreasing emission criteria. The overall yearly cost of VARSU is C_{ti} = 56,191$/year (Mikelis, 2008) and then the cost effectiveness of decreasing SO_X and NO_X emissions for exhaust gas will be diminished to 18.86 $/kg and 2.88 $/kg respectively. The maximum economic cost-effectiveness opportunity by using VARSU is decrement of CO_2 emission, which is diminished by 968.8 ton/year, with 0.054 $/kg cost effectiveness.

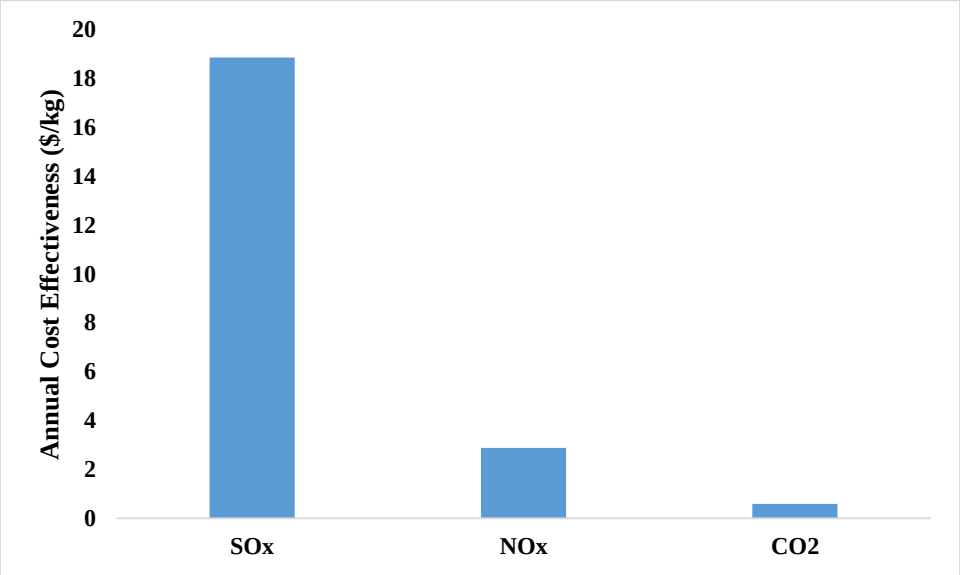

Figure 4-16 Yearly cost-effectiveness emission decrement for pollutants after implementing VARSU.

By using well to wake approach, the emissions of different pollutants from medium speed diesel auxiliary engine of the case study vessel is computed for 100 years and 20 years in terms of CO_2e100 and CO_2e20 as shown in Figure 4-17 and 4-18. In order to do that appropriate data about GWP and emission factors of different climate pollutants are used.

The GWP of CO_2, CH_4, N_2O and BC for 100 years are 1, 36, 298 and 900 and also for 20 years 1, 87, 268 and 3200 respectively. The well to tank of climate pollutants emission factors of marine gas oil (MGO) and medium speed diesel (MSD) auxiliary engine for CO_2, CH_4, N_2O and BC are 1, 0.5757, 0.00460, 0.00001, NA as well as for tank to wake are 3.206, 0.00006, 0.00017, 0.00026 in g/g fuel (Comer & Osipova, 2021). From the analysis of WTW carbon dioxide equivalent approach, findings show that about 4569.18 and 5465.33 tons of climate pollutants (CO_2, CH_4,

N_2O and BC) is totally emitted to the atmosphere in 100 years and 20 years respectively, from these emissions CO_2 by itself accounts 4078.51 tons as shown in Figure 4-17.

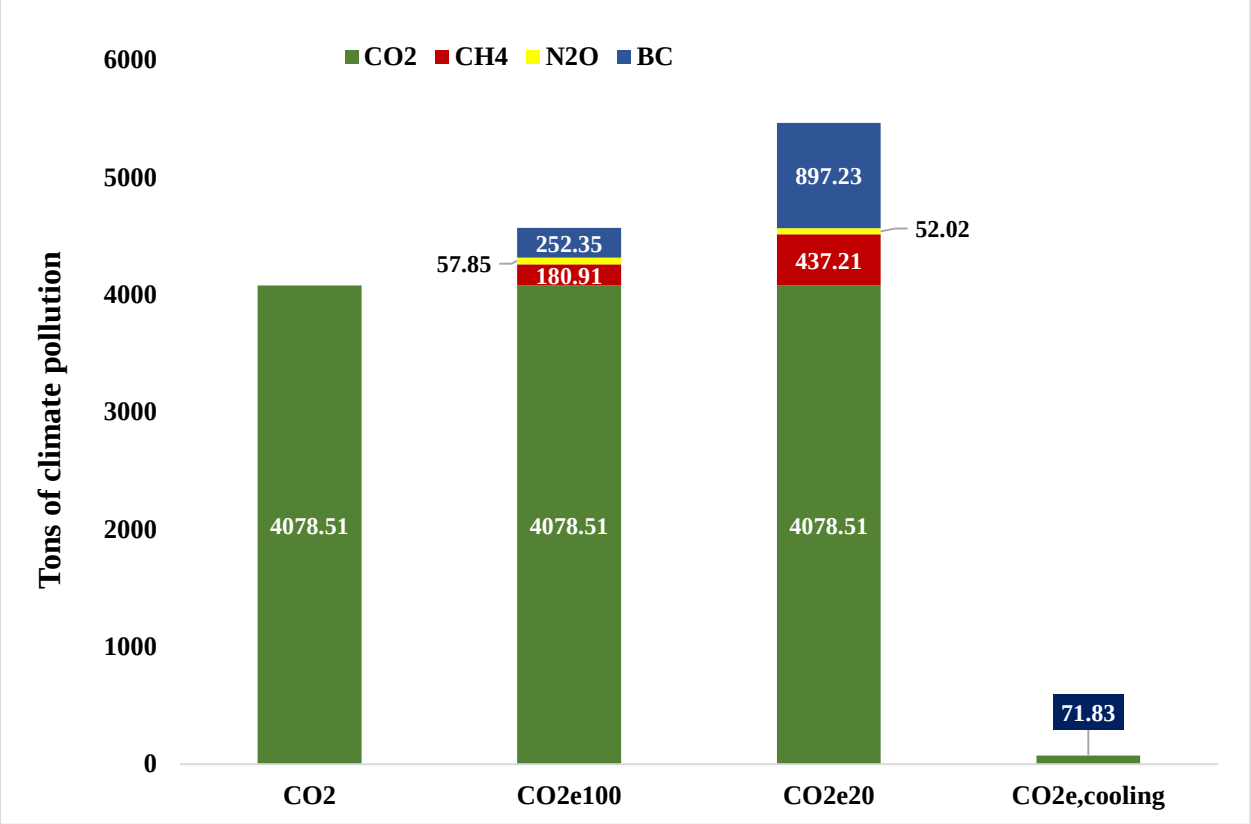

Figure 4-17 Well-to-wake emissions of climate pollutants before applying VARSU.

The amount of climate pollutant emission is before applying VARSU is high as shown above in Figure 4-17. However, by applying VARSU the overall emission of climate pollutant is reduced by 349.55 and 418.11 tons in 100 years and 20 years respectively as shown below in Figure 4-18. Hence, VARSU is an eco-friendly major climate pollutant reducer cooling system.

The other pollutants need detailed investigation to compute GWP since their impact on the climate is complex, for instance, NO_X has a green house, warming as well as cooling effects due to different factors, HC is a GHG and precursors to formation of tropospheric ozone, CO is not a direct greenhouse gas, but it has an indirect impact by increasing the lifetime of methane, PM absorb solar radiation which leads to warming, SO_X is not greenhouse gas but have cooling effect

due to formation of aerosols. Therefore, owing to these reason not well represented by a single GWP value and their impacts relies on factors like their atmospheric location, specific chemical composition as well as interactions with other compounds (Jalkanen et al., 2016).

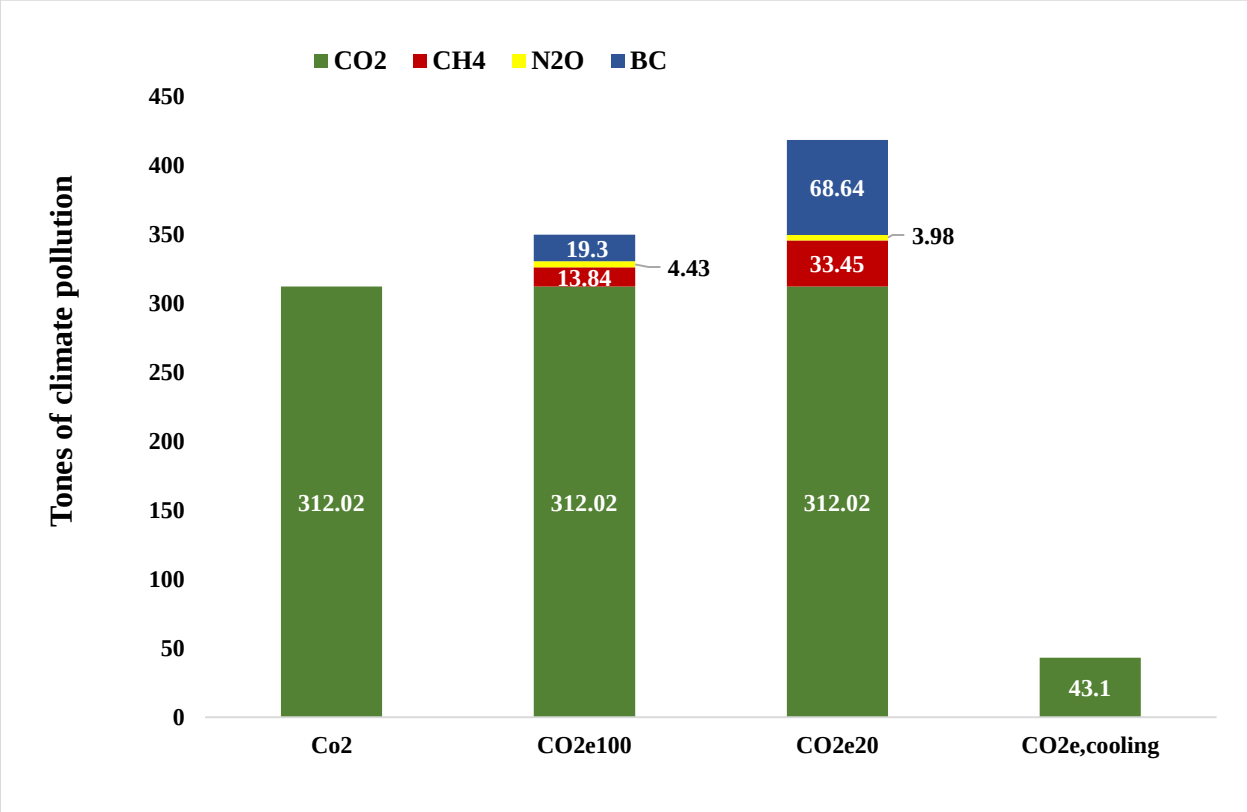

Figure 4-18 Well-to-wake emissions of climate pollutants before applying VARSU.

To determine CO_2e from cooling system equipment in equation (3.67), the values of different parameters are taken; Q_n = 1000 kg, k = 0.5%, X = 8%, Y = 90%, Z = 50%, C = 380kW and the GWP for refrigerant R404A = 4300 (Environnement et al., 2025). Hence, from the calculation the finding shows that about 71.83 tons of CO_2e is emitted to the atmosphere if the ship is not applying VARSU throughout the lifetime (30 years) as shown in Figure 4-17. However, if it is introducing VARSU onboard ship about 43.1 tons of CO_2e is reduced from the emission for the remaining lifespan of the vessel (18 years) as shown in Figure 4-18 because the vapor compression system that use refrigerant R404A for cooling is completely substituted by ecofriendly cooling system that is VARSU.

CHAPTER 5: CONCLUSION AND RECOMMENDATIONS

5.1. Conclusion

The present concerns about climate change and growing of fuel cost need a proper energy conservation technology to recover waste heat generated by marine transportation. Single−effect H_2O−LiBr absorption system can apply waste heat from proper sources to yield cooling effect for air conditioning system.

In this thesis, a thermodynamic, environmental and economic analysis was performed for a single−effect VARS with added auxiliary components such as mixing chamber, flash tank and liquid suction heat exchanger using H_2O−LiBr as an operating fluid and marine diesel engine exhaust gas as a supplied heat input to driven a cycle. By considering the thermodynamic analysis, an exhaust gas can supply above a desired heat successfully for a generator and produce above the desired cooling capacity of 380 kW. Theoretically a proposed, a combined and an ordinary cycle performances were compared. An overall system COP of a proposed cycle is raised by 38.23% in contrast to an ordinary cycle. Due to the addition of LSHX, a COP of proposed cycle is raised by 3% in contrast with combined cycle. At the end, the proposed cycle improves a refrigerant quality which goes to evaporator and the efficiency of the case study vessel's main diesel engine by 4.7 – 8.7%.

Based on economic and environmental analysis, the application of exhaust gas driven VARS will diminish fuel usage by 82.5 ton/year. This in turn decrease of NO_X and SO_X discharge by 19.49 ton/year and 2.98 ton/year, respectively. A maximum decrement will observe in CO_2 discharge, by 968.8 ton/year. Using of exhaust gas for VARS machine will save annually $94,523.34 at the end of the anticipated lifecycle of the vessel with 3% increment of fuel price. This application is economically efficient with capital as well as installation costs of $413,236 with payback period of 7 years. This results decrement in SO_X, NO_X, and CO_2 discharges with cost-effectiveness of 18.86 $/kg, 2.88 $/kg, as well as 0.054 $/kg, respectively and also reduces about 349.55 and 418.11 tons of CO_2e (blend of CO_2, CH_4, N_2O and BC) in 100years and 20 years using well to wake approach respectively. Thus, using of waste heat results reduction in environmental pollution and energy consumption of auxiliary engines in ship.

5.2. Recommendations

The possibility of using low grade thermal energy for cooling production is interesting if there is a continuous requirement for cooling effect in air conditioning system but the ship's engine must be in cruising mode to generate cooling effect. A VARS fulfills the cooling demand using waste heat from exhaust gas.

If this work is more advanced in the future, it could be utilized for the other vessels beyond the analysis applied in this thesis. The application area is vast since waste heat is rejected in different ways.

To investigate further about recovery of waste heat, a precise technique for desalination of salt using the combined dissipated heat from scavenge air as well as jacket cooling water is left for future work. Investigation is required in this regard for the possibilities of direct heating of salt with waste heat or if a heat exchanger is needed.

REFERENCES

Abed, A. M., Alghoul, M. A., Sirawn, R., Al-Shamani, A. N., & Sopian, K. (2015). Performance enhancement of ejector-absorption cooling cycle by re-arrangement of solution streamlines and adding RHE. *Applied Thermal Engineering*, *77*, 65–75. https://doi.org/10.1016/j.applthermaleng.2014.12.003

Alshammari, F., Pesyridis, A., Karvountzis-Kontakiotis, A., Franchetti, B., & Pesmazoglou, Y. (2018). Experimental study of a small scale organic Rankine cycle waste heat recovery system for a heavy duty diesel engine with focus on the radial inflow turbine expander performance. *Applied Energy*, *215*, 543–555.

Ammar, N. R. (2018). *THERMO-ECONOMIC ANALYSIS AND ENVIRONMENTAL ASPECTS OF ABSORPTION REFRIGERATION UNIT OPERATION ONBOARD MARINE VEHICLES : RO- PAX VESSEL CASE STUDY*. *25*(3), 94–103.

Aphornratana, S. (1995). *Theoretical and experimental investigation of a combined ejector-absorption refrigerator*. University of Sheffield, Department of Mechanical and Process Engineering.

Aphornratana, S., & Eames, I. W. (1998). Experimental investigation of a combined ejector-absorption refrigerator. *International Journal of Energy Research*, *22*(3), 195–207.

Arun Bangotra. (2017). Design - Analysis of Generator of Vapour Absorption Refrigeration System for Automotive Air- Conditioning. *International Journal of Engineering Research And*, *V6*(06), 121–125. https://doi.org/10.17577/ijertv6is060074

Behrendt, C. (2019). *CONDITIONS OF WASTE HEAT RECOVERY IN MARINE WASTE HEAT CONDITIONS OF WASTE HEAT RECOVERY IN MARINE WASTE HEAT RECOVERY*. *April*, 2–9.

Bellos, E., & Tzivanidis, C. (2018). Parametric analysis and optimization of a cooling system with ejector-absorption chiller powered by solar parabolic trough collectors. *Energy Conversion and Management*, *168*, 329–342.

Bo, Z., Mihardjo, L. W. W., Dahari, M., Abo-Khalil, A. G., Al-Qawasmi, A.-R., Mohamed, A. M., & Parikhani, T. (2021). Thermodynamic and exergoeconomic analyses and optimization of an auxiliary tri-generation system for a ship utilizing exhaust gases from its engine. *Journal of Cleaner Production*, *287*, 125012.

Browning, L., International, I. C. F., Hartley, S., & Facanha, C. (2009). Current Methodologies in Preparing Mobile Source Port-Related Emission Inventories. U.S. Environmental Protection Agency. *Final Report*, *April*, 1–18.

Butrymowicz, D., Gagan, J., Łukaszuk, M., Śmierciew, K., Pawluczuk, A., Zieliński, T., & Kędzierski, M. (2021). Experimental validation of new approach for waste heat recovery from combustion engine for cooling and heating demands from combustion engine for maritime applications. *Journal of Cleaner Production*, *290*, 125206.

Cao, T., Lee, H., Hwang, Y., Radermacher, R., & Chun, H.-H. (2015). Performance investigation

of engine waste heat powered absorption cycle cooling system for shipboard applications. *Applied Thermal Engineering*, *90*, 820–830.

Chaboki, Y. A., Khoshgard, A., Salehi, G., & Fazelpour, F. (2021). Energy, exergy, and environmental analysis of meeting cooling demand of a ship with waste heat recovery. *Energy Efficiency*, *14*, 1–14.

Chunnanond, K., & Aphornratana, S. (2004). Ejectors: applications in refrigeration technology. *Renewable and Sustainable Energy Reviews*, *8*(2), 129–155. https://doi.org/https://doi.org/10.1016/j.rser.2003.10.001

Comer, B., & Osipova, L. (2021). *Accounting for well-to-wake carbon dioxide equivalent emissions in maritime transportation climate policies APPROACH FOR CALCULATING WELL-TO-WAKE*. *March*.

Convention, U. N., Specialist, S. P., Sector, N. S., Initiative, B., Researcher, V., & Studies, A. (n.d.). *OCEAN SUSTAINABILITY IN THE 21 S T CENTURY*.

Environnement, M. De, Lutte, D., & Faune, D. (2025). *Greenhouse Gas Emissions Quantification Guide*.

Epa, U., of Transportation, O., Quality, A., & Division, C. (2016). *NATIONAL PORT STRATEGY ASSESSMENT: Reducing Air Pollution and Greenhouse Gases at U.S. Ports, Executive Summary (EPA-420-S-16-002, September 2016)*. *September*. https://www3.epa.gov/otaq/nearroadway.htm.

ESLSE. (2022). *Ethiopian Shipping Lines and Logistics Serices Profiles.* 1-21,. WWW.eslse.et,

EU. (2024). Regulation (EU) 2024/573 of the European Parliament and of the Council of 7 February 2024 on fluorinated greenhouse gases, amending Directive (EU) 2019/1937 and repealing Regulation (EU) No 517/2014. *Official Journal of the European Union*, *L*(573), 1–67. https://eur-lex.europa.eu/legal-content/DE/TXT/?uri=CELEX:32024R0573

Farshi, L. G., Mahmoudi, S. M. S., Rosen, M. A., Yari, M., & Amidpour, M. (2013). Exergoeconomic analysis of double effect absorption refrigeration systems. *Energy Conversion and Management*, *65*, 13–25.

Fernández-Seara, J., Vales, A., & Vázquez, M. (1998). Heat recovery system to power an onboard NH3-H2O absorption refrigeration plant in trawler chiller fishing vessels. *Applied Thermal Engineering*, *18*(12), 1189–1205.

Guangrong, Z. (2017). *Ship energy efficiency technologies: Now and the future*.

Holmberg, P., & Berntsson, T. (1990). Alternative working fluids in heat transformers. *Ashrae Transactions*, *96*(pt 1).

IMO. (2009). *Mepc 59/ Inf.10*. *April 2009*, 1–287.

IMO, Smith, T. W. P., Jalkanen, J. P., Anderson, B. A., Corbett, J. J., Faber, J., Hanayama, S., O'Keeffe, E., Parker, S., Johansson, L., Aldous, L., Raucci, C., Traut, M., Ettinger, S., Nelissen, D., Lee, D. S., Ng, S., Agrawal, A., Winebrake, J. J., & Hoen, M., A. (2014). Third IMO Greenhouse Gas Study 2014. *International Maritime Organization (IMO)*, 327.

https://doi.org/10.1007/s10584-013-0912-3

IMO, U. N. (2018). Body Adopts Climate Change Strategy for Shipping. *International Maritime Organisation,(IMO), London*.

Jalkanen, J., Johansson, L., & Kukkonen, J. (2016). *A comprehensive inventory of ship traffic exhaust emissions in the European sea areas in 2011*. 71–84. https://doi.org/10.5194/acp-16-71-2016

Johnson, H., Gabrielii, C., & Andersson, K. (2015). *Energy and Exergy Analysis of Ship Energy Systems – The Case study of a*. *18*(2), 82–93. https://doi.org/10.5541/ijot.70299

Kamali, M., Parham, K., & Assadi, M. (2018). Performance analysis of a single stage absorption heat transformer-based desalination system employing a new working pair of (EMIM)(DMP)/H2O. *International Journal of Energy Research*, *42*(15), 4790–4804.

Karamangil, M. I., Coskun, S., Kaynakli, O., & Yamankaradeniz, N. (2010). A simulation study of performance evaluation of single-stage absorption refrigeration system using conventional working fluids and alternatives. *Renewable and Sustainable Energy Reviews*, *14*(7), 1969–1978.

Keçeciler, A., Acar, H. İ., & Doğan, A. (2000). Thermodynamic analysis of the absorption refrigeration system with geothermal energy: an experimental study. *Energy Conversion and Management*, *41*(1), 37–48.

Khalil, S. J. (2024). *Thermodynamic Design of 10 TR Single-Effect LiBr-H 2 O Absorption Refrigeration System*. *29*(1), 74–84.

Koehler, W. J., Ibele, W. E., Soltes, J., & Winter, E. R. (1988). Availability simulation of a lithium bromide absorption heat pump. *Heat Recovery Systems and CHP*, *8*(2), 157–171.

Kumar, N. R. (2009). *This is to certify that thesis entitled " STUDY OF AUTOMOBILE AIR CONDITIONING Department of Mechanical Engineering*. 1–53.

Kurem, E., & Horuz, I. (2001). A comparison between ammonia-water and water-lithium bromide solutions in absorption heat transformers. *International Communications in Heat and Mass Transfer*, *28*(3), 427–438.

Lee, S. (2014). Translated Decisions of the Korean Courts on Japanese Forced Labor re Mitsubishi Heavy Industries: Introductory Remarks: 2009 Da 22549, Issued May 24, 2012 (Supreme Court) 2012 Na 4497, Issued July 30, 2013 (Busan High Court). *The Korean Journal of International and Comparative Law*, *2*(2), 203–204.

Man, B. (2018). *Two stroke Engines* (Issue July 2018).

Manzela, A. A., Hanriot, S. M., Cabezas-Gómez, L., & Sodré, J. R. (2010). Using engine exhaust gas as energy source for an absorption refrigeration system. *Applied Energy*, *87*(4), 1141–1148.

Mathapati, S. S., Gupta, M., & Dalimkar, S. (2014). A study on automobile air-conditioning based on absorption refrigeration system using exhaust heat of a vehicle. *International Journal of Engineering Research and General Science*, *2*(4), 80–86.

Mikelis, N. (2008). A statistical overview of ship recycling. *WMU Journal of Maritime Affairs*, *7*, 227–239. https://doi.org/10.1007/BF03195133

Ouadha, A., & El-Gotni, Y. (2013). Integration of an ammonia-water absorption refrigeration system with a marine Diesel engine: A thermodynamic study. *Procedia Computer Science*, *19*, 754–761.

Oyelakun, B., Abdul-azeez, A. A., Olayemi, O., & Ibrahim, A. A. (2025). *THE PAYBACK PERIOD (PBP) UNIFIED FORMULA : A SIMPLIFIED PROPOSED THE PAYBACK PERIOD (PBP) UNIFIED FORMULA : A SIMPLIFIED PROPOSED METHOD FOR CALCULATING PBP IN CAPITAL BUDGETING DECISION*. *February*.

Palacios-Bereche, R., Gonzales, R., & Nebra, S. A. (2012). Exergy calculation of lithium bromide-water solution and its application in the exergetic evaluation of absorption refrigeration systems LiBr-H2O. *International Journal of Energy Research*, *36*(2), 166–181. https://doi.org/10.1002/er.1790

Report, I., & Horizon, T. (2021). *Global Warming Potentials (GWPs)/ CO 2 -equivalent (CO 2 e) and the importance of time horizons*. 1–4.

Riffat, S., & Qiu, G. (2004). Comparative investigation of thermoelectric air-conditioners versus vapour compression and absorption air-conditioners. *Applied Thermal Engineering*, *24*, 1979–1993. https://api.semanticscholar.org/CorpusID:108779277

Sahriana, N., Suminar, T., & Pranoto, Y. K. S. (2020). Development of maritime insight learning tools for ocean literacy in children aged 5-6 years old. *Journal of Primary Education*, *9*(5), 536–545.

Salehi, S., Yari, M., Mahmoudi, S. M. S., & Farshi, L. G. (2019). Investigation of crystallization risk in different types of absorption LiBr/H2O heat transformers. *Thermal Science and Engineering Progress*, *10*, 48–58.

Salmi, W., Vanttola, J., Elg, M., Kuosa, M., & Lahdelma, R. (2017). Using waste heat of ship as energy source for an absorption refrigeration system. *Applied Thermal Engineering*, *115*, 501–516.

Samanta, S., & Basu, D. N. (2016). Energy and entropy-based optimization of a single-stage water–lithium bromide absorption refrigeration system. *Heat Transfer Engineering*, *37*(2), 232–241.

Seddiek, I. S. (2015). an Overview: Environmental and Economic Strategies for Improving Quality of Ships Exhaust Gases. *Transactions of the Royal Institution of Naval Architects Part A: International Journal of Maritime Engineering*, *157*(1 A), A53–A64. https://doi.org/10.5750/ijme.v157iA1.948

Shu, G., Liang, Y., Wei, H., Tian, H., Zhao, J., & Liu, L. (2013). A review of waste heat recovery on two-stroke IC engine aboard ships. *Renewable and Sustainable Energy Reviews*, *19*, 385–401.

Sirwan, R., Alghoul, M. A., Sopian, K., & Ali, Y. (2013a). Thermodynamic analysis of an ejector-flash tank-absorption cooling system. *Applied Thermal Engineering*, *58*(1–2), 85–97.

Sirwan, R., Alghoul, M. A., Sopian, K., & Ali, Y. (2013b). Thermodynamic analysis of an ejector-flash tank-absorption cooling system. *Applied Thermal Engineering*, *58*(1–2), 85–97. https://doi.org/10.1016/j.applthermaleng.2013.03.031

Sözen, A. (2001). Effect of heat exchangers on performance of absorption refrigeration systems. *Energy Conversion and Management*, *42*(14), 1699–1716.

Sun, D.-W., Eames, I. W., & Aphornratana, S. (1996). Evaluation of a novel combined ejector-absorption refrigeration cycle—I: computer simulation. *International Journal of Refrigeration*, *19*(3), 172–180.

Sun, D. (1997). Solar powered combined ejector-vapour compression cycle for air conditioning and refrigeration. *Energy Conversion and Management*, *38*, 479–491. https://api.semanticscholar.org/CorpusID:109026033

Vahvanen, J. (2020). *Waste heat to electricity recovery techniques on large ships*.

Yang, C., Faragher, R., Yang, Z., Hollebone, B., Fieldhouse, B., Lambert, P., & Beaulac, V. (2023). Characterization of chemical fingerprints of ultralow sulfur fuel oils using gas chromatography-quadrupole time-of-flight mass spectrometry. *Fuel*, *343*, 127948. https://doi.org/10.1016/j.fuel.2023.127948

Zhang, Q., Luo, Z., Zhao, Y., & Pavel, S. (2021). Thermodynamic analysis and multi-objective optimization of a transcritical CO2 waste heat recovery system for cruise ship application. *Energy Conversion and Management*, *227*, 113612.

Zhu, S., Zhang, K., & Deng, K. (2020). A review of waste heat recovery from the marine engine with highly efficient bottoming power cycles. *Renewable and Sustainable Energy Reviews*, *120*, 109611.

APPENDIX A

Ethiopian Shipping and Logistics Services Enterprise		Document No.:		SMS/GEF/009
		Category		CR
Title:	Main Engine Performance Record	Issue Date	Revision No.	Action
		1985	04	F&L

						Vessel.....MV GAMBELLA.....	
Engine type.....Man B&W...		Engine No.....SE6540-0266.....				Date of mesurement.....31/08/2022.....	
P.....6810.....KW		N.....146.....				Service hour 32485	
Voyage From NINGBO to SINGAPORE		wind force 4				Fuel lever pos.....6.7.....	
Drought fore/aft...6.3/7.4.....m		Sea.....moderate.....				Load Indicator Pos.....40%.....	
Load .....T		Wind & sea in relation to vessel				SPEED SETTING 57	
Speed .....11.5.....Knots		NEX4					
Atms. Temp/presure...24/1015.....0c/m/bar						Engine .....125.....min-1.....	
						Governor term shaft pos.....	
Cylinder	1	2	3	4	5	6	Turbocharger
Exh. Gas temp Pyro	378	410	385	403	381	376	t exh gas bef. Turbine 0C.....434...
bef. Cyl. (max 0c) therm	109	107	104	107	107	110	t.tubine cool W. outlet 0c.....
Cyl. Cool outlet (80-90 0c)	79	82	79	83	81	79	turbin speed min -1.....15661...

Piston C. outlet.(max 850c)	53	54	53	53	54	54	P.exh. Gas back press. Mm W/g.....
Combution pressure	136	133	131	134	134	131	
FuelLubrication oil							Freshwater
Type.....VLSFO.....		Type.....ATLANTA MARINE3005.....				(bar) (0c)	
S.gravity kg/dm3.....		Oty. in system 1.....				Cyl. Cool inlet .....3.4..... ...67.....	
Consumption T/day.....20.....		Consumption 1/day.....				Pist. Cool. Inlet	
Visco. (CST).....8.1.....		Treatement.....Purifiers.....				Charge. Air cool inlet .....2.6..... .....37.....	
P.bef. Eng.(bar).....7.5.....		P m/bring bar.....2.4.....				Charge air cool outlet ....42....	
P.init boast pump (bar).....4.....		P x/hd.brng.bar.....				Seawater 30	
P.outl. Boost pump(bar).....10.....		P actuator (bar)				Inlet cooler.....38.....	
T bef eng. 0c.....115.....		P lubricator drive (bar).....				Outlet cooler.....	
t bef preheater 0c		t inlet eng. 0c.....44.....				Centeral cooling water	
t service tank 0c.....89.....		t outl. Cool 0c.....44.....				Inlet cooler.....2.6.....	
Δ p eng inlet bar.....		t. inlet eng. 0c				Outlet cooler...41.2....	
.		t.inlet cool 0c.....55.....					
Thrust bearing		Cylinder oil				Remarks	
P inlet bar.....2.4.....		Type...TALUSIA UNIVERSAL.....					
t inlet 0c.....44.3.....		Consumption 1/day.....180.....					

t outlet 0c.....55.....		Exhaust gas colour.....CLEAR.....
Air	Charge air	Remarks
P. staring E. in .....21.....	P bef cool bar.....	
P. con. E. in.....7.....	P aft cool (bar).....1.9.....	
P. air spring .....7.....	t bef. Cool (bar).....172.....	
.	t aft. Cool (bar).....56.....	Date 31/08/2022 Name:- DEMELASH ABAY

Note:
Chief engineer to modify the form and make it ship specific
One copy to chief engineer file and one copy to TD

VESSEL NAME: MV GAMBELLA

MAIN ENGINE FUEL CONSUMPTION & SPEED

S/N	MAIN ENGINE Fuel used : VLSFO	Consumption on Ballast voyage		Consumption on Loaded voyage		Remark
		Fuel Consumption (Metric Ton)	SPEED (KNOT)	Fuel Consumption	SPEED (KNOT)	
1	Economy(120RPM)	17.5	10.7	18.6	10.3	
2	Normal(125RPM)	19.7	11.5	20.65	11.1	
3	Maximum(131RPM)	22.5	12	23.7	11.7	

AUXILARY ENGINE FUEL CONSUMPTION

S/N	Fuel Used: MGO	Machinery	Fuel Consumption (Metric Ton)	Remark
1	Cargo loading	Two gen. sets + boiler	3.5	
2	Idle waiting /at	One gen. set + boiler	2.9	

All Above is an approximate calculation in current vessel status and in NORMAL WEATHER CONDITION.
PLEASE NOTE , RECENT PAST RECORDS SHOW THAT VESSEL OPERATED AT 120RPM AT ALL TIMES

BASIC DESIGN DATA 基本设计参数:

Main engine主机型号 :	6S40ME-B9-TII		
Engine load主机负荷95%	ISO NCR	:	
Exhaust gas quantity主机废气排量	kg /h	:	54500
Exhaust gas temp. inlet boiler	deg . C	:	258.2
废气进锅炉的温度			
Exhaust gas temp. outlet: boiler	deg. C	:	170
废气出锅炉的温度			
Steam output废气部分蒸汽产量	kg/h	:	~1150
Total pressure loss across the			
boiler incl. inlet/outlet boxes	mm WC	:	110
废气经过锅炉的压力损失90%	mm WC		110
100%工况	mm WC		130

APPENDIX B

List of Capacities for 6S40ME-B9-TII at NMCR - IMO NO_x Tier II compliance

		Seawater cooling						Central cooling					
		Conventional TC			High eff. TC			Conventional TC			High eff. TC		
		1 x TCA55-21	1 x A170-L34	1 x MET53MA	*	*	*	1 x TCA55-21	1 x A170-L34	1 x MET53MA	*	*	*
Pumps													
Fuel oil circulation	m³/h	2.8	2.8	2.8	N.A.	N.A.	N.A.	2.8	2.8	2.8	N.A.	N.A.	N.A.
Fuel oil supply	m³/h	1.8	1.8	1.8	N.A.	N.A.	N.A.	1.8	1.8	1.8	N.A.	N.A.	N.A.
Jacket cooling	m³/h	60.0	60.0	60.0	N.A.	N.A.	N.A.	60.0	60.0	60.0	N.A.	N.A.	N.A.
Seawater cooling *	m³/h	230.0	230.0	230.0	N.A.	N.A.	N.A.	220.0	220.0	220.0	N.A.	N.A.	N.A.
Main lubrication oil *	m³/h	140.0	140.0	145.0	N.A.	N.A.	N.A.	140.0	140.0	145.0	N.A.	N.A.	N.A.
Central cooling *	m³/h	-	-	-	-	-	-	175	175	175	-	-	-
Scavenge air cooler(s)													
Heat diss. app.	kW	2,820	2,820	2,820	N.A.	N.A.	N.A.	2,810	2,810	2,810	N.A.	N.A.	N.A.
Central water flow	m³/h	-	-	-	N.A.	N.A.	N.A.	96	96	96	N.A.	N.A.	N.A.
Seawater flow	m³/h	147	147	147	N.A.	N.A.	N.A.	-	-	-	N.A.	N.A.	N.A.
Lubricating oil cooler													
Heat diss. app. *	kW	620	610	610	N.A.	N.A.	N.A.	620	610	610	N.A.	N.A.	N.A.
Lube oil flow *	m³/h	140.0	140.0	145.0	N.A.	N.A.	N.A.	140.0	140.0	145.0	N.A.	N.A.	N.A.
Central water flow	m³/h	-	-	-	N.A.	N.A.	N.A.	79	79	79	N.A.	N.A.	N.A.
Seawater flow	m³/h	83	83	83	N.A.	N.A.	N.A.	-	-	-	N.A.	N.A.	N.A.
Jacket water cooler													
Heat diss. app.	kW	1,080	1,080	1,080	N.A.	N.A.	N.A.	1,080	1,080	1,080	N.A.	N.A.	N.A.
Jacket water flow	m³/h	60	60	60	N.A.	N.A.	N.A.	60	60	60	N.A.	N.A.	N.A.
Central water flow	m³/h	-	-	-	N.A.	N.A.	N.A.	79	79	79	N.A.	N.A.	N.A.
Seawater flow	m³/h	83	83	83	N.A.	N.A.	N.A.	-	-	-	N.A.	N.A.	N.A.
Central cooler													
Heat diss. app. *	kW	-	-	-	N.A.	N.A.	N.A.	4,510	4,500	4,500	N.A.	N.A.	N.A.
Central water flow	m³/h	-	-	-	N.A.	N.A.	N.A.	175	175	175	N.A.	N.A.	N.A.
Seawater flow	m³/h	-	-	-	N.A.	N.A.	N.A.	220	220	220	N.A.	N.A.	N.A.
Starting air system, 30.0 bar g, 12 starts. Fixed pitch propeller - reversible engine													
Receiver volume	m³	2 x 2.5	2 x 2.5	2 x 2.5	N.A.	N.A.	N.A.	2 x 2.5	2 x 2.5	2 x 2.5	N.A.	N.A.	N.A.
Compressor cap.	m³	150	150	150	N.A.	N.A.	N.A.	150	150	150	N.A.	N.A.	N.A.
Starting air system, 30.0 bar g, 6 starts. Controllable pitch propeller - non-reversible engine													
Receiver volume	m³	2 x 1.5	2 x 1.5	2 x 1.5	N.A.	N.A.	N.A.	2 x 1.5	2 x 1.5	2 x 1.5	N.A.	N.A.	N.A.
Compressor cap.	m³	90	90	90	N.A.	N.A.	N.A.	90	90	90	N.A.	N.A.	N.A.
Other values													
Fuel oil heater	kW	73	73	73	N.A.	N.A.	N.A.	73	73	73	N.A.	N.A.	N.A.
Exh. gas temp.	°C	265	265	265	N.A.	N.A.	N.A.	265	265	265	N.A.	N.A.	N.A.
Exh. gas amount	kg/h	56,400	56,400	56,400	N.A.	N.A.	N.A.	56,400	56,400	56,400	N.A.	N.A.	N.A.
Air consumption	kg/h	15.3	15.3	15.3	N.A.	N.A.	N.A.	15.3	15.3	15.3	N.A.	N.A.	N.A.

* For main engine arrangements with built-on power take-off (PTO) of a MAN Diesel recommended type and/or torsional vibration damper the engine's capacities must be increased by those stated for the actual system

For List of Capacities for derated engines and performance data at part load please visit http://www.manbw.dk/ceas/erd/

Data at nominel MCR (L_1)			SFOC at nominal MCR (L_1)
			Conventional TC
Engine	kW	r/min	g/kWh
5 S40ME-B9	5,675	146	175
6 S40ME-B9	6,810		
7 S40ME-B9	7,945		
8 S40ME-B9	9,080		

Mass of Water and Oil

No. of cylinders	Mass of water and oil in engine in service					
	Mass of water			Mass of oil		
	Jacket cooling water kg	Scavenge air cooling water kg	Total kg	Engine system kg	Oilpan kg	Total kg
5	225	260	485	170	250	420
6	270	260	530	195	365	560
7	315	260	575	220	290	510
8	360	260	620	245	365	610

APPENDIX C

TMU-380 marine air conditioner

Instruction manual

Jiangsu Zhaosheng Air Conditioning Co., Ltd.

Tel: 0523-87598768 87591611

Fax: 0523-87592899

http//www: zhaoshenggroup.com

November 2010

1. Purpose and characteristics of CLN, TMU air conditioning device

This air conditioning device is used for air conditioning in various cabins of ships as an air handling device for centralized air conditioning systems. That is, the filtration and cooling of air are concentrated in the device, and the treated air is sent to each cabin through the air duct to ensure a certain temperature, humidity and cleanliness.

The air conditioning device consists of a semi-enclosed compressor, a condenser, an air conditioner (including Freon air cooler, steam heater, steam humidifier, centrifugal fan, return air mixing box, etc.), as well as an electric control box, an instrument panel, refrigeration system pipelines and valves, etc. The size and position of the return air mixing box and the outlet pipe are manufactured according to requirements.

All refrigerant pipelines and cables of this device have been disconnected and sealed before leaving the factory, and the compression condensing unit and air conditioner refrigeration system have been pressure tested and vacuum tested. After the user installs the device in place, connect the refrigerant pipeline, cable system and power supply according to the refrigeration system schematic diagram, connect them completely, re-do the pressure test and vacuum test, and then perform liquid filling and debugging.

The air conditioning box of this device is a frame strip combination structure made of molds. The box adopts double-layer panels and is covered with rubber-plastic cotton boards for insulation.

2. Main technical data of the device and specifications of main supporting equipment

I. Air conditioning device

(1) Model CLN-380 marine compression condensing unit

TMU-380 marine direct air conditioner

(2) Refrigeration type Direct evaporation type

(3) Refrigeration capacity 380KW (Tc=+40□C, To=+5□C)

(4) Heating capacity 380KW

(5) Compressor energy adjustment range Pressure adjustable

(6) Air volume 16000m3/h

(7) External residual pressure ~1800Pa

(8) Heating steam volume 580m3/h saturated steam

(9) Humidification volume 50kg/h saturated steam

(10) Compressor power 2×55kw

(11) Fan power 18.5kw

(12) Refrigerant R404A

(13) Cooling water temperature 32□C

(14) Power supply AC380V 3ϕ 50Hz

(15) Operation control mode Automatic, manual

(16) Safety protection device High pressure, low pressure, water pressure, motor overload and phase failure protection, compressor exhaust overtemperature protection.

2.2 Compression condensing unit

(1) 2 compressors

Open compressor model 5H60 Carrier

Motor input power 55KW

Electricity AC 440V 3ϕ 60Hz

Motor model Y250M-4-H

(2) 2 marine condensers

Type Horizontal shell and tube, inlet and outlet flange connection

Cooling water flow 60X2m3/h

Inlet and outlet diameter DN100

2.3 Air conditioner

(1) Evaporator

Material Copper tube copper sleeve

(2) Steam heater

Material Copper tube copper sleeve

(2) Humidifier

Stainless steel tube

(2) Air filter (detachable and washable)

Material Concave and convex brocade wire mesh

(3) Centrifugal fan

Model KHF-500

Air volume 16000m3/h

Static pressure 2300Pa

(3) Matching motor (protection level: IP44, insulation level: F grade)

Model Y180M-4-H (B3)

Power 18.5 kW

Electricity AC440V 3ϕ 60Hz

2.4 Others

(1) Low pressure controller KP1 Danfoss

(2) Low pressure gauge DT-60

(3) High pressure controller KP5 Danfoss

(4) High pressure gauge DT-60

(5) Water pressure controller YWK-50-C

(6) Water pressure gauge DT-60

(7) Temperature controller A19A Johnson

(8) Liquid supply solenoid valve EVR-25 Danfoss

(9) Thermal expansion valve THR-60S ALCO

(10) Dry filter ATDS-9611

(11) Thermometer WNG-11

APPENDIX D

By using the selected design parameters of the system, the concentrations of strong and weak solutions of LiBr can be computed

- Refrigerant temperature and pressure in evaporator: $T_e = 5^oC$, $p_e = 0.872kPa$
- Generator temperature: $T_g = 85^oC$
- Condenser temperature and pressure: $T_c = 40^oC$, $p_c = 7.38kPa$
- Absorber temperature: $T_a = 35^oC$

$$\chi_{ws} = \frac{49.04+1.125T_a-T_e}{134.65+0.47T_a} = 55.21\%$$

$$\chi_{ss} = \frac{49.04+1.125T_g-T_c}{134.65+0.47T_g} = 59.95\%$$

Then using the concentration values, circulation ratio can be determined

$$\lambda = \frac{\dot{m}_{ss}}{\dot{m}_r} = \frac{\chi_{ws}}{\chi_{ss}-\chi_{ws}}$$

$$\lambda = 11.65$$

$$\dot{m}_{ws} = \dot{m}_{ss} + \dot{m}_r = \dot{m}_r(\lambda + 1)$$

By using mass and energy balance on generator, the mass flow rates can be determined from equations

$$\dot{m}_3 = \dot{m}_4 + \dot{m}_7 \quad (3.33)$$

$$\dot{m}_3 h_3 = \dot{m}_4 h_4 + \dot{m}_7 h_7 + Q_g \quad (3.34)$$

Where

$\dot{m}_3 = \dot{m}_{ws}$; $\dot{m}_4 = \dot{m}_{ss}$ and $\dot{m}_7 = \dot{m}_r$

$h_7 = h_v$ at T_g and $p_3 = p_4 = p_5 = p_g = p_c$

The heat input to generator (Q_g) is determined from the equations:

$$Q_g = \dot{m}_{exh} C_{P,exh}(T_{g,in} - T_{g,out})$$

$$C_{P,exh} = (962.097 + 0.1509T_{exh})J/kgK$$

$T_{g,in} = T_{exh\ gas,in} = 170 \pm 15^oC$, in this sample calculation take $T_{g,in} = T_{exh\ gas,in} = 155^oC$

$T_{g,out} = T_{exh\ gas,out} = 120^oC$

$C_{p,exh\ @\ T=120^oC} = 1.021kJ/kgK$

$C_{p,exh\ @\ T=155^oC} = 1.027kJ/kgK$

$\dot{m}_{exh} = 13.29kg/s$

Substituting the above values;

$Q_g = 509.14kW$

By using the above equation (3.34)

$$Q_g = \dot{m}_{ss}h_4 + \dot{m}_r h_7 - \dot{m}_{ws}h_3$$

$$= \dot{m}_r(\lambda h_4 + h_7 - (\lambda + 1)h_3)$$

From steam tables $h_7 = h_v$ at $T_g = 85^oC = 2651.9$ kJ/kg

From Duhring enthalpy calculations:

$h_4 = h$ at $T_g = 85^oC$ and $\chi_{ss} = 59.95\%$; $h_4 = 202.33kJ/kg$

$h_1 = h_2 = h$ at $T_a = 35^oC$ and $\chi_{ws} = 55.21\%$; $h_2 = 84.06kJ/kg$

By using equation (3.32) below h_3 is determined by taking effectiveness $\varepsilon = 0.7$

$$\varepsilon_{SHX} = \frac{h_3 - h_2}{h_4 - h_2} \quad (3.32)$$

$h_3 = 166.85kJ/kg$

Hence, by substituting the values into equation (3.34) the mass flow rates becomes:

$\dot{m}_r = 0.17kg/s$

$\dot{m}_{ss} = 1.98kg/s$

$\dot{m}_{ws} = 2.15kg/s$

By considering an ordinary cycle, the heat transfer rates(Q) in condenser, evaporator, and absorber can be computed.

From equations (3.45) and (3.46), a condenser heat transfer rate (Q_c) is determined;

$$\dot{m}_7 = \dot{m}_8 \quad (3.45)$$

$$\dot{m}_7 h_7 = \dot{m}_8 h_8 + Q_C \quad (3.46)$$

Where

$\dot{m}_8 = \dot{m}_r = 0.17kg/s$

From steam table: $h_8 = h_f$ at T_8; $T_8 = T_c$; $p_7 = p_7 = p_8 = p_c$; $h_8 = 167.57kJ/kg$

Thus,

$Qc = 422.34kW$

From equations (3.58) and (3.59), an evaporator heat transfer rate (Q_c) is determined;

$$\dot{m}_9 = \dot{m}_{10} \quad (3.58)$$

$$\dot{m}_9 h_9 = \dot{m}_{10} h_{10} + Q_e \quad (3.59)$$

Where

$\dot{m}_9 = \dot{m}_{10}$

From steam table: $h_9 = h_8$; $h_{10} = h_v$ at T_{10}; $T_9 = T_{10} = T_e$ and $p_9 = p_{10} = p_e$

$h_9 = 167.57kJ/kg$

$h_{10} = 2510.6kJ/kg$

Thus,

$Q_e = 398.32kW$

From equations (3.26) and (3.27), an absorber heat transfer rate (Q_a) is determined;

$$\dot{m}_1 = \dot{m}_6 + \dot{m}_{10} \quad (3.26)$$

$$\dot{m}_1 h_1 = \dot{m}_6 h_6 + \dot{m}_{10} h_{10} - Q_a \quad (3.27)$$

Where

$\dot{m}_1 = \dot{m}_{ws}$; $\dot{m}_6 = \dot{m}_{ss}$ and $\dot{m}_{10} = \dot{m}_r$

$h_1 = h$ at T_a and χ_{ws}; $h_6 = h_5$; $h_{10} = h$ at T_{10a} and $p_1 = p_6 = p_a = p_e = p_{sat}$ at T_e

From equation (3.31) below, h_5 is determined;

$$\dot{m}_2 h_2 + \dot{m}_4 h_4 = \dot{m}_3 h_3 + \dot{m}_5 h_5 \quad (3.31)$$

Where

$\dot{m}_2 = \dot{m}_3 = \dot{m}ws$; $\dot{m}_4 = \dot{m}_5 = \dot{m}_{ss}$

Thus

$h_5 = 112.43$ kJ/kg $= h_6$

Substituting the values;

$Q_a = 468.68kW$

COP of VARS for ordinary cycle is determined as:

$$\text{COP} = \frac{Q_e}{Q_g + W_P}$$

By neglecting work of pump, COP becomes:

$$\text{COP} = 0.7823$$

In the proposed and the combined cycle, the heat transfer rate in generator and absorber is the same as ordinary cycle.

Therefore, to compute a heat transfer rates in condenser, first compute the unknown parameters in a mixing chamber and flash tank using equations;

$$\dot{m}_{7a} = \dot{m}_{10c} + \dot{m}_7 \quad (3.37)$$

$$\dot{m}_{7a}h_{7a} = \dot{m}_{10c}h_{10c} + \dot{m}_7 h_7 \quad (3.38)$$

$$\omega = \frac{\dot{m}_{10c}}{\dot{m}_7} \quad (3.39)$$

$$\dot{m}_{7a} = (1 + \omega)\dot{m}_7 \quad (3.40)$$

$$h_{7a} = \frac{h_7 + \omega(h_{10c})}{1+\omega} \quad (3.41)$$

$$\dot{m}_{10c}h_{10c} = \dot{m}_{8b}h_{8b} = \dot{m}_{10b}h_{10b} \quad (3.42)$$

$$\dot{m}_{10c} = \dot{m}_{8b} + \dot{m}_{10b} \quad (3.43)$$

$$\dot{m}_{10b} = \dot{m}_{10a} - \dot{m}_{10} \quad (3.44)$$

Where

$\dot{m}_7 = \dot{m}_{10} = \dot{m}_r$

$\dot{m}_{10a} = \dot{m}_{8a}$; $p_7 = p_{7a} = p_{10c} = p_c$

$\dot{m}_{8b}$ is determined below from equation (3.52)

From steam table: $h_7 = h_v$ at T_7, $T_7 = T_g$; $h_{8b} = h_v$ at T_{ft}; $h_{10b} = h_{10a} = h_{10}$; h_{10c} is determined above from equation (3.42).

By taking the entrainment ratio $\omega = 0.6$;

$\dot{m}_{10c} = 0.102$ kg/s

$\dot{m}_{7a} = 0.272$ kg/s

From equation (3.51). the flash tank pressure and temperature is determined;

$$P_{ft} = \sqrt{P_e P_c} \quad (3.51)$$

P_{ft} = 2.538 kPa and $T_{ft} = T_{sat\ @pft}$ = 21.32°C

By using flash tank mass and energy balance $\dot{m}_{8b}$ is computed

$$\dot{m}_8 = \dot{m}_{8a} + \dot{m}_{8b} \quad (3.49)$$

$$\dot{m}_8 h_8 = \dot{m}_{8a} h_{8a} + \dot{m}_{8b} h_{8b} \quad (3.50)$$

Where

$\dot{m}_8 = \dot{m}_{7b} = \dot{m}_{7a}$

$T_8 = T_{8a} = T_{8b} = T_{ft}$; $T_{ft} = T_{sat}$ at P_{ft}

From steam table: $h_8 = h_f$ at T_c; $h_{8a} = h_f$ at T_{ft}; $h_{8b} = h_v$ at T_{ft}

Thus

h_{8a} = 89.33 kJ/kg

h_{8b} = 2540.47kJ/kg

Hence, the unknown parameter $\dot{m}_{8b}$ is determined from equation (3.52) and is given as:

$$\dot{m}_{8b} = \frac{\dot{m}_{8a}(h_8 - h_{8a})}{h_{8b} - h_{8a}} \quad (3.52)$$

$\dot{m}_{8b} = 0.032\ \dot{m}_{8a}$

Where

$\dot{m}_8 = \dot{m}_{8a} + \dot{m}_{8b}$; $\dot{m}_8$ = 0.272kg/s

Thus;

$\dot{m}_{8a}$ = 0.264 kg/s

$\dot{m}_{8b}$ = 0.008 kg/s

Using mass and energy balance equations in the LSHX

$$\dot{m}_{8a} = \dot{m}_9 = \dot{m}_{9b} = \dot{m}_{10a} \quad (3.53)$$

$$\dot{m}_{8a} h_{8a} + \dot{m}_{9b} h_{9b} = \dot{m}_9 h_9 + \dot{m}_{10a} h_{10a} \quad (3.54)$$

The effectiveness of LSHX is given as:

$$\varepsilon_{LSHX} = \frac{T_9 - T_{8a}}{T_{9b} - T_{8a}} \quad (3.55)$$

Where

From steam table: $h_9 = h_f$ at T_9; $T_{9a} = T_{9b} = T_e$; $h_{8a} = h_f$ at T_8; $h_{9b} = h_v$ at T_{9b}; $p_{8a} = p_9 = p_{ft}$

and h_{10a} is determined from the above equation (3.54)

By taking $\varepsilon_{LSHX} = 0.7$; the outlet temperature of LSHX (T_9) becomes;

$T_9 = 9.89^oC$

Thus,

$h_9 = 41.55$ kJ/kg = h_{9a};

$h_{9b} = 2510.6$ kJ/kg and then

$h_{10a} = 2558.38$kJ/kg = $h_{10b} = h_{10}$

It is known that the mass in VARS the mass of desorbed refrigerant in the generator is the same as the mass of extracted by absorber from the evaporator, i.e. $\dot{m}_7 = \dot{m}_{10} = \dot{m}_r$.

Hence, $\dot{m}_{10b}$ is determined as;

$$\dot{m}_{10b} = \dot{m}_{10a} - \dot{m}_{10}$$

$\dot{m}_{10b} = 0.094$ kg/s

Then substitute the above values into equation (3.42), h_{10c} is determined.

$h_{10c} = 2557.00$ kJ/kg

Then substitute the above values into equation (3.38), h_{7a} is determined.

$h_{7a} = 2616.30$ kJ/kg

Therefore, using equations (3.45) and (3.46) a heat transfer rate in condenser becomes;

$$\dot{m}_{7a} = \dot{m}_{7b} \quad (3.45)$$

$$\dot{m}_{7a}h_{7a} = \dot{m}_{7b}h_{7b} + Q_C \quad (3.46)$$

Where

From steam table: $h_{7b} = h_f$ at T_{7b}; $T_{7b} = T_c$; $p_{7a} = p_{7b} = p_8 = p_c$

Thus,

$Q_c = 666.05$kW

By using mass and energy balance equations of evaporator, a heat transfer rate of evaporator can be determined for proposed and combined system;

$$\dot{m}_{9a} = \dot{m}_{9b} \quad (3.58)$$

$$\dot{m}_{9b}h_{9b} = \dot{m}_{9a}h_{9a} + Q_e \quad (3.59)$$

For combined system, in this case Q_e is determined without LSHX;

Thus,

$$Q_e = \dot{m}_{9b}h_{9b} - \dot{m}_{8a}h_{8a}$$

Q_e = 639.22kW

$COP_{Combined}$ = 1.2555

For the proposed system, in this case Q_e is determined with LSHX;

Thus,

$$Q_e = \dot{m}_{9b}h_{9b} - \dot{m}_{9a}h_{9a}$$

Q_e = 651.83kW

$COP_{Proposed}$ = 1.2803